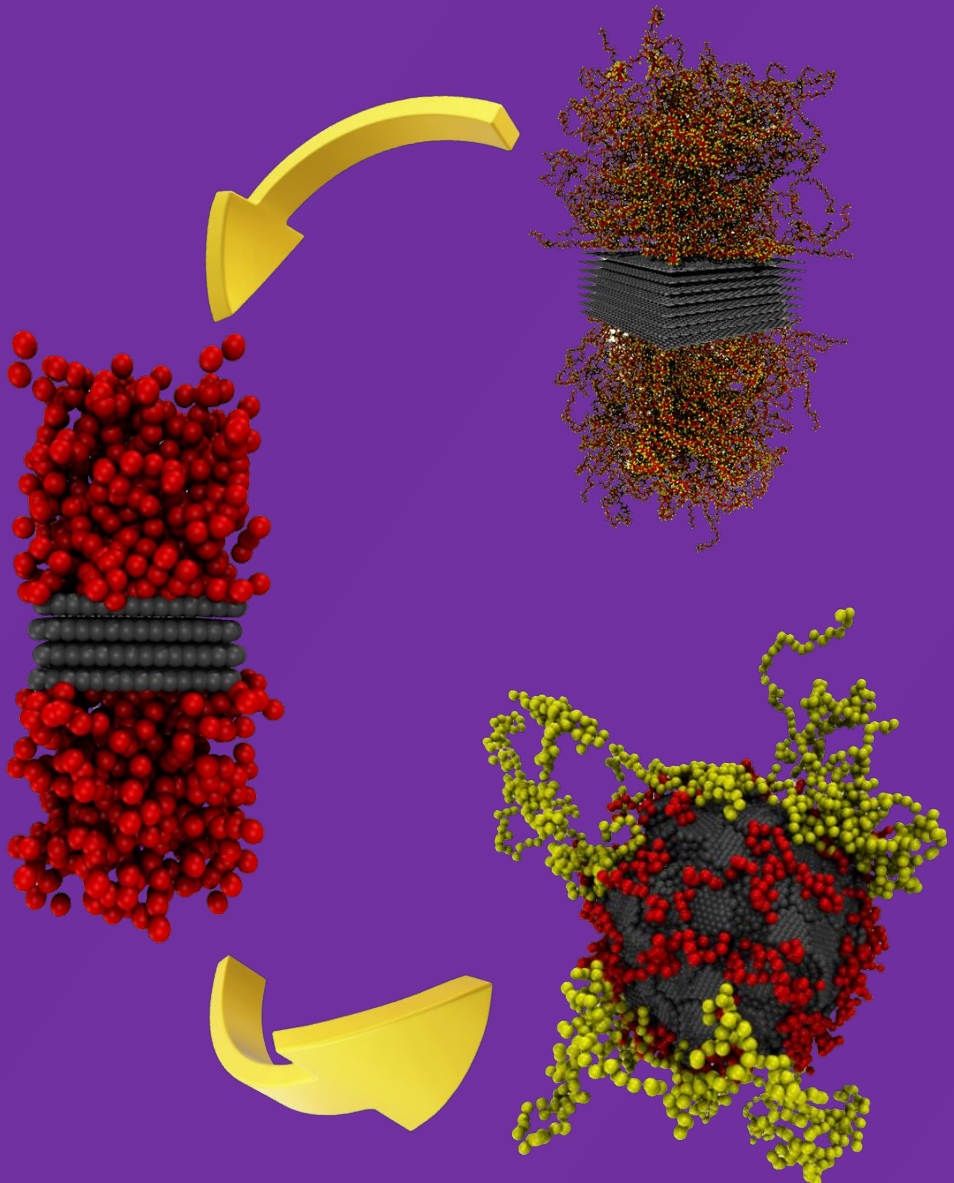




# Mesoscale Modeling of Carbon Black/Polymer Interfaces: Linking Atomistic and Coarse-Grained Particle-Field Representations

Stefano Caputo



Università degli Studi di Salerno  
Dipartimento di Chimica e Biologia "A. Zambelli"  
XXXII ciclo di dottorato



# Mesoscale Modeling of Carbon Black/Polymer Interfaces: Linking Atomistic and Coarse-Grained Particle-Field Representations

**Tutor:**

Prof. Giuseppe Milano

**Ph. D. Student:**

Stefano Caputo  
8800100030

**External Tutor:**

Dr. Alexandra Romina Alburnia

**Ph. D. Course Coordinator:**

Prof. Riccardo Zanasi

2019 - 2020



# Contents

<b>1 Introduction.....</b>	<b>1</b>
<i>References .....</i>	<i>2</i>
<b>2 Hybrid Particle-Field Molecular Dynamics.....</b>	<b>3</b>
2.1 <i>Theoretical Scheme .....</i>	<i>3</i>
2.2 <i>Implementation Scheme .....</i>	<i>9</i>
<i>References .....</i>	<i>13</i>
<b>3 Carbon Black.....</b>	<b>14</b>
3.1 <i>Overview .....</i>	<i>14</i>
3.2 <i>Morphology and Structure .....</i>	<i>16</i>
3.3 <i>Molecular Models of Carbon Black.....</i>	<i>18</i>
<i>References .....</i>	<i>19</i>
<b>4 Multiscale Modeling of CB/PE Interfaces .....</b>	<b>20</b>
4.1 <i>All-atom Simulations of PE and PE/Graphite .....</i>	<i>22</i>
4.1.1 <i>Atomistic Model of PE .....</i>	<i>22</i>
4.1.2 <i>Simulation Details .....</i>	<i>23</i>
4.1.3 <i>Force-field testing: Calculated vs Experimental Properties .....</i>	<i>25</i>
4.1.4 <i>Atomistic Model of PE/Graphite System.....</i>	<i>27</i>
4.2 <i>CG Models of PE and Graphitic Structures.....</i>	<i>30</i>
4.2.1 <i>Mapping Scheme: Graphite and PE.....</i>	<i>31</i>
4.2.2 <i>Simulations of CG PE chains .....</i>	<i>36</i>

4.2.3 CG Model of PE on Graphite .....	43
<b>4.3 CG Model of CB Nanoparticle.....</b>	<b>48</b>
4.3.1 Models and Parameters .....	48
4.3.2 Primary Nanoparticle Structure Generation .....	53
4.3.2.1 Simulation Details.....	53
4.3.2.2 Results and Discussion.....	53
<b>4.4 CG Model of PE on Graphite/CB: Monodisperse and Bidisperse Polymer Melts.....</b>	<b>60</b>
4.4.1 Simulation Details .....	60
4.4.2 Graphite/CB Monodisperse Polymer Melt Systems.....	61
4.4.3 Graphite/CB Bidisperse Polymer Melt Systems .....	64
<b>4.5 Conclusions and Perspectives.....</b>	<b>76</b>
<b>References .....</b>	<b>79</b>
<b>5 All-atom Model of Atactic Poly(2-vinylpyridine) .....</b>	<b>81</b>
5.1 Atomistic Model of Atactic P2VP .....	84
5.2 Simulation Details .....	88
5.3 Results and Discussion .....	90
5.3.1 Relaxation of Atactic P2VP Melt with PF-MD Method.....	90
5.3.2 Structural Properties.....	97
5.4 Conclusions.....	99
References .....	100
<b>Appendix.....</b>	<b>104</b>

---

## Introduction

---

Polymer nanocomposites are materials given by a combination of inorganic nanoparticles, denoted as fillers, with at least one dimension is in the range 1-100 nm, and an organic polymeric component, referred as matrix.<sup>1</sup>

Over the last two decades, these materials have attracted increasingly interest due to their high impact in industrial formulations and technological applications. In particular, the addition of nanoparticles to a polymer can influence in a substantial way several physicochemical properties, such as mechanical strength, electrical and thermal conductivity, gas permeability, chemical resistance and many others. These improved properties, which manifest on a macroscopic level, are due to the presence of different interactions taking place among the polymer and the filler nanoparticles at the nanoscale. For many industrial applications, it is required an accurate control of the dispersion state of the nanoparticles within the polymeric matrix, but this can be a challenging task, especially when increasing the filler content.<sup>2</sup> To this aim molecular simulations represent a valuable and reliable tool to get insights on nano and microscale level phenomena and thus to better understand which

factors can influence the dispersion of nanoparticles in polymeric systems.

This thesis is concerned with the study of polymer / nanoparticle interfaces, by means of molecular dynamics (MD) simulations, with the aim to get different structural and dynamical properties information of the adsorbed polymer chains. In particular systems containing carbon black (CB) nanoparticles embedded in melts of polyethylene (PE) of varying  $M_w$ , have been simulated, using a multiscale approach starting from atomistic to the coarse-grained level. Simulations and specific models have been developed by applying hybrid particle-field molecular dynamics (PF MD) technique, which is straightforward, suitable method for the simulation of large length and timescale phenomena, typical of high  $M_w$  polymer melts. Another part of the thesis deals with the modeling of atactic poly(2-vinylpyridine). In particular, force fields have been tested that can reproduce experimental structural properties of this polymer.

## References:

- (1) R. K. Gupta, E. Kennel, K.-J. Kim, *Polymer Nanocomposites Handbook*, CRC Press, **2010**.
- (2) S. K. Kumar, V. Ganesan, R. A. Riggleman, *J. Chem. Phys.* **2017**, *147*, 020901.

---

## Hybrid Particle-Field Molecular Dynamics

---

### *2.1 Theoretical Scheme*

The hybrid PF-MD method has been widely validated and successfully employed in many previous works to equilibrate polymer melt systems of both atomistic and coarse-grained models, and to prepare polymer composite materials.<sup>1,2,3,4</sup>

Here a theoretical description of the method is given. Further details and a full treatment of the approach can be found in other articles<sup>5,6</sup> where the derivation has been first introduced.

The main feature of PF-MD method is that the non-bonded forces calculation (most computationally expensive term in a MD simulation), can be replaced by the interaction of each atom with an external potential depending on the local density of particles at a given position  $r$ .<sup>5</sup>

In the spirit of self-consistent field theory (SCFT), a many-body problem can be reduced to a problem of deriving the partition function of a single particle in an external potential  $V(\mathbf{r})$ .<sup>5</sup> In this framework, the Hamiltonian of the system can be divided in two parts:

$$\hat{H}(\Gamma) = \hat{H}_0(\Gamma) + \hat{W}(\Gamma), \quad (1)$$

where  $\Gamma$  is used to denote a set of positions of all atoms in the system, specifying a point in the phase space. The symbol  $\hat{\cdot}$  in equation (1) indicates that the associated physical quantity is a function of the microscopic states described by the phase space  $\Gamma$ .

$\hat{H}_0(\Gamma)$  is the Hamiltonian of a reference ideal system composed of  $M$  noninteracting molecules but with all the intramolecular interaction terms (bond, angle) that are generally considered in molecular simulations. On the other hand, the deviation from the reference system due to the intermolecular nonbonded interactions is accounted for by the term  $\hat{W}(\Gamma)$  in equation (1).

Considering the canonical ( $NVT$ ) ensemble, the partition function of the system can be expressed as

$$Z = \frac{1}{M!} \int d\Gamma \exp\{-\beta[\hat{H}_0(\Gamma) + \hat{W}(\Gamma)]\}. \quad (2)$$

The density distribution of atoms from microscopic point of view can be obtained considering that the microscopic density distribution can be defined as a sum of delta functions centered at the center of mass of each particle as

$$\hat{\phi}(\mathbf{r}; \Gamma) = \sum_{p=0}^M \sum_{i=0}^{N_M} \delta(\mathbf{r} - r_i^{(p)}), \quad (3)$$

where  $M$  is the total number of molecules in the system and  $N_M$  is the number of particles contained in a molecule.

The deviation  $\widehat{W}(\Gamma)$  from the reference state  $\widehat{H}_0(\Gamma)$  originates from the interactions between molecules. Here it is assumed that  $\widehat{W}(\Gamma)$  depends on  $\Gamma$  only through the particle density  $\widehat{\phi}(\mathbf{r}; \Gamma)$  as

$$\widehat{W}(\Gamma) = \widehat{W}(\widehat{\phi}(\mathbf{r}; \Gamma)). \quad (4)$$

Using the assumption in equation (4) and the property of  $\delta$  functional that obeys

$$\int D\{f(\mathbf{r})\} \delta[f(\mathbf{r}) - g(\mathbf{r})] F[g(\mathbf{r})] = F[f(\mathbf{r})], \quad (5)$$

the partition function in equation (2) can be rewritten as

$$Z = \frac{1}{M!} \int d\Gamma \int D\{\varphi(\mathbf{r})\} \delta[\varphi(\mathbf{r}) - \widehat{\phi}(\mathbf{r}; \Gamma)] \\ \times \exp\{-\beta[\widehat{H}_0(\Gamma) - \widehat{W}(\varphi(\mathbf{r}))]\}. \quad (6)$$

Using the Fourier representation of the delta functional, one obtains

$$\delta[\varphi(\mathbf{r}) - \hat{\phi}(\mathbf{r}; \Gamma)] = \int D\{w(\mathbf{r})\} \times \exp \left[ i \int w(\mathbf{r}) (\varphi(\mathbf{r}) - \hat{\phi}(\mathbf{r}; \Gamma)) d\mathbf{r} \right]. \quad (7)$$

Inserting equation (7) into equation (6) leads to

$$Z = \frac{1}{M!} \int d\Gamma \int D\{\varphi(\mathbf{r})\} \int D\{w(\mathbf{r})\} \times \exp \left[ i \int w(\mathbf{r}) (\varphi(\mathbf{r}) - \hat{\phi}(\mathbf{r}; \Gamma)) d\mathbf{r} \right] \times \exp \{ -\beta [\hat{H}_0(\Gamma) - \hat{W}(\varphi(\mathbf{r}))] \}. \quad (8)$$

At this point the partition function  $z$  of a system made of a single molecule in an external potential  $V(\mathbf{r}) = i/\beta(w(\mathbf{r}))$  is defined

$$z[V(\mathbf{r})] = \int d\Gamma \exp \left\{ -\beta \left[ \hat{H}_0(\Gamma) + \int \hat{\phi}(\mathbf{r}; \Gamma) V(\mathbf{r}) d\mathbf{r} \right] \right\}. \quad (9)$$

Using the equation (9) and rearranging equation (8) one obtains

$$Z = \frac{1}{M!} \int d\Gamma \int D\{w(\mathbf{r})\} \exp \left\{ -\beta \left[ -\frac{1}{\beta} \ln z + W(\varphi(\mathbf{r})) \right] \right\} - \int V(\mathbf{r}) \varphi(\mathbf{r}) d\mathbf{r} \right\}. \quad (10)$$

In terms of this partition function, the mean field approximation is obtained by replacing the sum over the canonical ensemble in equation (10) with a Gaussian integral around the most probable state that minimizes the argument of the exponential function on the right side of equation (10). The condition for the determination of the most probable state is given using functional derivatives:

$$\begin{cases} \frac{\delta}{\delta\phi(\mathbf{r})} \left\{ -\beta \left[ -\frac{1}{\beta} \ln z + W(\phi(\mathbf{r})) - \int V(\mathbf{r}) \phi(\mathbf{r}) d\mathbf{r} \right] \right\} = 0 \\ \frac{\delta}{\delta V(\mathbf{r})} \left\{ -\beta \left[ -\frac{1}{\beta} \ln z + W(\phi(\mathbf{r})) - \int V(\mathbf{r}) \phi(\mathbf{r}) d\mathbf{r} \right] \right\} = 0 \end{cases} \quad (11)$$

This leads to

$$\begin{cases} V(\mathbf{r}) = \frac{\delta W[\phi]}{\delta\phi(\mathbf{r})} \\ \phi(\mathbf{r}) = -\frac{1}{\beta z} \frac{\delta z}{\delta V(\mathbf{r})} = \langle \hat{\phi}(\mathbf{r}; \Gamma) \rangle = \phi(\mathbf{r}). \end{cases} \quad (12)$$

According to the derivation given above, it is possible to obtain an expression for a density dependent external potential acting on each molecule. If one assumes a multicomponent system, where each component is specified by an index  $K$ , then the interaction term  $W$  takes the following form:

$$W[\{\phi_K(\mathbf{r})\}] = \int d\mathbf{r} \left[ \frac{k_B T}{2} \sum_{KK'} \chi_{KK'} \phi_K(\mathbf{r}) \phi_{K'}(\mathbf{r}) + \frac{1}{2\kappa} \left( \sum_K \phi_K(\mathbf{r}) - 1 \right)^2 \right], \quad (13)$$

where the second addend of the integrand of equation (13) is the relaxed incompressibility condition and  $\kappa$  is the compressibility that is assumed to be sufficiently small.

The corresponding mean field potential can be given by

$$V_K(\mathbf{r}) = \frac{\delta W[\{\phi_K(\mathbf{r})\}]}{\delta \phi_K(\mathbf{r})} = k_B T \sum_{K'} \chi_{KK'} \phi_{K'}(\mathbf{r}) + \frac{1}{\kappa} \left( \sum_K \phi_K(\mathbf{r}) - 1 \right). \quad (14)$$

In the case of a mixture of two components A and B, the mean field potential acting on a particle of type A at position  $\mathbf{r}$  is given by

$$V_A(\mathbf{r}) = k_B T [\chi_{AA} \phi_A(\mathbf{r}) + \chi_{AB} \phi_B(\mathbf{r})] + \frac{1}{\kappa} (\phi_A(\mathbf{r}) + \phi_B(\mathbf{r}) - 1). \quad (15)$$

The potential acting on particle B can be derived in a similar way. Then the force acting on a particle A at position  $\mathbf{r}$ , due to interaction with density field is

$$F_A(\mathbf{r}) = -\frac{\partial V_A(\mathbf{r})}{\partial \mathbf{r}} = -k_B T \left( \chi_{AA} \frac{\partial \phi_A(\mathbf{r})}{\partial \mathbf{r}} + \chi_{AB} \frac{\partial \phi_B(\mathbf{r})}{\partial \mathbf{r}} \right) - \frac{1}{\kappa} \left( \frac{\partial \phi_A(\mathbf{r})}{\partial \mathbf{r}} + \frac{\partial \phi_B(\mathbf{r})}{\partial \mathbf{r}} \right). \quad (16)$$

## 2.2 Implementation Scheme

As reported in the works of Milano and Kawakatsu<sup>5,6</sup> a description of the implementation scheme is given here. What is needed in order to connect particle and field models is a scheme to obtain a smooth coarse-grained density function  $\phi(\mathbf{r})$  directly from the particle positions  $\Gamma$ .

This can be expressed as

$$\bar{S}\{\hat{\phi}(\mathbf{r}; \Gamma)\} = \phi(\mathbf{r}) \quad (17)$$

where  $\bar{S}$  indicates the mapping from the particle positions to the coarse-grained density. The iteration scheme used in the hybrid PF-MD approach is summarized in figure 1. The starting value of the density dependent mean field potential is obtained from the initial configuration of the system (at time  $t_0$ ). The potential energy is given

by the sum of the intramolecular interaction potentials (bond, angles) and the density dependent mean field potential. A new configuration is obtained by integrating the equation of motion of the particles from time  $t_0$  to time  $t_0 + \Delta t$ . At each predefined density update time ( $\Delta t_{\text{update}}$ ) the density is updated according to the updated positions of the particles in the simulation box. From the updated value of the density, a new value of the potential energy is calculated and then new forces are obtained.

The density field is obtained by mapping particle positions on a mesh, thus dividing the simulation box in cells. Then, according to the positions of each particle inside a cell, a fraction of particle is assigned to each vertex of the cell. This procedure is schematized in figure 2. The density and its derivatives used for the calculation of the forces and the potential energy due to particle-field interactions are both defined on three-dimensional lattice points obeying the periodic boundary conditions.

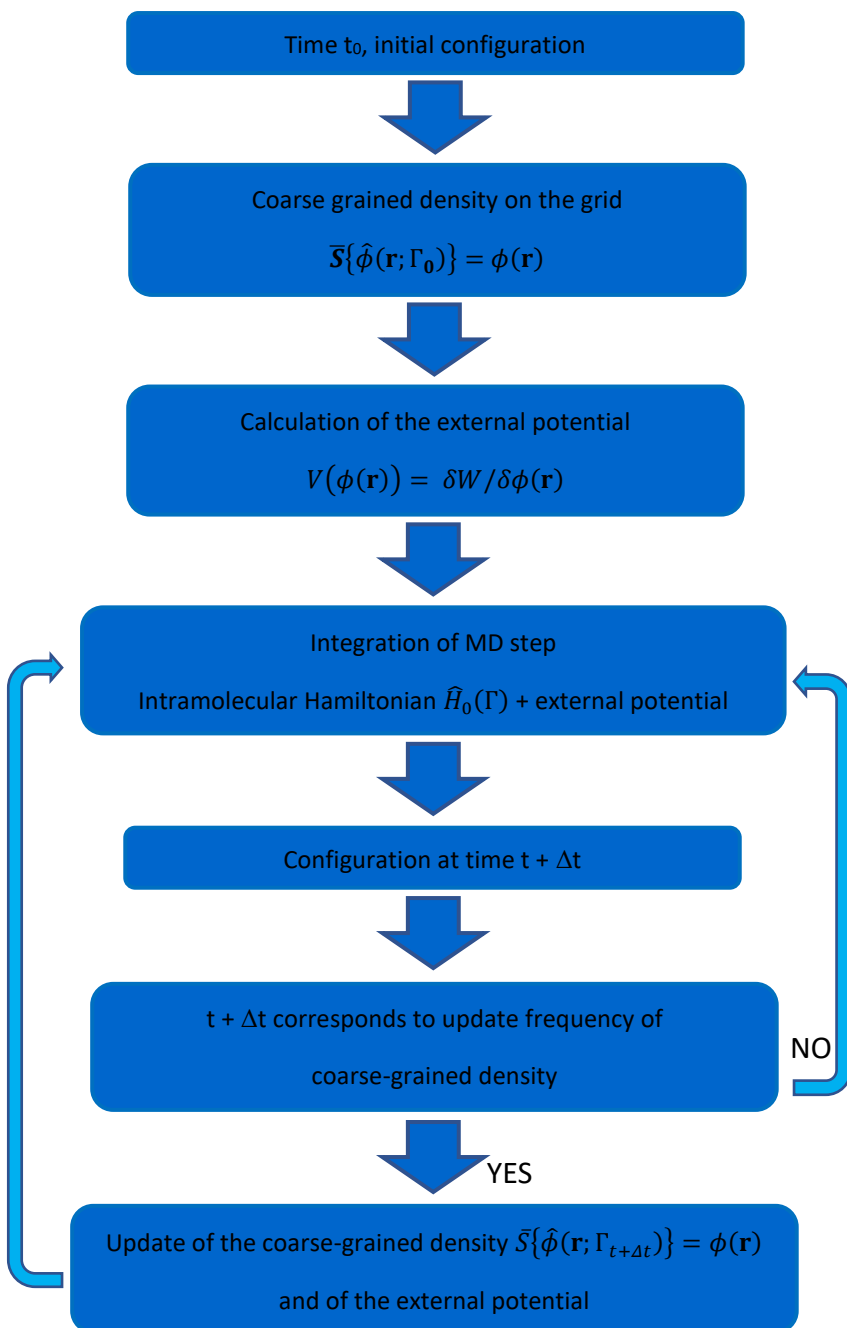


**Figure 1:** Iteration scheme for the hybrid PF-MD simulations

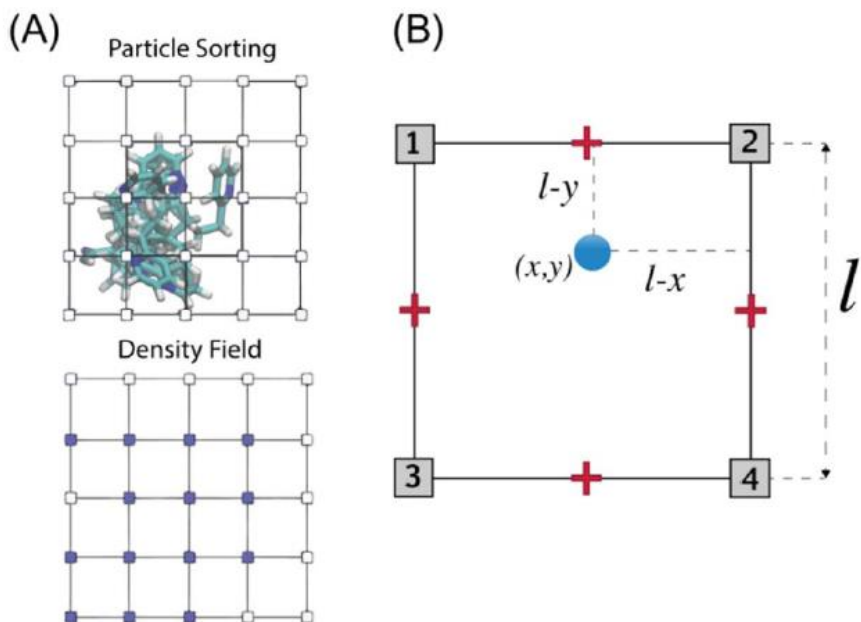


**Figure 2:** (A) Example, using a two-dimensional system, of the assignment of the coarse-grained density to lattice points (for a polymer chain). (B) Criterion for the assignment of a particle fraction to lattice points. The squares indicate the lattice points where the density is defined. The density gradients, used to calculate forces, are defined at the center of each edge (red crosses).

As depicted in figure 2B the fraction of particle assigned to a lattice point, is proportional to the area of the rectangles. In particular, in figure 2B, a fraction of particle proportional to the area  $(l-y \times l-x)$  is assigned to point 3. The grid size  $l$  is an important spatial parameter since it describes the extent to which the density is spread over the lattice points. Once the coarse-grained density has been calculated from particle positions, the spatial derivatives of the density field are evaluated. Spatial derivatives can be obtained by differentiation of

the density lattice. Then, the potential energy and forces acting on particles in the system, can be calculated using values obtained from the interpolation of the density and its spatial derivatives in equations 15 and 16.

### References:

- (1) A. De Nicola, T. Kawakatsu, G. Milano, *J. Chem. Theory Comput.* **2014**, *10*, 5651.
- (2) A. De Nicola, A. Correa, G. Milano, P. La Manna, P. Musto, G. Mensitieri, G. S. Scherillo, *J. Phys. Chem. B* **2017**, *121*, 3162.
- (3) A. De Nicola, T. Kawakatsu, C. Rosano, M. Celino, M. Rocco, G. Milano, *J. Chem. Theory Comput.* **2015**, *11*, 4959.
- (4) A. De Nicola, T. Kawakatsu, G. Milano, *Macromol. Chem. Phys* **2013**, *214*, 1940.
- (5) G. Milano, T. Kawakatsu, *J. Chem. Phys.* **2009**, *130*, 214106.
- (6) G. Milano, T. Kawakatsu, *J. Chem. Phys.* **2010**, *133*, 214102.

---

## Carbon Black

---

### *3.1 Overview*

Carbon black (CB) is a generic term for an important family of industrial products involving thermal, furnace, channel and acetylene blacks (based on the specific production process).<sup>1</sup> It essentially consists of elemental carbon in the form of almost spherical nanoparticles coalesced into aggregates and then aggregates make up bigger structures called agglomerates. Carbon black is obtained by the partial combustion or thermal decomposition of hydrocarbons,<sup>1</sup> and based on the specific manufacturing process, materials with different morphologies as well as nanoparticle dimensions can be obtained.

Carbon black produced with the furnace process, which is the most commonly used method nowadays, is called “furnace black”, distinguishing it from other types of carbon black manufactured with other processes. Below a list of the most important methods of production is given<sup>1</sup>.

#### **- Furnace Black Process**

In this process, carbon black is produced by blowing petroleum oil or coal oil into high-temperature gases to combust them partially. This method is the most suitable for mass production of CB since it gives

high yield and allows wide control over its properties, mainly particle size and structure. This is currently the most common method used for manufacturing carbon black.

#### **- Channel Process**

In this case, carbon black is produced by bringing partially combusted fuel, which is generated with natural gas as raw material, into contact with channel steel and then collecting the product. This method gives carbon black with several functional groups on the surface, and thus can be used in some painting applications.

#### **- Acetylene Black Process**

As the name suggests, this process gives carbon black by thermally decomposing acetylene gas. It provides carbon black with higher structures and higher crystallinity.

#### **- Lampblack Process**

This method obtains carbon black by collecting soot from fumes deriving by burning oils or pine wood. This method however is not suitable for mass production, but its products can be used as raw material for ink sticks as it provides carbon black with specific color. Carbon black is the most widely used nanomaterial, as a filler, in a wide variety of polymeric materials. Most commonly CB is employed as a filler in rubbers for the tyre industry since it greatly enhances the mechanical properties of the compounds. Due to its high tinting strength and thermal stability it is suitable for coloring resins and films that are heat-formed. Moreover CB is excellent for absorbing

ultraviolet light. Resins with carbon black are used in automobile bumpers, wire coverings and steel pipe linings.

Carbon black particles can also provide good electrical conductivity and therefore it is widely used as conductive filler in plastics, elastomer, paints, adhesives, films, and pastes, for applications where antistatic properties are needed.

### *3.2 Morphology and Structure*

At the nanoscale level carbon black is made of almost spherical nanoparticles, named primary particles or nodules. These nanoparticles, whose diameter is in the range 20 – 200 nm,<sup>1</sup> are composed of many graphite-like units. In particular, within a primary particle, there are two regions: an amorphous core, composed of smaller graphitic units distributed in a random order, and a graphitized shell, made of larger graphitic units stacked in a turbostratic order.<sup>1</sup> Several nanoparticles coalesced together form an aggregate, which is the primary dispersable unit, and in turn these aggregates tend to form bigger structures known as agglomerates. The structure of carbon black is schematically shown in figure 3.<sup>2</sup>

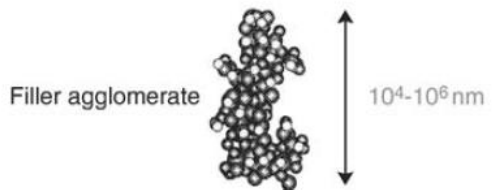
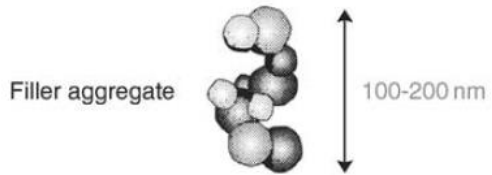
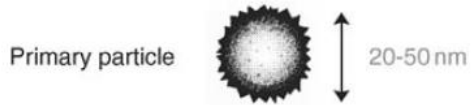
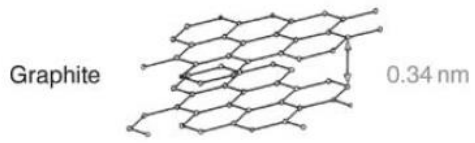


**Figure 3:** Structure of carbon black

### *3.3 Molecular Models of Carbon Black*

Although carbon black structure and composition is widely characterized experimentally, through a series of different techniques, such as X-ray diffraction (XRD), electron microscopy, gas adsorption,<sup>1</sup> there are very few computational models available in the literature. Generally, in MD simulations, carbon black is treated as a graphitic surface, for example in simulations of molecules adsorption, such as water,<sup>3</sup> methanol and ethanol,<sup>4</sup> or to investigate the effect of surface modification on the stability of CB dispersion in water.<sup>5</sup> However, representing CB as graphitic surface, is still an approximation, since, in the reality, it is made of spherical (or quasi-spherical) NP, and indeed the shape<sup>6</sup> and curvature<sup>7</sup> of a filler substrate can influence structural and dynamical properties of the surrounding polymer. The only detailed model of CB nanoparticle is the one reported by Ban et al.<sup>8</sup> in which a simulation protocol has been developed to generate all-atom NP with a core-shell structure, reproducing accurately XRD patterns and densities. However this model, being all-atom one, contains already a huge number of particles and this makes it not suitable for MD simulations of CB nanoparticles in polymer melts on the timescale of  $\mu\text{s}$  and for high  $M_w$  polymer chains, since it would require a prohibitive computational cost.

For this reason, we have developed a coarse-grained (CG) model of CB nanoparticle, able to reproduce its experimental density and morphological features.

This CB primary particle model contains a considerably lower number of particles (30102 beads) respect to the all-atom one of Ban et. al (~500000 beads), thus making possible the simulation of large polymer / NP systems. The detailed procedure we set up and employed to generate the NP is described in chapter 4.

## References:

- (1) J. B. Donnet, *Carbon Black*, CRC Press, **1993**.
- (2) T. A. Vilgis, G. Heinrich, M. Klüppel, *Reinforcement of Polymer Nano-composites*, Cambridge University Press, **2009**.
- (3) G. R. Birkett, D. D. Do., *J. Phys. Chem.* **2007**, *111*, 5735.
- (4) G. R. Birkett, D. D. Do., *Mol. Simul.* **2006**, *32*, 887.
- (5) S. Dong, J. Yan, N. Xu, J. Xu, H. Wang, *Surf. Sci.* **2011**, *605* (9–10), 868.
- (6) S. T. Knauert, J. F. Douglas, F. W. Starr, *J. Polym. Sci. Part B Polym. Phys.* **2007**, *45*, 1882.
- (7) H. Eslami, M. Rahimi, F. Müller-Plathe, *Macromolecules* **2013**, *46*, 8680.
- (8) S. Ban, K. Malek, C. Huang, Z. Liu, *Carbon*, **2011**, *49*, 3362.

---

## Multiscale Modeling of CB/PE Interfaces

---

CB-filled polymer composites have attracted significant scientific and industrial interest for many years because they possess improved mechanical, thermal, and electrical properties<sup>1,2,3</sup>.

The mechanical and electrical properties of these composites are strongly affected by the CB particle morphology and dispersion. In CB, primary particles are held together by weak forces (dispersion and/or electrostatic interactions), which, during melt mixing, compounding or other processing technique, within a polymeric matrix, prevent an easy break-up of the CB aggregates. In principle the dispersion qualities can be improved by chemically modifying (i.e. grafting or crosslinking) the filler, but functionalization, however, involves further steps in the production process of the final composite material.

Therefore, a better understanding of the factors that influence the dispersion of bare CB in polymers, such as filler wettability, is necessary, and answers can come from the study of the underlying molecular-level phenomena that take place at the CB/polymer interface.

The aim of the work presented in this thesis, as already reported in the introduction, is to perform PF-MD simulations, of systems containing CB nanoparticles embedded in mono or bidisperse polyethylene melts of varying  $M_w$ . Up to date, there are no computational studies of this type available in the literature. Here we address this task following a multiscale approach, that is summarized below, and described in detail in the following sections:

**I)** Choice of a suitable force-field for polyethylene and testing of its performance through the reproduction of target structural properties.

**II)** Starting from atomistic simulations of polyethylene/graphite interface, we derived a density profile of the polymer phase, respect to the graphitic surface.

**III)** Choice of a mapping scheme for the polymer chains, and the graphitic surface. All the bonded interactions in the CG polymer model have been obtained from reference atomistic simulations. Subsequently, simulations of a model CG system have been used to parametrize polymer/graphite interaction (within the PF-MD framework), in the CG representation, through matching of all-atom and CG polymer density profiles.

**IV)** A model of CB primary particle has been developed by using a well-defined procedure. The validity of the model has been assessed through the comparison of the calculated NP morphology and density with the experimental ones

V) Simulations of CG systems containing high  $M_w$  polymer melts in contact with either CG graphite surface and CB NP, in order to obtain structural and dynamical properties of the chains in the polymer phase.

## *4.1 All-atom Simulations of PE and PE/Graphite*

### *4.1.1 Atomistic Model of PE*

The parameters used to perform all-atom simulations of PE homopolymer and PE in contact with graphite, were taken from the L-OPLS force-field<sup>4</sup>, which is a version of the OPLS-AA<sup>5</sup> force field optimized specifically for long chain hydrocarbons, and it has been already applied successfully in other works.<sup>6,7,8</sup> A schematic picture of the PE chemical structure together with the atom types and charges scheme is reported in Figure 5. In particular, terminal carbons and hydrogens are labeled as  $C_T$  and  $H_T$  respectively, while backbone carbons and hydrogens are denoted as  $C_2$  and  $H_2$ .

All the other bonded (bond, angle, dihedral) and non-bonded (LJ) parameters, can be found in Ref.<sup>4</sup>

Parameters used to describe graphene layers in the graphitic structure were instead taken from the standard OPLS-AA force -field.

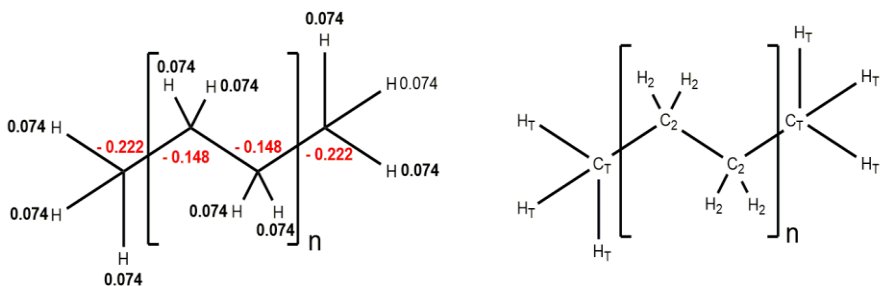


**Figure 5.** Polyethylene (PE) monomer structure with partial charges scheme (left) and atom types (right)

#### 4.1.2 Simulation Details

All the systems simulated, were first pre-equilibrated using PF-MD, implemented in the OCCAM software<sup>9</sup>, in order to remove unphysical atom overlaps, using a procedure similar to the ones already applied to equilibrate other polymer melt systems.<sup>10</sup> In particular two subsequent runs, with decreasing grid sizes, from  $l = 0.4 \text{ nm}$  to  $l = 0.2 \text{ nm}$ , were performed. The resulting configurations were then energy minimized, after the reintroduction of short-range correlations (Lennard-Jones and Coulombic interactions), which are not treated explicitly with the PF-MD method. Subsequently standard MD simulations were executed, first in the *NVT* (for 5 ns) and then in the *NPT* ensemble, using GROMACS software.<sup>11</sup> Table 1 contains information on systems composition for the runs performed in the *NPT* ensemble.

**Table 1.** Composition of the systems and simulation details, for the standard MD simulations in the NPT ensemble.

<b>System</b>	<b>No. of PE Chains</b>	<b>No. of Monomers in PE chains</b>	<b>Tot. No. Particles</b>	<b>Box size [nm] (x,y,z)</b>	<b>Time (ns)</b>	<b>T (K)</b>
PE melt	191	20	23302	6.276 5.599 5.793	100	293
PE melt	191	20	23302	6.815 6.500 6.291	180	550
PE melt	40	1072	257360	14.120 14.120 14.120	140	423
PE/Graphite	388	20	59342	5.880 6.542 15.550	240	550

For all the simulations in the *NVT* and *NPT* ensemble, the temperature was kept fixed by means of a velocity rescale algorithm<sup>12</sup> with a coupling constant  $\tau_T = 0.02$  ps. In the *NPT* runs the pressure was held constant at 1.013 bar using the Berendsen algorithm<sup>13</sup> with a coupling constant  $\tau_P = 0.2$  ps. A time step of 2 fs was employed in all simulations. A cutoff distance of 1.1 nm was used for both van der Waals and Coulomb interactions. The non-bonded interactions were excluded between first and third neighbors. The LINCS constraint algorithm<sup>14</sup> was employed to fix all the carbon-hydrogen distances.

### 4.1.3 Force-field testing: Calculated vs Experimental Properties

The L-OPLS force field we have chosen to perform our all-atom simulations, is able to correctly reproduce several experimental properties (density, heat of vaporization, viscosities)<sup>4</sup> for a several types of hydrocarbons. However, since there was no report on the performance of this force-field for C<sub>40</sub>H<sub>82</sub> chains (PE with 20 repeating units), we decided to calculate structural properties, mainly mass density and X-ray diffraction pattern, and compare them with experimental data available. In particular, the computed mass density for C<sub>40</sub>H<sub>82</sub>, at 298 K, is 0.820 g/cm<sup>3</sup> while the experimental one is 0.817 g/cm<sup>3</sup>,<sup>15</sup> resulting in an error of less then 1 %, thus indicating a very accurate reproduction of this property.

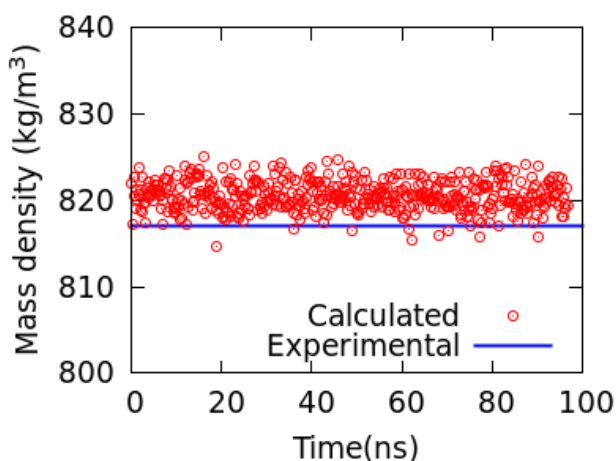


**Figure 6.** Behavior of the calculated mass density over time (red circles) and experimental mass density (blue line).

The comparison of calculated and experimental<sup>16</sup> X-ray diffraction pattern is reported in figure 7. In particular, we observe a good reproduction of the main peak relative to the amorphous phase of PE. For clarity, here we report also the whole experimental diffraction pattern of a PE sample<sup>16</sup> (figure 8), which contains other peaks relative to the crystalline phase. These peaks are not present in the calculated X-ray spectrum, since the L-OPLS force field is not able to reproduce crystalline phases of PE. However, since our simulations are performed in the melt state, at temperatures above the melting point of PE, this does not constitute an issue for our purposes.

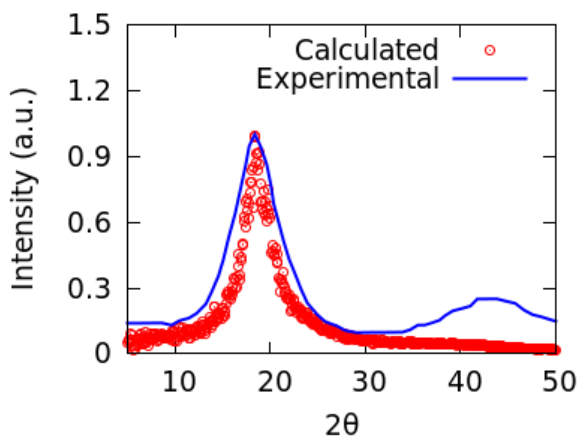


**Figure 7.** Calculated (red circles) and experimental (blue line) X-ray diffraction patterns at 300 K. The intensity has been normalized with respect to the highest peak.

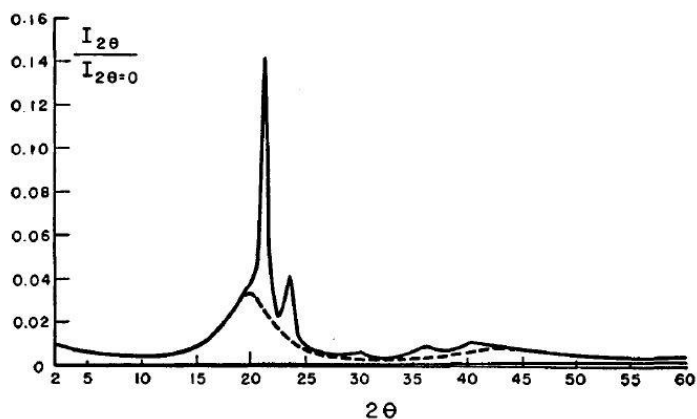


**Figure 8.** Experimental diffraction pattern of PE sample at 300 K.

Overall the L-OPLS force field results in very good reproduction of structural properties of the  $C_{40}H_{82}$  chains, and thus it can be used for the parametrization of the CG model of PE.

#### 4.1.4 Atomistic Model of PE/Graphite System

At the all-atom level, we modeled the CB surface as a semi-infinite graphitic structure (as depicted in figure 9). The simulation box was orthorombic, and periodic boundary conditions were applied. Eight graphene layers were used to represent the graphitic structure.

Simulation details are reported in table 1, for the production run in the *NPT* ensemble. The simulation setup employed is the same as the one reported in section 4.1.2. Also in this case a relaxation procedure has been applied to the system, using the PF-MD method with a grid

size  $l = 0.2 \text{ nm}$ , in order to get a well relaxed initial all-atom configuration.

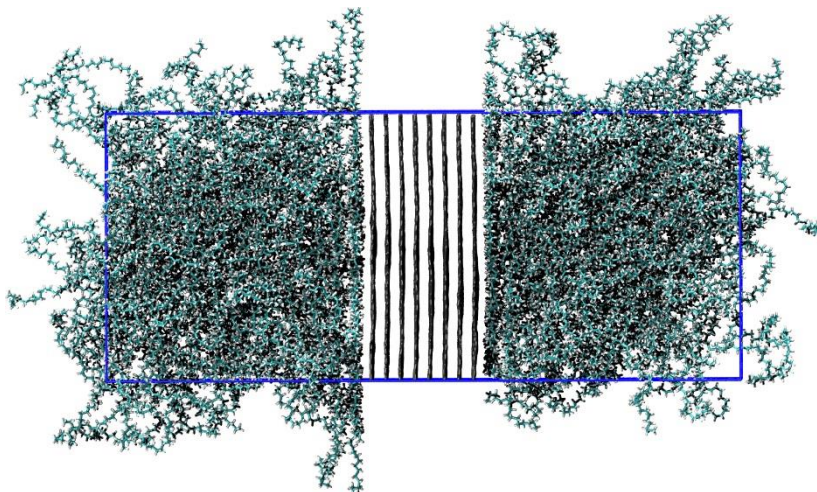


**Figure 9.** Snapshot of the polyethylene/graphite system. 8 graphene layers were used to represent CB surface.

The organization of the polymer chains respect to the graphite surface, was analyzed by dividing the system into bins separated by planes parallel to the solid surface, having width of  $1 \text{ \AA}$ , and computing the value of the mass density in each bin. This gives a polymer density profile, along the direction normal to the graphite plane, as reported in the plot of figure 10. The mass density profile of the graphite is also showed. Values were obtained averaging over the last  $40 \text{ ns}$  of the simulation, when the system has already reached an equilibrium condition.

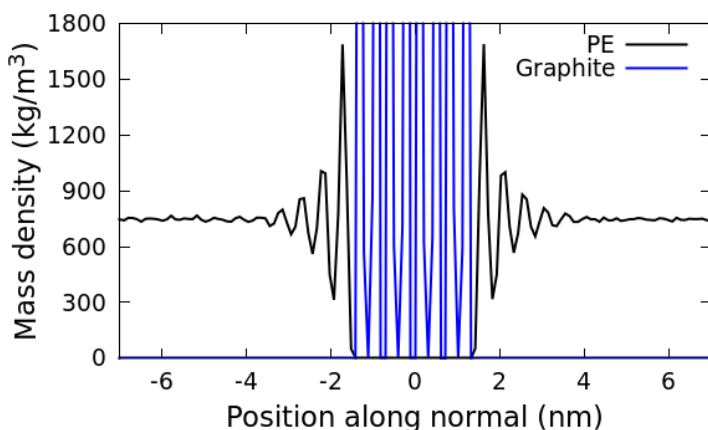


**Figure 10.** Mass density profile of PE and graphite. The profile has been calculated along the direction normal to the graphite surface.

In proximity of the graphite, the density profile attains its highest value, then exhibits a characteristic oscillatory behavior wherein other three peaks can be observed, at distances equal to 2.1, 2.6, and 3.1 *nm* from the graphite plane. Similar density profiles with the characteristic oscillatory features have been also reported in previous simulations of polymer/graphite interfaces.<sup>17,18,19</sup> At distances beyond 4 *nm* from graphite, the density attains a constant value equal (720  $kg/m^3$ ), which is close to the value of the pure PE melt (690  $kg/m^3$ )<sup>18,20</sup>, at the same temperature (550 K). The density profile we obtained from this simulation, has been used for the parametrization of the interaction between PE and graphitic surface in the CG representation, which will be described in the following section.

## *4.2 CG Models of PE and Graphitic Structures*

Coarse graining methods involve the reduction of the number of degrees of freedom in a system, retaining only those that are relevant for a particular range of interest. In practice this is achieved by grouping several atoms into pseudoatoms, or beads, and determining the interaction potential among beads. In particular, since for entangled polymer melts the longest relaxation time scales at least as  $N^3$  (where  $N$  is the number of atoms in the system)<sup>10,21</sup>, use of CG models becomes necessary when simulating systems of long polymer chains, where several orders of magnitude (from the scale of chemical bond, to that of the radius of gyration), are involved. In addition, with CG models, a smoother free-energy landscape is created, compared to fully atomistic simulations. The main consequence that arises from this representation is that faster dynamics are obtained respect to the fully atomistic model, and this allows to probe longer time and length scales in simulations. With this in mind, we developed a coarse-grained model for both polyethylene chains and for units in the carbon black nanoparticle and graphite surface. In the following sections, the mapping schemes and the parametrization of the interactions of the CG model we established are described in detail.

### 4.2.1 Mapping Scheme: Graphite and PE

The mapping scheme was first chosen for the CG model of graphite.

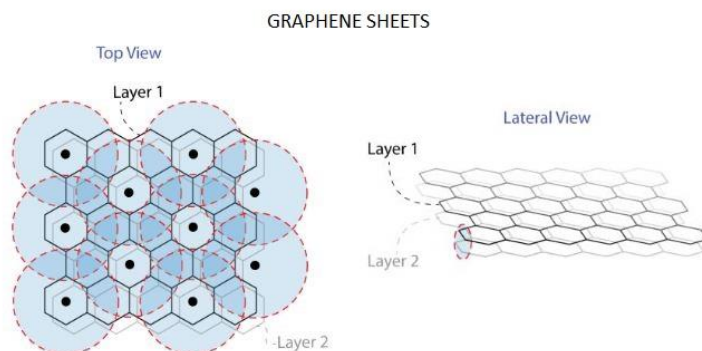


**Figure 11.** Mapping scheme used for the graphene sheets. CG beads are reported in light blue, with their center of mass represented by black dots. The underlying all-atom structure (aromatic carbons) is also reported. Each CG bead maps on 11 carbon atoms.

Considering that the equilibrium distance of carbon-carbon bonds in aromatic rings of a graphene sheet is  $1.42 \text{ \AA}$  (from the OPLS-AA<sup>5</sup> force field), then using the mapping scheme reported in figure 11, the bead diameter (or alternatively the distance between two beads centers of mass) is  $0.73 \text{ nm}$ . In this way each CG layer maps two all-atom graphene sheets (as can be observed from figure 11). Once established the coarse-grained model of graphene sheets, then the starting point to build the mapping scheme of polyethylene, is that

the mean distance between beads within a polymeric chain should be the same as that in the beads of graphite, in order to have comparable length scales. To make the best choice among several mapping schemes, the first step was the generation of CG simulation trajectory derived from the fully atomistic ones. Then distributions for bond lengths  $P(r)$  and angles  $P(\theta)$  for mapped CG representations were calculated. The resulting distributions were used to derive CG bond and angle potentials. The most suitable mapping scheme was obtained by placing the center of mass of CG beads each four monomers within a polyethylene chain (figure 12).

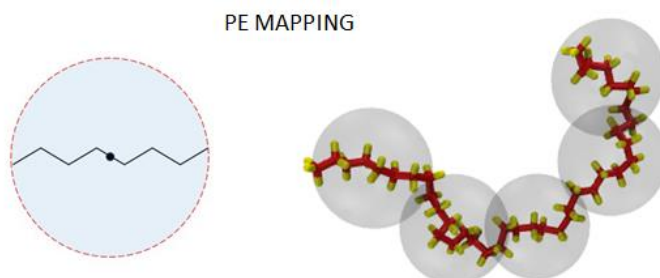


**Figure 12.** CG mapping of PE: one CG bead (left) and 20 monomers chain (right). Each CG bead corresponds to 8 carbon atoms.

In particular, a distribution of bond lengths centered around 0.715  $nm$  was obtained, as reported in figure 13, and thus the bead dimension is almost the same as in the case of graphene sheets (0.73  $nm$ )

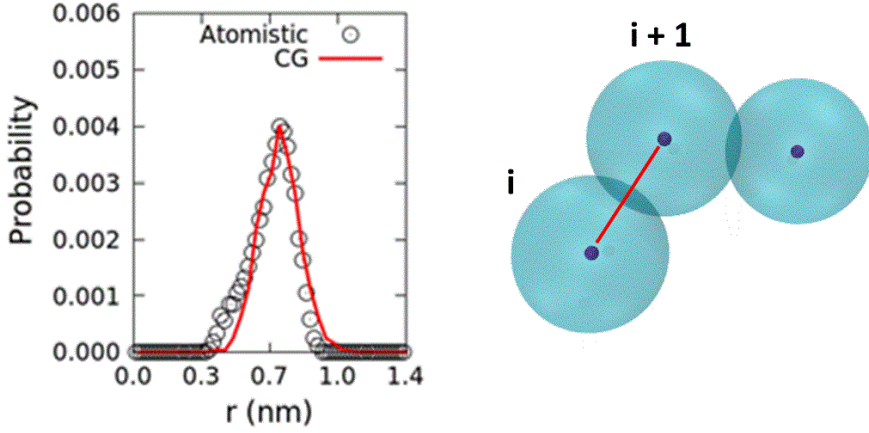


**Figure 13.** Bond length distribution between two consecutive CG beads  $i$  and  $i+1$

This distribution was then used to derive CG bond potential. The initial guess potential is given by:

$$V_{bond}(r) = k_B T \ln(P(r)/r^2) \quad (18)$$

Where  $k_B = 1.380649 \times 10^{-23} \frac{J}{K}$  is the Boltzmann constant, and  $T$  is the temperature in Kelvin.

The bond is described by a harmonic bond potential (Eq. 19)

$$V_{bond}(\mathbf{r}_{ij}) = \frac{1}{2} K_{bond} (\mathbf{r}_{ij} - \mathbf{r}_{ij}^0)^2 \quad (19)$$

Where  $K_{bond}$  is the bond constant and  $\mathbf{r}_{ij}^0$  is the equilibrium bond length. Starting from the value of the initial guess potential,  $K_{bond}$

and  $\mathbf{r}_{ij}^0$  are obtained by varying them until the resulting bond length distribution matches the reference one from the mapped atomistic trajectory.

Once optimized the harmonic bond potential parameters, the harmonic angle bending potential is calculated. As for the case of the bonds, the initial guess potential is given by:

$$V_{angle}(r) = k_B T \ln(P(\theta)/\sin \theta) \quad (20)$$

In this case the angle potential depends on the cosine of the angle  $\Theta$  (Eq. 21):

$$V_{angle}(\theta_{ijk}) = \frac{1}{2} K_{angle} (\theta_{ijk} - \theta_{ijk}^0)^2 \quad (21)$$

Where  $K_{angle}$  is the bond constant and  $\theta_{ijk}^0$  is the equilibrium bond length. Also in this case  $K_{angle}$  and  $\theta_{ijk}^0$  are varied until matching of the reference distribution (figure 14). The final set of parameters for bond and angle potentials is summarized in the table 2.

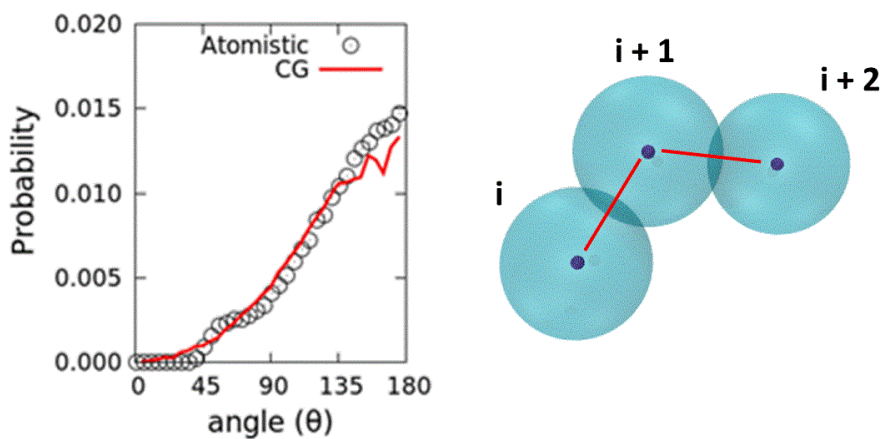


**Figure 14.** Angle bending distribution between three consecutive CG beads  $i$ ,  $i+1$  and  $i+2$

**Table 2.** Equilibrium value of harmonic bond and angle potential, for CG model of PE. Bead type is C.

<b>Bond</b>	$K_{bond}$ (kJ mol <sup>-1</sup> nm <sup>-2</sup> )	$r_{ij}^0$ (nm)
C-C	400	0.715

<b>Angle</b>	$K_{angle}$ (kJ mol <sup>-1</sup> rad <sup>-2</sup> )	$\theta_{ijk}^0$ (deg)
C-C-C	7.5	165.00

### 4.2.2 Simulations of CG PE Chains

To test the validity of the CG model of PE, gyration radii were calculated from *NVT* simulations, using the PF-MD method, and compared with the experimental ones obtained from small-angle neutron scattering (SANS) measurements<sup>22</sup>. Four different systems with varying  $M_w$  of the PE chains were simulated. Details of the simulated systems are reported in table 3. The grid size in the PF-MD simulations was set to 0.73 nm (approximately one bond length in the CG model), and the timestep was 0.03 ps.

**Table 3.** Details of the PF-MD simulations of CG PE melts.

<b>System</b>	<b>No. of PE Chains</b>	<b>No. of Monomers in PE chains</b>	<b>Tot. No. Particles</b>	<b>Box size [nm] (x,y,z)</b>	<b>Time (<math>\mu</math>s)</b>	<b>T (K)</b>
PE melt	191	20	955	6.145 6.145 6.145	0.35	423 468
PE melt	1925	1072	515900	50 50 50	5.13	423 468
PE melt	350	5880	514500	50 50 50	18.5	423 468
PE melt	193	10696	516082	50 50 50	16.4	423 468

The plot of the Rg as function of PE M<sub>w</sub> is reported in figure 15, while their values are written in table 4.

**Table 4.** Values of calculated and experimental<sup>22</sup> Rg of CG PE melts, at T = 423 K

No. of monomers	Calculated Rg (nm)	Exp. Rg (nm)
20	0.81 ± 0.01	1.09
1072	7.91 ± 0.04	7.96
5880	17.95 ± 0.09	18.68
10696	21.82 ± 0.07	25.19

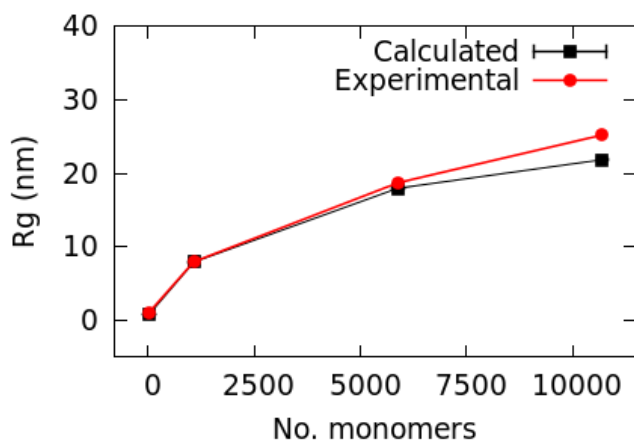


**Figure 15.** Plot of gyration radii obtained by PF-MD simulations of CG PE melts, as function of M<sub>w</sub>, compared with available data from SANS experiments.<sup>22</sup>

T = 423 K

From the plot figure 15 and the values reported in table 4, a good agreement between  $R_g$  calculated from CG simulations and experimental data is observed, for almost the whole range of molecular weights, thus confirming a good description of the structural properties of the CG model.

From the simulations of coarse-grained PE melt, we calculated also diffusion coefficients. This is an important quantity, since it allows to estimate a timescale for dynamical properties.<sup>21</sup> In particular, diffusion coefficients can be computed from the mean-squared displacements  $\Delta r^2$  of the chains center of mass through the Einstein relation:

$$D \approx \frac{1}{6} \frac{d}{dt} \langle \Delta r^2 \rangle \quad (22)$$

where the angle brackets denote an ensemble average over all the molecules in the system. Figure 16 shows the plot for the dependence of diffusion coefficients on the molecular weight, while computed and experimental values are reported in table 5.

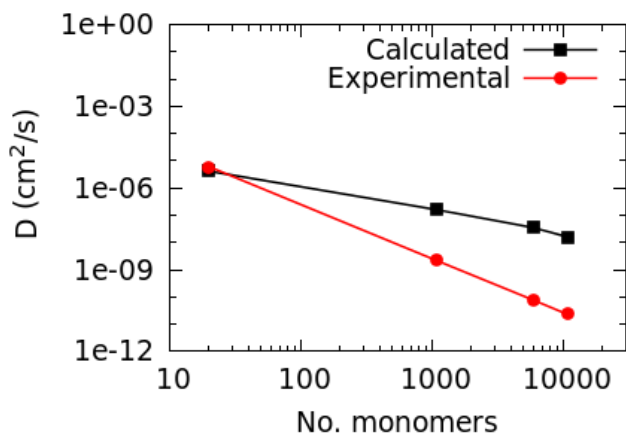


**Figure 16.** Dependence of the calculated and experimental<sup>23</sup> diffusion coefficients on the chain length.  $T = 468$  K.

**Table 5.** Values of calculated and experimental<sup>23</sup> diffusion coefficients of CG PE chains, at  $T = 468$  K

No. of monomers	$D_{\text{calculated}}$ ( $\text{cm}^2/\text{s}$ )	$D_{\text{experimental}}$ ( $\text{cm}^2/\text{s}$ )	$D_{\text{calculated}}/D_{\text{experimental}}$
20	$4.1 \times 10^{-6}$	$6 \times 10^{-6}$	0.68
1072	$1.6 \times 10^{-7}$	$2.2 \times 10^{-9}$	72
5880	$3.5 \times 10^{-8}$	$7.7 \times 10^{-11}$	450
10696	$1.6 \times 10^{-8}$	$2.3 \times 10^{-11}$	700

The values of calculated diffusion coefficients span from  $4.1 \cdot 10^{-6} \text{ cm}^2/\text{s}$ , for the lowest  $M_w$  (PE with 20 monomers), to  $1.6 \cdot 10^{-8} \text{ cm}^2/\text{s}$ , for the highest  $M_w$  (PE with 10696 monomers). The ratio of the calculated ( $D_{\text{calc}}$ ) to experimental ( $D_{\text{exp}}$ ) diffusion coefficients, varies between 0.68 and 700, thus showing that faster dynamics are achieved for the coarse-grained simulations with respect to the

experiments. Moreover, the increase in the value of the ratio  $D_{\text{calc}}/D_{\text{exp}}$  is related to the absence of entanglement effects in PF-MD simulations, as already reported in another work using this method.<sup>10</sup>

Another dynamical property that we calculated is the self-intermediate scattering function (SISF), which we used to estimate the scaling of dynamics between the coarse-grained and the all-atom model.

The SISF is defined as the spatial Fourier transform of the self Van Hove correlation function, which is the volumetric probability density of finding a particle  $i$  in the vicinity of some distance  $r$  from the origin, given that it was at the origin at time  $t = 0$ .<sup>24</sup> SISF can be expressed with the following equation:

$$F_s(q, t) = \frac{1}{N} \left\langle \sum_{j=0}^N e^{iq \cdot (r_j(t) - r_j(0))} \right\rangle \quad (23)$$

where  $N$  is the number of particles over which the function is computed,  $q$  is the scattering vector, and  $r_j$  is the position of the  $j$ -th particle.

In particular we calculated SISF for a melt of PE with chains of 1072 monomers, both at the all-atom level, using standard MD simulations, and at the coarse-grained level, using PF-MD simulations. The function was evaluated at two  $q$  values:  $8.6 \text{ nm}^{-1}$

(corresponding to the length of a single bond in the CG model) and at  $0.78 \text{ nm}^{-1}$  (corresponding to the  $R_g$  of the chains). The plot of the SISFs is reported in figure 17.

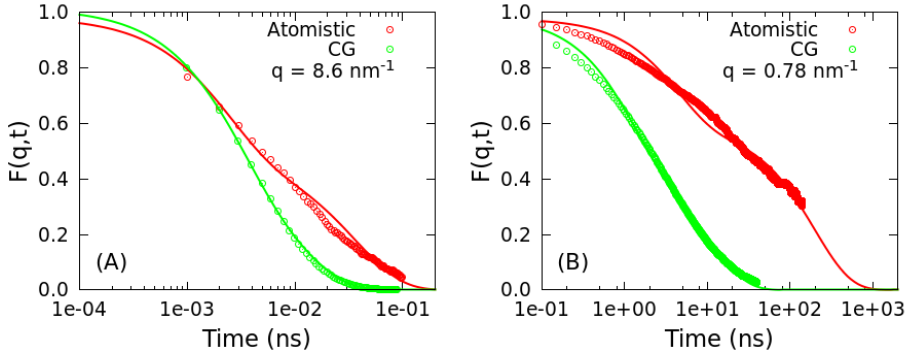


**Figure 17.** Self-intermediate scattering function  $F_s(q, t)$  of PE chains (1072 monomers). **A)**  $F_s(q, t)$  for all-atom (red circles) and CG (green circles) chains at  $q = 8.6 \text{ nm}^{-1}$ . **B)**  $F_s(q, t)$  for all-atom (red circles) and CG (green circles) chains at  $q = 0.78 \text{ nm}^{-1}$ . Solid lines are the fit represented by equation 24.

Relaxation times of the SISFs of figure 17, can be obtained using the following equation:

$$F_s(q, t) = (1 - A)e^{-(t/\tau_v)^{3/2}} + A e^{-(t/\tau_\alpha)^\beta} \quad (24)$$

where  $\tau_v$  is the short vibrational relaxation timescale and the  $t^{3/2}$  dependence, for the vibrational relaxation part, derives from a Gaussian approximation of  $F_s(q, t)$  with displacements intermediate between ballistic and Brownian motion.<sup>25</sup>

Fitted parameters using equation 24 are reported in table 6.

**Table 6.** Parameters and relaxation times from the fitting of SISF data with equation (4(12)) for PE chains (1072 monomers) at  $q = 8.6 \text{ nm}^{-1}$  and  $q = 0.78 \text{ nm}^{-1}$

System	$q \text{ (nm}^{-1}\text{)}$	A	$\tau_v \text{ (ns)}$	$\tau_\alpha \text{ (ns)}$	$\beta$
All-atom	8.6	0.627	0.002	0.036	0.732
		$\pm$ 0.002	$\pm$ /	$\pm$ 0.001	$\pm$ 0.020
CG	8.6	0.615	0.003	0.011	0.712
		$\pm$ 0.006	$\pm$ /	$\pm$ /	$\pm$ 0.005
All-atom	0.78	0.741	4.310	200	0.793
		$\pm$ 0.002	$\pm$ 0.050	$\pm$ 1	$\pm$ 0.002
CG	0.78	0.671	1.120	10.8	0.731
		$\pm$ 0.004	$\pm$ 0.010	$\pm$ 0.07	$\pm$ 0.003

From the comparison of both the short ( $\tau_v$ ) and long ( $\tau_\alpha$ ) relaxation times, between the atomistic and coarse-grained simulations, some differences can be observed. In particular, when  $q = 8.6 \text{ nm}^{-1}$ , since we are analyzing dynamics happening on small length scales ( $\sim 0.73 \text{ nm}$  in the real space) the relaxation times are quite similar in both models, with a slightly lower  $\tau_\alpha$  for the coarse-grained simulation. When  $q = 0.78 \text{ nm}^{-1}$ , the length scale we are probing is that of the  $R_g$  of the PE chains (with 1072 monomers), and thus the analysis is

performed on dynamics taking place on larger length scales. In this case the longest relaxation time  $\tau_\alpha$  for the coarse-grained model is more than one order of magnitude lower than the corresponding  $\tau_\alpha$  of the all-atom model. This result clearly confirms the efficiency of the coarse-grained model, since dynamic properties can be equilibrated in lower times, thus giving the possibility to perform simulations on large length and time scales, that could not be accessed with the all-atom model.

#### 4.2.3 CG Model of PE on Graphite

This section deals with the parametrization of the non-bonded interactions among polymer and graphite/carbon black units. Since this has been done within the PF-MD framework, we recall here the expression for the mean field potential acting on each particle in the system, already presented in chapter 2:

$$V_K(\mathbf{r}) = k_B T \sum_{K'} \chi_{KK'} \phi_{K'}(\mathbf{r}) + \frac{1}{\kappa} \left( \sum_K \phi_K(\mathbf{r}) - 1 \right) \quad (25)$$

In particular, the terms needed to perform the PF-MD simulations of polymer/graphite systems, are  $\chi_{KK'}$ , which describes the non-bonded interaction between particles of type  $KK'$ , (in this case

between polyethylene and graphite CG beads), and the compressibility  $\kappa$ .

The first step in the parametrization procedure was to generate a coarse-grained system of polyethylene and graphite with the same dimensions and number of chains as in the all-atom model presented in section 4.1.4, and using the mapping scheme showed in section 4.2.1. Details of the simulation are reported in table (7).

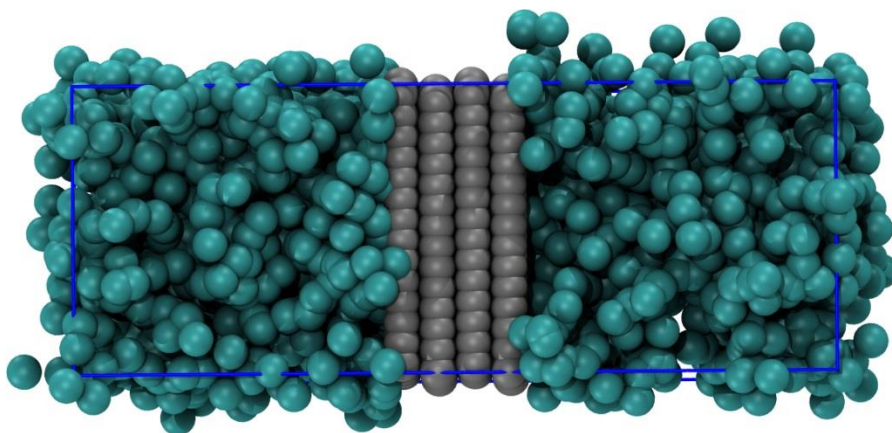


**Figure 18.** Snapshot of the coarse-grained polyethylene/graphite system. 4 graphene layers (which map the 8 layers in the all-atom system) were used to represent CB surface.

**Table 7.** Details of the PF-MD simulation of CG PE/graphite system

<b>System</b>	<b>No. of PE Chains</b>	<b>No. of Monomers in PE chains</b>	<b>Tot. No. Particles</b>	<b>Box size [nm] (x,y,z)</b>	<b>Time (<math>\mu</math>s)</b>	<b>T (K)</b>
PE	388	20	3024	5.886	0.6	550
+				6.575		
Graphite				15.550		

The property used to parametrize the non-bonded interaction parameters, in the PF-MD model, was the polymer density profile. In particular, the final set of parameters  $\chi_{KK'}$  and  $\kappa$  was obtained by varying them until the computed density profile, derived from the coarse-grained simulation, matched the profile derived from the atomistic reference simulation. Another important parameter, taken into account when performing the parametrization, was the grid size  $l$ , since it describes the extent to which the potential acting on particles is coarsened, and thus it directly affects the polymer structure and density throughout the system. In particular we found the best grid size value to be 0.73 nm.

Initially, the  $\chi_{KK'}$  interaction parameter, we used was the same between all the polymer/graphite beads in the system. However, this gave poor results since all the  $\chi_{KK'}$  values tested led to the unphysical situation in which the polymer chains crossed the graphitic layers. For this reason, we decided to employ two different pairs of

$\chi_{KK'}$  parameters, describing the interaction of the polymer with the inner and the outer graphene sheets respectively.

In particular a repulsive interaction was set for the polymer/inner layers interaction (positive value of  $\chi_{KK'}$ ), while for the polymer/outer layers an attractive interaction was specified (negative value of  $\chi_{KK'}$ ). This setup is depicted in figure 19.

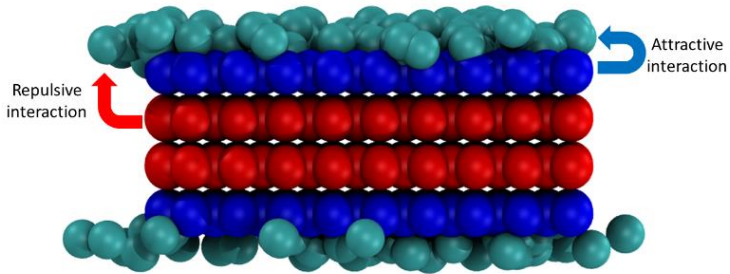


**Figure 19.** Schematic representation of the interaction between polymer (green beads) and repulsive (red) and attractive (blue) graphite beads.

With this setup, we tested several pairs of  $\chi_{KK'}$  interaction parameters some of which are reported in the plot of figure 20.

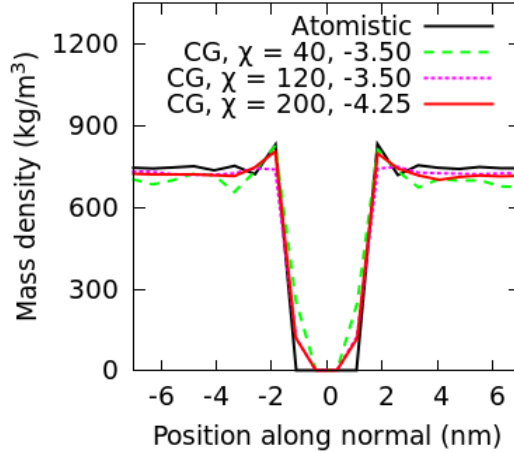


**Figure 20.** Polymer density profiles used for the parametrization. The reference profile (black curve) is derived by atomistic trajectory centered on CG sites. Three pairs of  $\chi_{KK'}$  interaction parameters are plotted (green, pink and red lines).

As can be seen from the plot in figure 20, the polymer density profile, of the coarse-grained model, that best matches the all-atom reference one, is obtained when using  $\chi_{KK'} = 200 \frac{kJ}{mol RT}$  (for the repulsive interaction) and  $\chi_{KK'} = -4.25 \frac{kJ}{mol RT}$  (for the attractive interaction). The compressibility  $\kappa$ , which affected mainly the polymer densities in the bulk phase (far from the interface), was set to 1.

### *4.3 CG Model of CB Nanoparticle*

In this section the development of a coarse-grained model of a primary carbon black nanoparticle will be presented. The nanoparticle, generated through a simulated annealing procedure, was spherical. This choice is based on the analysis of many available experimental data<sup>26</sup> showing that primary particles have a spherical shape, and that, in most of the carbon black applications, their average diameter is around 20 *nm*.

#### *4.3.1 Models and Parameters*

Graphene sheets of different sizes (figure 21), were used as building blocks: one type was used to generate the amorphous core while the other to construct the graphitized shell around the inner core. In particular, in the all-atom representation, core and shell units, consisted of 33 and 294 carbon atoms respectively. Using the same mapping scheme adopted for the graphene sheets (showed in section 4.1.2) carbon black core and shell units, in the coarse-grained representation, consisted of 4 and 43 beads respectively. The mapping scheme adopted for the CG model of core and shell units is showed in figure 21 along with the all atom representation.

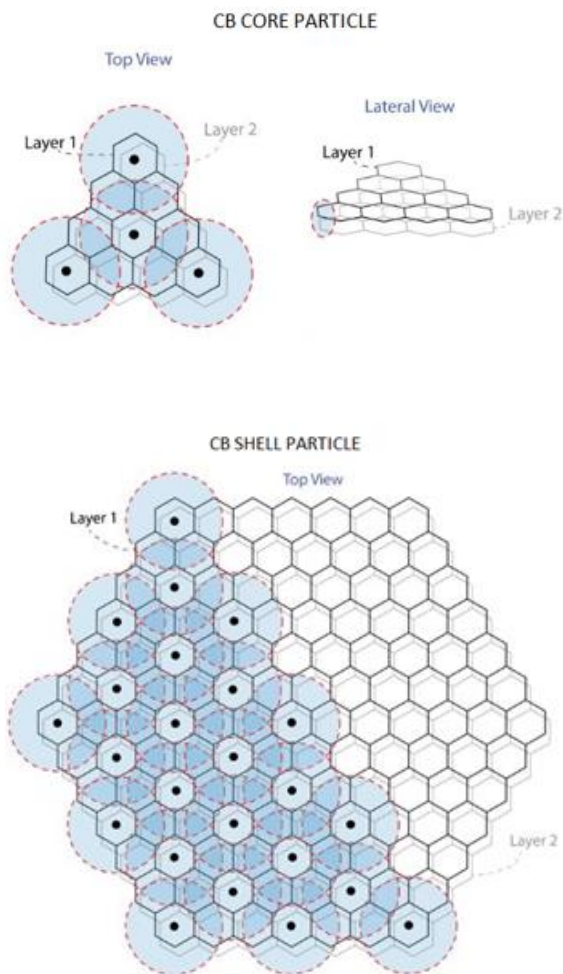


**Figure 21.** Mapping scheme used for core and shell units of carbon black nanoparticle. CG beads are reported in light blue, with their center of mass represented by black dots. The underlying all-atom structure (aromatic carbons) is also reported. In the core unit, each CG bead maps 16.5 carbon atoms, while in the shell unit each CG bead maps 13.7 carbon atoms.

With the scheme we adopted, a single CB nanoparticle of 20 nm diameter, can be represented using  $3 \cdot 10^4$  beads, instead of  $5 \cdot 10^5$  atoms (in the all-atom model). This clearly results in a reduction of the computational cost, since for an MD simulation the computational complexity to treat such a molecule, scales at least as  $O(N^2)$  (being  $N$  the number of beads in the system).

Since the carbon black nanoparticle structure was generated using standard MD, we treated the non-bonded interactions among coarse-grained beads, with a Lennard-Jones potential (equation 26). The first step was to determine the interaction parameters among coarse-grained beads, mainly  $\sigma$ , which is the distance at which interparticle potential is zero, and  $\varepsilon$ , which is the depth of the potential well.

$$V(r_{ij}) = 4\varepsilon_{ij} \left[ \left( \frac{\sigma_{ij}}{r_{ij}} \right)^{12} - \left( \frac{\sigma_{ij}}{r_{ij}} \right)^6 \right] \quad (26)$$

These parameters were parametrized based on the non-bonded potential of interaction among atoms in the all-atom structures.

More in detail, short energy minimizations were performed on two all-atom couples of core (or shell) units, keeping the distance between the pairs fixed (figure 22). Then the value of the Lennard Jones potential was computed at several separation distances, giving thus a potential energy curve that served as reference. The same

procedure of energy minimizations was then performed on coarse-grained pairs of core/shell units, using trial  $\sigma$  and  $\varepsilon$  values. The final set of parameters was the one that better reproduced the reference all-atom potential energy curve (figure 23).

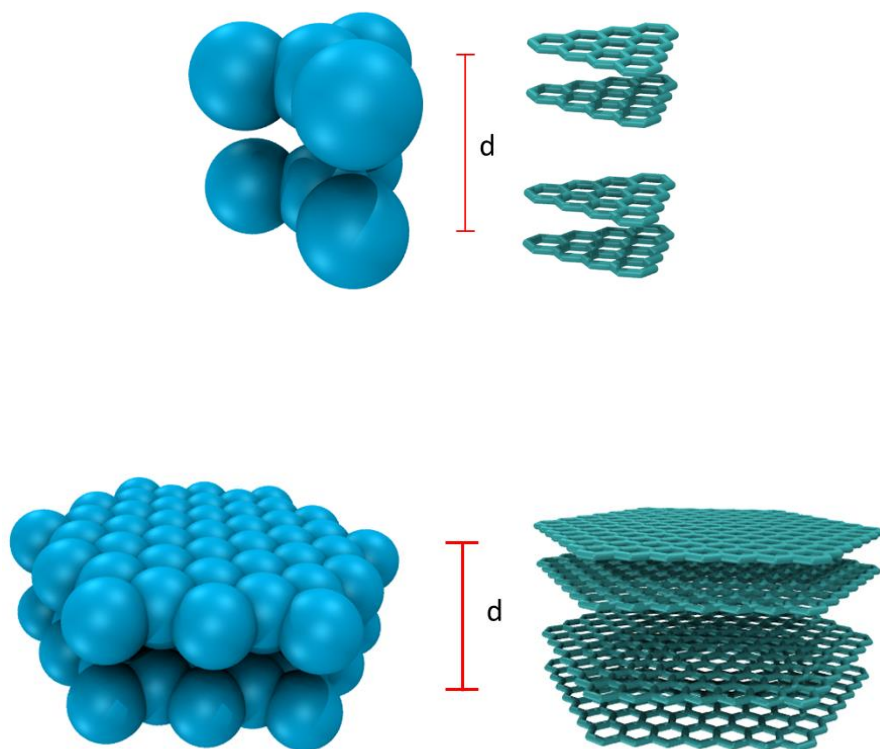


**Figure 22.** Scheme of configurations used to calculate the potential energy at varying distances  $d$ . Carbon black core units, in the coarse-grained (left) and all-atom (right) representations are showed.

In particular, the parametrized values were  $\sigma = 0.635 \text{ nm}$  and  $\epsilon = 8.55 \text{ kJ/mol}$ .

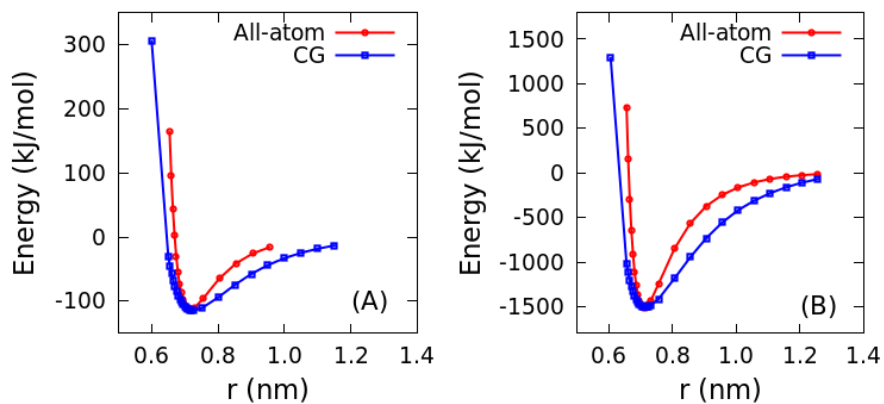


**Figure 23.** Plots of the Lennard-Jones potential energy obtained using the energy minimization procedure. All-atom (red line, dots) and coarse-grained (blue line, squares) potential energy curves for the carbon black core units A) and shell units B).

## 4.3.2 Primary Nanoparticle Structure Generation

### 4.3.2.1 Simulation Details

For all the energy minimization and MD runs described in the following section, the timestep was set to 0.03 *ps*, the cutoff for Van der Waals interactions was 1.5 *nm*, while the non-bonded interaction parameters (from section 4.3.1) were  $\sigma = 0.635$  *nm* and  $\varepsilon = 8.55$  *kJ/mol*. For the MD runs, the temperature was controlled using a velocity rescale algorithm<sup>12</sup> with a coupling constant  $\tau_T = 0.3$  *ps*.

### 4.3.2.2 Results and Discussion

The initial structure of the carbon black nanoparticle was generated starting from the inner amorphous core. In particular, using the Packmol software<sup>27</sup>, 796 core units were placed randomly into a spherical volume of 10 *nm* diameter. Then using the GROMACS software<sup>11</sup>, the structure was energy minimized in two subsequent runs of 150 *ps*, first keeping position restraints on all the molecules, and then removing them.

The resulting structure was then equilibrated performing two successive simulated annealing runs of 15 *ns* in the *NVT* ensemble. As for the energy minimization runs, also here the first run was done keeping positions restraints on all the molecules, while the second one removing them. Details of the simulated annealing setup are reported in figure 24, which shows the temperature variations as function of time, during the simulation.

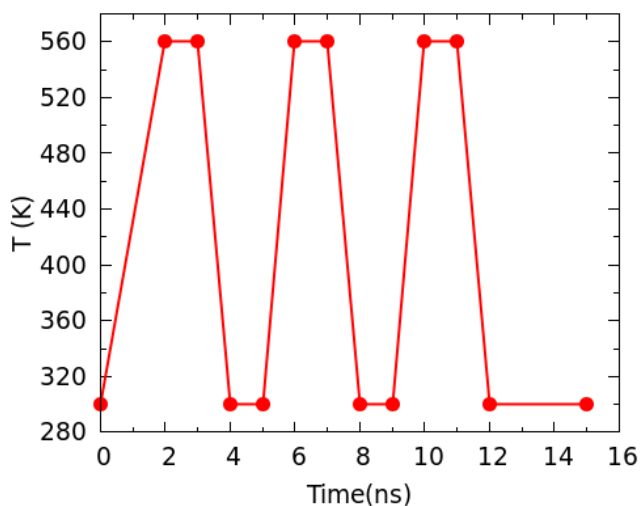


**Figure 24.** Variation of the temperature during the simulated annealing simulation.

In particular, as can be observed from figure 24, the initial temperature of 300 K was raised gradually to 560 K in the first 2 ns. Then three cycles followed, in which the temperature was varied between 560 and 300 K in 1 ns and kept constant for 1 ns once the target temperature was reached. The final temperature was 300 K. Radial density profiles of the initial configuration of the nanoparticle core and after the equilibration procedure, are shown in figure 25.

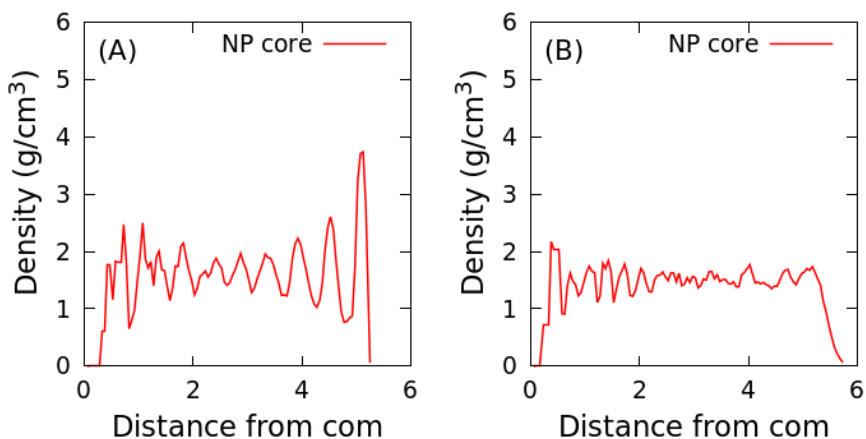


**Figure 25.** Radial density profile of the initial nanoparticle core structure generated from Packmol (A) and after simulated annealing simulations (B).

From the plots in figure 25 it is clear that after the equilibration procedure, the nanoparticle core has a more homogeneous density compared to the initial structure.

Next, the outer shell of the nanoparticle was built starting from the structure of the core previously obtained. In particular 626 CG shell molecules were placed concentrically around the nanoparticle core, in a shell of 10 *nm* length. The packed shell units were stacked one onto the other and with their surface tangent to the sphere surface.

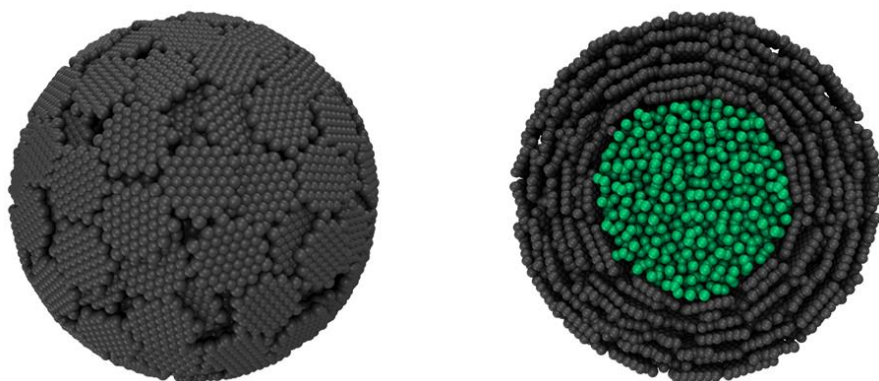


**Figure 26.** Initial structure of the CB nanoparticle. Whole particle (left), section of particle (right). Beads of the shell units are depicted in grey, while beads of the core in green.

However, as can be observed from figure 26, in the initial structure of the CB nanoparticle, the surface is almost completely flat, while from experimental characterizations<sup>28</sup>, it has been observed that sites with different structures are present. Moreover, there were still some unphysical voids within the shell, thus not resulting in a homogenous packing of the molecules.

For this reason, as in the case of the core, a minimization procedure was performed on the whole nanoparticle. In particular, two energy minimizations of 600  $\mu s$  were executed. In the first run position restraints on all the core molecules were imposed, while in the second they were removed. Next, two subsequent simulated annealing simulations of 15  $ns$ , were performed in the *NVT* ensemble. The temperature changes applied during the annealing were the

same used for the equilibration of the nanoparticle core (figure 24). The first run was executed keeping position restraints on the molecules of the core, while in the second run, they were removed. Radial density profiles of the whole nanoparticle before and after the equilibration procedure are shown in figure 27.

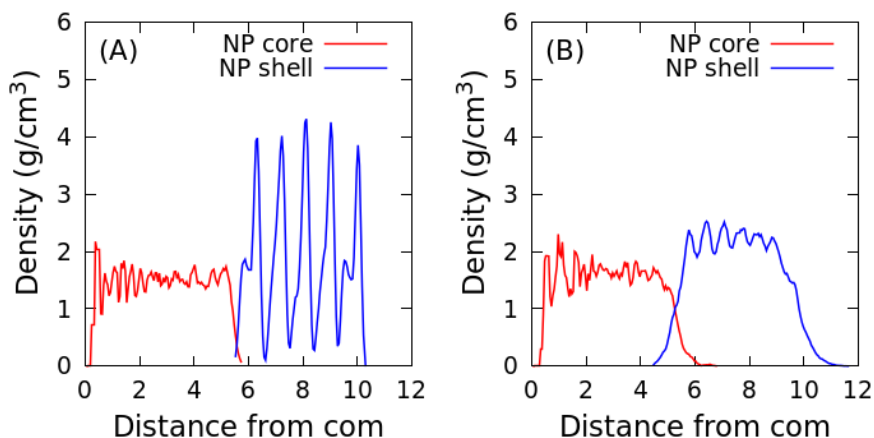


**Figure 27.** Radial density profile of the whole nanoparticle structure before (A) and after simulated annealing simulations (B).

From the plots of figure 27, it can be observed that starting from the initial structure, where shell molecules are placed around the core in a well defined way, the equilibration procedure brings to a new structure where the density is smoother throughout the whole nanoparticle.

The mean density, resulting from the contribution of the inner core and the outer graphitized shell, is around 2 g/cm<sup>3</sup>, which agrees well

with the experimental one measured by X-ray diffraction<sup>26</sup> (2.05 – 2.25 g/cm<sup>3</sup>), thus confirming the accuracy of the model we propose here.

An even more interesting result for this model of carbon black nanoparticle comes from the analysis of its morphology. In particular, with the whole procedure of equilibration described above, it was possible to obtain a structure with a heterogeneous surface containing experimentally observed structures<sup>28</sup> such as crystallite edges, slit shaped cavities and graphitic planes, as can be observed in figure 28. These morphological arrangements are important features since from an experimental point of view, they are considered superior adsorption sites for polymer chains<sup>29</sup>. Moreover, as it will be showed in the following section, the heterogeneity of the surface has a main influence on the structuring of chains at the polymer/nanoparticle interface, in bidisperse polymer melts.

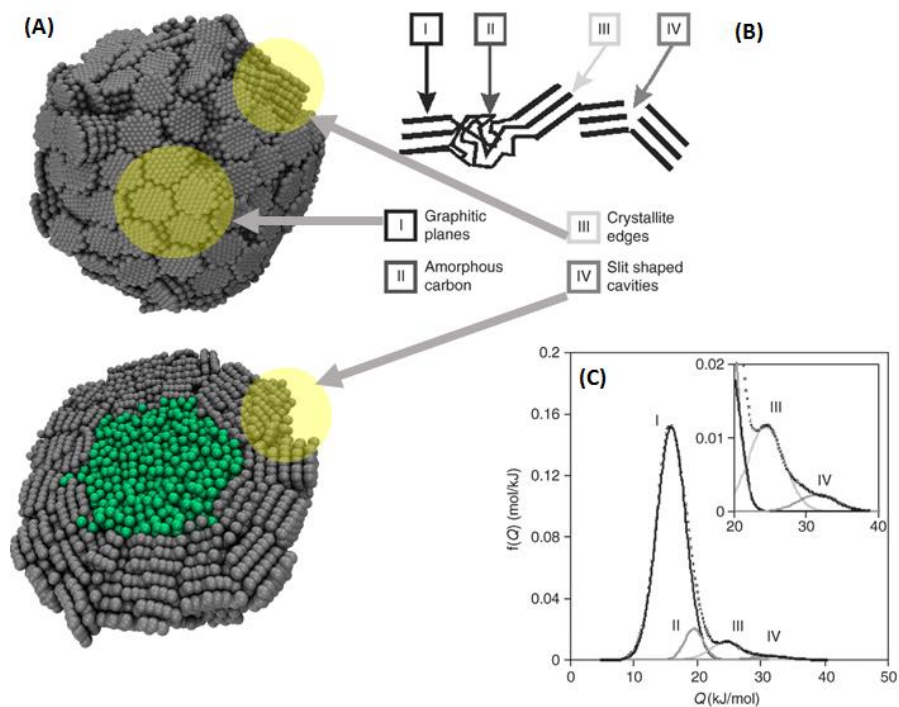


**Figure 28.** CB primary nanoparticle obtained from the annealing procedure (A). Experimental ethene adsorption isotherms<sup>28</sup> (C), from which different morphological arrangements are found (B).

## 4.4 CG Model of PE on Graphite/CB: Monodisperse and Bidisperse Polymer Melts

This section is about CG simulations of polyethylene melts of high  $M_w$  in contact with either graphite or carbon black nanoparticle. In particular, simulations were performed with the aim of comparing the effects of the filler shape and morphology on the structuring of the polymer/filler interface, in both monodisperse and bidisperse polymer melts.

### 4.4.1 Simulation Details

All the simulations were performed using the PF-MD method implemented in the OCCAM software<sup>9</sup>. Simulations were runned in the  $NVT$  ensemble using a timestep of 0.03  $ps$ . The relevant parameters for the PF-MD simulations were the ones reported in section 4.2.3. In particular, values of  $\chi_{KK'} = 200 \frac{kJ}{mol RT}$  and  $\chi_{KK'} = -4.25 \frac{kJ}{mol RT'}$ , were used to describe polymer/filler interactions, while the compressibility  $\kappa$  was set to 1 and the grid size was 0.73  $nm$ . However, for the carbon black nanoparticle it was necessary to tag all the beads on the surface and assign them the value  $\chi_{KK'} = -4.25 \frac{kJ}{mol RT}$  for the interaction with the polymer beads, while the remaining beads, under the surface, were assigned the value  $\chi_{KK'} = 200 \frac{kJ}{mol RT}$ .

#### 4.4.2 Graphite/CB Monodisperse Polymer Melt Systems

Details on the simulated systems are reported in table 8. In all the systems, the graphite and the carbon black nanoparticle were kept fixed.

**Table 8.** Details of the PF-MD simulations of monodisperse polymer melts with graphite and carbon black

System	No. of PE Chains	No. of Monomers in PE chains	Tot. No. Particles	Box size [nm] (x,y,z)	Time ( $\mu$ s)	T (K)
PE Graphite	636	1072	192128	29.430 26.300 59.181	0.44	550
PE Graphite	116	5880	192200	29.430 26.300 59.190	3.78	550
PE Graphite	150	10696	440124	35.136 39.450 77.19	1.95	550
PE CB	1736	1072	495350	50 50 50	0.57	550
PE CB	316	5880	494622	50 50 50	1.02	550
PE CB	174	10696	495378	50 50 50	0.675	550

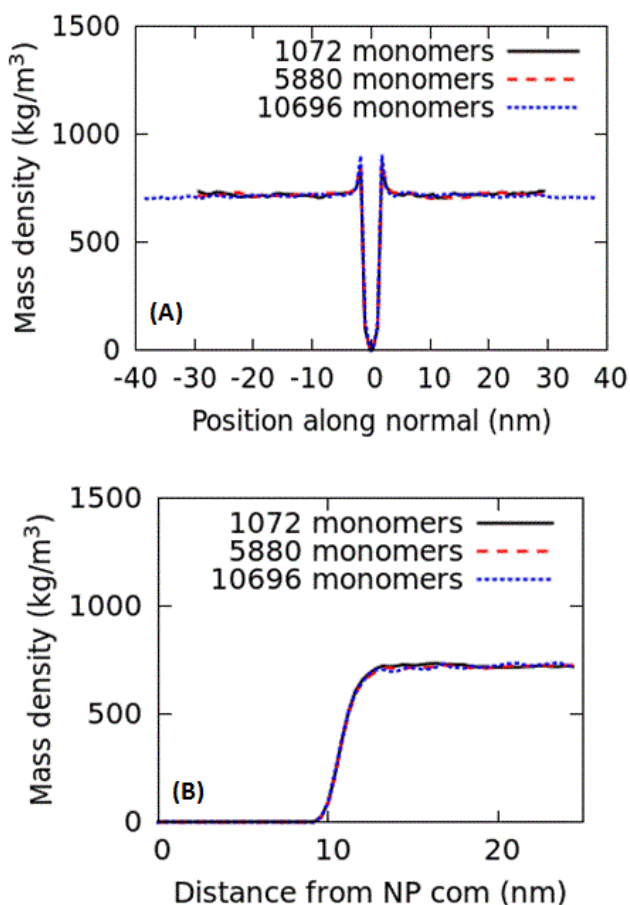


**Figure 29.** Polymer density profiles with respect to the surface of graphite (A) and CB (B). In plot A the zero corresponds to the middle point between the graphene planes. In plot B the zero coincides with the center of mass of the nanoparticle.

The main output of the simulations were the computed polymer density profiles of respect to the graphite or carbon black surfaces. In the first case the profile was obtained calculating the density of the polymer in slabs of 0.73 nm parallel to the graphite plane. For the CB

system, the profile was obtained by computing the polymer density in concentric shells centered at the center of mass of the nanoparticle. Results are shown in figure 29.

Analyzing the plots, it can be observed that irrespective of the molecular weight of the polymer chains, the density profiles remains the same, in either the systems with graphite and carbon black primary particle.

Instead, a difference is apparent when comparing the systems containing graphite with the ones containing carbon black: in the first case there is an increase of the polymer density near the filler surface (sharp peaks in figure 29 A), while in the second case this is not observed, indicating a density that is the same as the bulk density for all the distances from the nanoparticle surface. This difference can be attributed to the different shape of the fillers (plain surface in the first case and spherical in the second one), which influences the structural properties of the polymer at the interface.

#### *4.4.3 Graphite/CB Bidisperse Polymer Melt Systems*

For the bidisperse case, three different melts were considered. In particular, two of the systems had a low  $M_w$  fraction containing chains of 20 monomers (0.563 kg/mol) and a high  $M_w$  fraction with chains of either 1072 or 5880 monomers (30 kg/mol and 165 kg/mol respectively). The third system consisted instead of a fraction of chains with 1072 monomers while the other one contained chains of 10696 monomers (300 kg/mol). Regarding the composition of the systems, in all cases the ratio of low to high  $M_w$  fraction was 1 to 1. As in this case of monodisperse systems, graphite and carbon black nanoparticle were kept fixed in all simulations.

The length of the simulations was such that polymer chains could travel a sufficiently long distance to rearrange their position close to the interface with the graphitic surface (or CB nanoparticle). This allows to correctly sample the configurations for the analysis of the polymer density profiles. In particular, the density profiles obtained from the simulations are showed in figure 30.

**Table 9.** Details of the PF-MD simulations of bidisperse polymer melts with graphite and carbon black

<b>System</b>	<b>No. of PE Chains</b>	<b>No. of Monomers in PE chains</b>	<b>Tot. No. Particles</b>	<b>Box size [nm] (x,y,z)</b>	<b>Time (<math>\mu</math>s)</b>	<b>T (K)</b>
PE/Graphite bidisperse	17310	20 1072	191338	29.430 26.300 59.190	6.24	550
PE/Graphite bidisperse	17052	20 5880	191910	29.430 26.300 59.190	8.26	550
PE/Graphite bidisperse	1652	1072 10696	842660	35.136 39.450 152.19	7.32	550
PE/CB bidisperse	47413	20 1072	495451	50 50 50	4.24	550
PE/CB bidisperse	46702	20 5880	495082	50 50 50	7.71	550
PE/CB bidisperse	4015	1072 10696	1984312	80 80 80	5.04	550

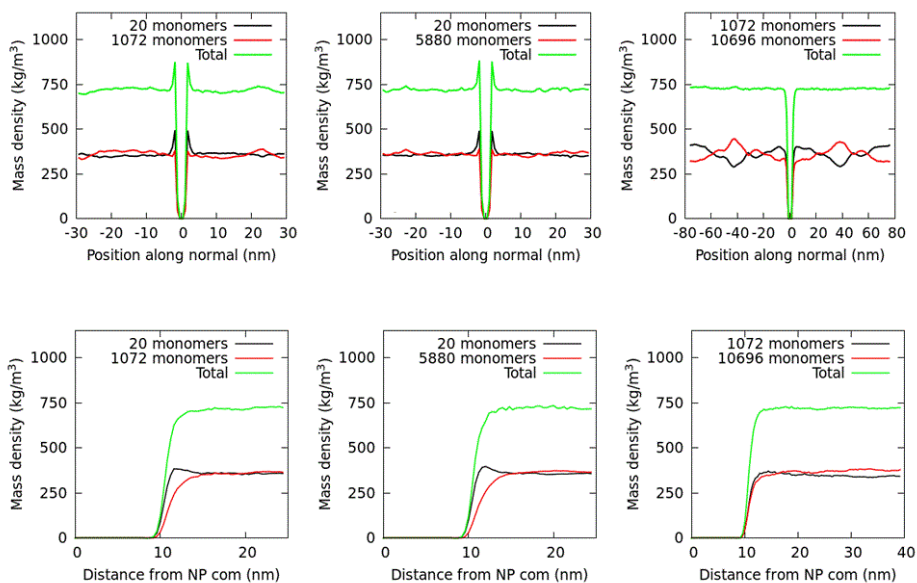


**Figure 30.** Polymer density profiles in bidisperse systems with respect to the surface of graphite (top) and CB nanoparticle (bottom). Green curves are the total density profiles while the red and black curves are the low and high  $M_w$  fractions respectively. In the systems with graphite (top) the zero corresponds to the middle point between the graphene planes, while in the systems with the CB nanoparticle (bottom) the zero coincides with the center of mass of the nanoparticle.

The first observation is that the total density profiles (green curves) have the same shape as the ones in the monodisperse systems, in particular, for the systems with graphite, the density reaches a maximum in proximity of the surface, while in systems with the CB nanoparticle the total density is the same as the bulk density, in all the range of distances from the surface.

Instead, considering the separate contribution of the two fractions to the total polymer density profiles, it can be clearly observed that in proximity of the surface, of either graphite or carbon black nanoparticle, the most abundant fraction is the one with the lowest  $M_w$ . This holds for all the systems in which the low  $M_w$  fraction is the one containing chains of 20 monomers, while for the systems with the highest  $M_w$  (1072 and 10696 monomers) no remarkable phase separation can be observed at the polymer/filler interface. To better understand the results obtained from the density profiles, free energies for the exchange of a bead in a long chain with a bead in a short chain, as function of the distance  $r$  from the filler surface, were computed. In particular, this quantity can be derived using the following expression<sup>30</sup>:

$$\Delta G_{long \rightarrow short} = RT \ln \left( \frac{g(r)_{long}}{g(r)_{short}} \right) \quad (26)$$

Where  $g(r)_{long}$  and  $g(r)_{short}$  are the values of the densities at different distances  $r$  from the surface,  $R$  is the gas constant and  $T$  the temperature in Kelvin.

Results obtained applying the equation 26 are showed in figure 31.

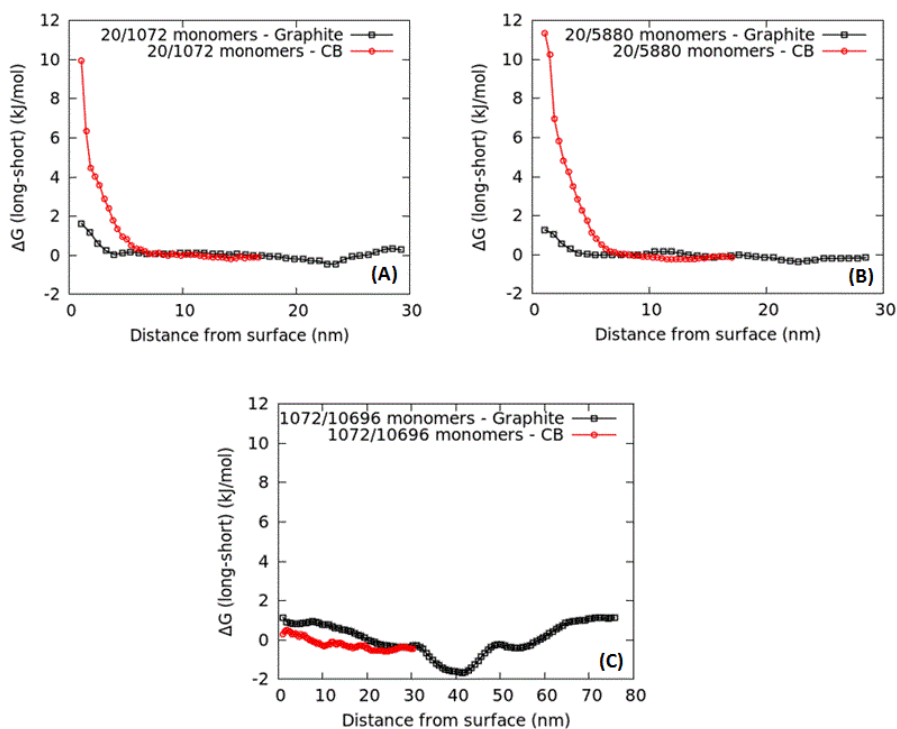


**Figure 31.** Free energy for the exchange of a bead in a long polymer chain with a bead in short polymer chain as function of the distance  $r$  from the surface of graphite (black curve) or carbon black nanoparticle (red curve). Analysis are reported for bidisperse systems with chains of 20/1072 monomers (A), 20/5880 monomers (B), 1072/10696 monomers (C).

Considering the systems where the low  $M_w$  fraction is that containing chains of 20 monomers (figure 31 A and B), it can be observed that for short distances from the surface of the fillers, (2-3 nm for graphite and 5 nm for CB nanoparticle), the free energy of substitution attains positive values, thus indicating, at those distances, an energy penalty

for the exchange of beads of long chains with those of short chains. At larger distances the mixing becomes substantially random. The energy penalty found for these systems is less remarkable for the systems with low  $M_w$  chains of 1072 monomers and high  $M_w$  chains of 10696 monomers (figure 31 C).

This free energy of exchange can be expressed as the sum of an enthalpic and an entropic contribution, as follows:

$$\Delta G = \Delta H - T\Delta S \quad (27)$$

Considering that the enthalpic term is the same for both chain/chain and chain/filler interactions, then it is clear that the energy penalty is entirely due to entropic contributions.

In order to give a possible explanation for the entropic effect on the phase separation in bidisperse systems, the conformations of polymer chains near the surface of the fillers were analyzed, since the number of conformations contributes to the total number of microstates, which are directly related to the entropy.

In particular, chain conformations were analyzed in terms of adsorbed trains, tails and loops (figure 32), whose definition<sup>17</sup> is given below:

- **Trains:** successive segments within the adsorbed layer (i.e. at a distance less than 0.73 nm).
- **Tails:** sequences of segments terminated at one side by a chain end and at the other side by a segment pertaining to a train.
- **Loops:** sequences of segments that connect two trains, with their centers outside the adsorbed layer.

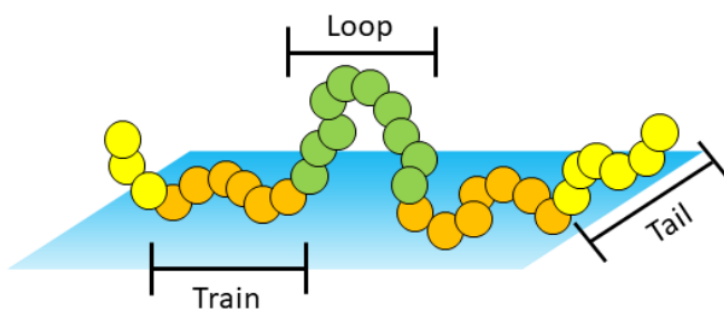


**Figure 32.** Schematic representation of the different conformations of adsorbed chains, in terms of trains (orange), tails (yellow) and loops (green). The light blue plane represents a generic surface.

Statistics for the adsorbed polymer chains conformations, were computed for both monodisperse and bidisperse melts.

In order to compare the results obtained, the average number of trains, tails and loops was normalized by the value of the surface area of the fillers. Data are reported in table 10 and table 11, for the systems containing the carbon black nanoparticle and the graphite respectively. For the bidisperse systems, analysis is reported for both low and high  $M_w$  polymer chains.

**Table 10.** Statistics of trains, tails and loops for the systems containing PE and CB nanoparticle.

<b>System</b>	<b>Type of chain</b>	<b>Trains/nm<sup>2</sup></b>	<b>Loops/nm<sup>2</sup></b>	<b>Tails/nm<sup>2</sup></b>
PE (20/1072)	20	0.190	0.016	0.346
(Bidisperse)	monomers	±	±	±
		0.003	0.001	0.004
PE (20/1072)	1072	0.058	0.025	0.061
(Bidisperse)	monomers	±	±	±
		0.002	0.001	0.001
PE (20/5880)	20	0.124	0.008	0.230
(Bidisperse)	monomers	±	±	±
		0.002	/	/
PE (20/5880)	5880	0.022	0.012	0.017
(Bidisperse)	monomers	±	±	±
		0.001	/	/
PE (1072/10696)	1072	0.091	0.043	0.095
(Bidisperse)	monomers	±	±	±
		0.002	0.002	0.002
PE (1072/10696)	10696	0.074	0.048	0.051
(Bidisperse)	monomers	±	±	±
		0.002	0.002	/
PE (1072)	1072	0.168	0.082	0.171
(Monodisperse)	monomers	±	±	±
		0.003	0.003	0.002
PE (5880)	5880	0.160	0.099	0.122
(Monodisperse)	monomers	±	±	±
		0.003	0.002	0.001
PE (10696)	10696	0.159	0.111	0.093
(Monodisperse)	monomers	±	±	±
		0.004	0.004	0.002

**Table 11.** Statistics of trains, tails and loops for the systems containing PE and graphite.

<b>System</b>	<b>Type of chain</b>	<b>Trains/nm<sup>2</sup></b>	<b>Loops/nm<sup>2</sup></b>	<b>Tails/nm<sup>2</sup></b>
PE (20/1072)	20	0.725	0.116	0.592
(Bidisperse)	monomers	±	±	±
		0.005	0.003	0.005
PE (20/1072)	1072	0.346	0.287	0.110
(Bidisperse)	monomers	±	±	±
		0.004	0.006	/
PE (20/5880)	20	0.671	0.107	0.550
(Bidisperse)	monomers	±	±	±
		0.005	0.002	0.006
PE (20/5880)	5880	0.380	0.354	0.047
(Bidisperse)	monomers	±	±	±
		0.005	0.002	/
PE (1072/10696)	1072	0.106	0.060	0.090
(Bidisperse)	monomers	±	±	±
		0.002	0.001	0.001
PE (1072/10696)	10696	0.070	0.056	0.029
(Bidisperse)	monomers	±	±	±
		/	/	/
PE (1072)	1072	0.807	0.684	0.224
(Monodisperse)	monomers	±	±	±
		0.007	0.008	0.001
PE (5880)	5880	0.798	0.760	0.094
(Monodisperse)	monomers	±	±	±
		0.006	0.006	/
PE (10696)	10696	0.834	0.793	0.077
(Monodisperse)	monomers	±	±	±
		0.004	0.004	/

In general, from the value reported in table 10 and 11, the absolute values of trains, tails and loops per square nanometer are higher for the systems with graphite respect to the one with the carbon black nanoparticle. This is not surprising for the higher values of the monomer density at the interface for systems interacting with graphitic planes. However, the most interesting comparison is the one between bidisperse and monodisperse systems, in particular when the high  $M_w$  polymer fraction of the former is the same of the latter (e.g. bidisperse with 20/1072 monomers chains vs. monodisperse 1072 monomers chains). Results are showed in figure 33 and 34.

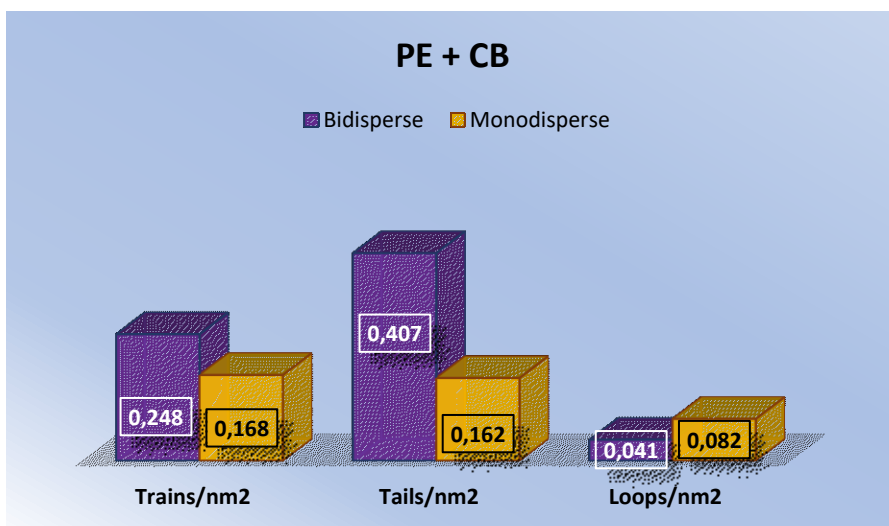


**Figure 33.** Statistics of the trains, tails and loops for PE + CB system. Bidisperse (20 / 1072 monomers) and monodisperse (1072 monomers) systems are reported in purple and orange respectively.

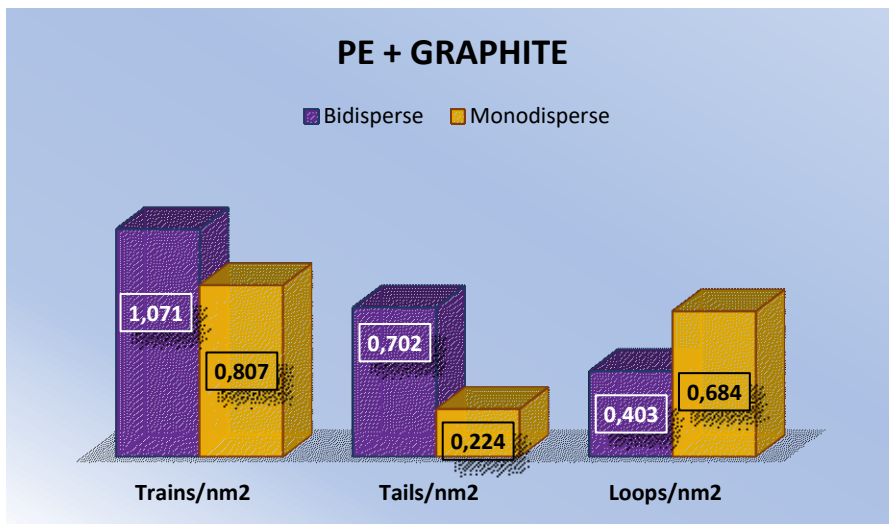


**Figure 34.** Statistics of the trains, tails and loops for PE + Graphite system. Bidisperse (20 / 1072 monomers) and monodisperse (1072 monomers) systems are reported in purple and orange respectively

Comparing the data between bidisperse and monodisperse systems, the number of trains and tails (per square nanometer) is almost the same, while the number of the loops differs in a remarkable way. This holds for both the systems with graphite and carbon black primary nanoparticle.

In particular, in monodisperse systems, the number of loops per square nanometer is almost double the number of loops found in bidisperse systems. This result can be interpreted in the following way: in bidisperse systems it is more favorable to adsorb low  $M_w$  chains instead of high  $M_w$  ones, because adsorption of the latter

requires an increase in the number of the loops that these chains have to adopt. Considering that for loop segments the number of possible conformations is lower respect to that in segments of a free chain, this translates into a reduction of the total entropy, which is not thermodynamically favorable.

This consideration explains the results obtained from the calculation of free energy of exchange of beads in long chains with beads of short chains at the polymer/filler interface. However, this cannot explain alone the observed phase separation, since the absolute values of free energy of exchange are different when comparing the bidisperse systems with graphite and carbon black nanoparticle.

A more complete picture is obtained when taking into account the effects of the carbon black nanoparticle surface disorder. In particular, the primary nanoparticle presents surface cavities which are not present in the graphite structure. The dimension of these cavities is such that they can be filled only by polymer chains of low  $M_w$  (20 monomers), while bigger chains (1072 monomers) with a  $R_g$  ( $\sim 8$  nm) comparable to the nanoparticle radius, cannot occupy them. In graphite instead, since the surface is completely flat, chains can adsorb in each point of it, irrespective of their dimension. These considerations explain why the energy penalty for the exchange of beads from long to short chains at the polymer/filler interface is higher in presence of the nanoparticle (respect to graphite).

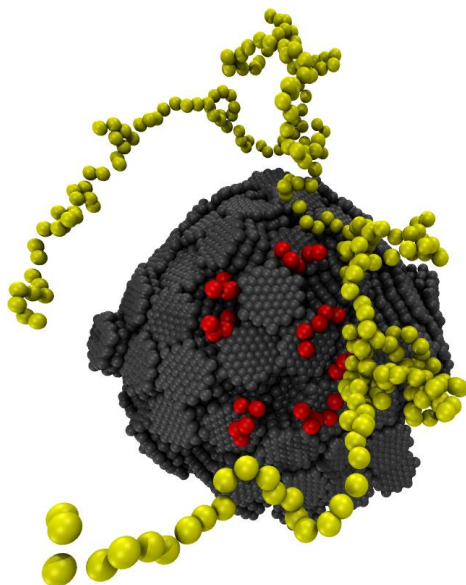


**Figure 35.** Snapshot of system containing PE chains of 20 monomers (red) and 1072 monomers (yellow) and CB nanoparticle, showing how short chains fit into different cavities of the surface respect to long chains.

#### *4.5 Conclusions and perspectives*

The main result of this chapter, and this thesis in general, has been the development of a CG molecular model of a carbon black primary particle, which has been used in simulations with polyethylene melts, in order to obtain information on the polymer structuring at the interface with this filler.

In particular, a strategy has been set up to obtain such nanoparticle structure, and along with that, a CG model of linear polyethylene has been developed. The proposed models are not generic, since they have been built based on atomistic reference properties, thus giving

more reliable results, comparable with experimental available data. Moreover, this is a realistic CB nanoparticle model, since its dimension (20 nm diameter) and the different sites that appear on the surface, are all features proved by experimental characterizations. To the best of our knowledge this is the only CG, yet detailed model, of carbon black nanoparticle present in the current literature.

Simulations of monodisperse and bidisperse polyethylene melt systems containing either graphite or CB nanoparticle were performed, and the main output were polymer density profiles. In particular from the analysis of the results, the main conclusions are:

- Shape of the filler is important, since in systems with graphite an increased value of the density is attained in proximity of the surface, while in systems with CB nanoparticle the density is the same as the bulk density for all the range of distances from the surface.
- In bidisperse polyethylene melts a phase separation occurs at the polymer/filler interface, with an abundance of the low  $M_w$  chains fraction respect to the high  $M_w$  fraction, near the surface of either graphite or CB nanoparticle. The driving force behind this effect is purely due to entropic contributions which are related to the possible conformations that a polymer chain can adopt at the interface with the filler, and

most important the surface disorder of the filler, which also induces phase separation.

Overall these results and the further applications of the proposed model can help to understand experimental results and to address improvement of the dispersion of fillers in polymer matrices.

As future perspectives, the model that has been proposed in this work, can be further developed to include surface modification of the nanoparticle (such as oxidized functional groups), and also polymer modification (chain branching, inclusion of different co-monomers), and to study the effect that these modifications have on the interfacial properties. Moreover, the model can be extended to multiparticle systems, in order to simulate the aggregation of more primary particles into aggregates and understand which factors can affect this process.

## References:

- (1) M. E. Spahr, R. Rothon, *Encyclopedia of Polymers and Composites*, Springer Berlin Heidelberg, **2015**.
- (2) J. C. Huang, *Advances in Polymer Technology*, **2002**, 21,299.
- (3) A. Kausar, *J. Plast. Film Sheeting* **2018**, 34, 256.
- (4) S. W. I. Siu, K. Pluhackova, R. A. Böckmann, *J. Chem. Theory Comput.* **2012**, 8 (4), 1459–1470.
- (5) W. L. Jorgensen, D. S. Maxwell, J. Tirado-Rives, *J. Am. Chem. Soc.* **1996**, 118 (45), 11225–11236.
- (6) K. M. Salerno, A. Agrawal, B. L. Peters, D. Perahia, G. S. Grest, *Eur. Phys. J. Spec. Top.* **2016**, 225, 1707.
- (7) S. Güryel, M. Walker, P. Geerlings, F. De Proft, M. R. Wilson, *Phys. Chem. Chem. Phys.* **2017**, 19, 12959.
- (8) J. P. Ewen, C. Gattinoni, F. M. Thakkar, N. Morgan, H. A. Spikes, D. Dini, *Materials*, **2016**, 9, 651.
- (9) Y. Zhao, A. De Nicola, T. Kawakatsu, G. Milano, *J. Comput. Chem.* **2012**, 33, 868–880.
- (10) A. De Nicola, T. Kawakatsu, G. Milano, *J. Chem. Theory Comput.* **2014**, 10, 5651–5667.
- (11) H. J. C. Berendsen, D. Van Der Spoel, R. Van Drunen, *Comput. Phys. Commun.* **1995**, 91, 43–56.
- (12) G. Bussi, D. Donadio, M. Parrinello, *J. Chem. Phys.* **2007**, 126, 14101.
- (13) Berendsen, H. J. C.; Postma, J. P. M.; Van Gunsteren, W. F.; DiNola, A.; Haak, J. R. Molecular Dynamics with Coupling to an External Bath. *J. Chem. Phys.* **1984**, 81, 3684.
- (14) B. Hess, H. Bekker, H. J. C. Berendsen, J. G. E. M. Fraaije, *J. Comput. Chem.* **1997**, 18 (12), 1463–1472.

- (15) W. M. Haynes, *Handbook of Chemistry and Physics*, CRC Press, **2002**.
- (16) S. Krimm, A. V. Tobolsky, *J. Polym. Sci.* **1951**, *7*, 57.
- (17) V. A. Harmandaris, K. Ch. Daoulas, V. G. Mavrantzas, *Macromolecules* **2005**, *38*, 5796.
- (18) A. P. Sgouros, G. G. Vogiatzis, G. Kritikos, A. Boziki, A. Nikolakopoulou, D. Liveris, D. N. Theodorou, *Macromolecules* **2017**, *50*, 8827.
- (19) M. Solar, K. Binder, W. Paul, *J. Chem. Phys.* **2017**, *146*, 203308.
- (20) J. Ramos, J. F. Vega, J. Martinez-Salazar, *Macromolecules* **2015**, *48*, 5016.
- (21) G. Milano, F. Müller-Plathe, *J. Phys. Chem. B* **2005**, *109* (39), 18609–18619.
- (22) J. Schelten, D. G. H. Ballard, G. D. Wignall, G. Longman, W. Schmatz, *Polymer*, **1976**, *17*, 751.
- (23) D. S. Pearson, G. Ver Strate, E. von Meerwall, F. C. Schilling, *Macromolecules* **1987**, *20*, 1133.
- (24) N. P. Walter, A. Jaiswal, Z. Cai, Y. Zhang, *Comput. Phys. Commun.* **2018**, *228*, 209.
- (25) F. W. Starr, J. F. Douglas, D. Meng, S. K. Kumar, *ACS Nano* **2016**, *10*, 10960.
- (26) J. B. Donnet, *Carbon Black*, CRC Press, 1993.
- (27) L. Martínez, R. Andrade, E. G. Birgin, J. M. Martínez, *J. Comput. Chem.* **2009**, *30* (13), 2157–2164.
- (28) T. A. Vilgis, G. Heinrich, M. Klüppel, *Reinforcement of polymer nano-composites*, Cambridge University Press, **2009**.
- (29) J. B. Donnet, *Carbon*, **1994**, *32* (7), 1305
- (30) G. Milano, F. Müller-Plathe, *J. Phys. Chem. B*, **2004**, *108*, 7415.

---

## All-atom Model of Atactic Poly(2-vinylpyridine)

---

In this chapter an all atom model of P2VP is presented, based on the well-known OPLS-AA<sup>1</sup> force field, which is suitable to model a wide range of complex mixtures and/or interfaces in composite materials. Poly(2-vinyl pyridine) (P2VP) is characterized by the presence of the 2-vinylpyridine substituent, in which the nitrogen atom provides peculiar physical-chemical features compared to similar polymers, such as poly(styrene) (PS), in terms of morphology and polar character. This allows, for example, to interact with other polar molecules or to act as metal ligand.<sup>2</sup> Applications of P2VP include, for example, polyethylene glycol (PEO)-P2VP block-copolymers, which have been used as stimuli responsive material, induced by pH, to form hydrophilic vesicles in solution.<sup>3</sup> In the PS-b-P2VP block copolymer, the capability of the pyridine group to form hydrogen bonds was used to control the supramolecular assembly of hydroxylated gold nanoparticle.<sup>4</sup> More in general, the stimuli-response behavior exhibited by P2VP material, mainly when it is in co-polymer, make it a good candidate for new “smart” materials for the so-called “4D printing”.<sup>5,6,7,8</sup>

The P2VP-PS block co-polymers, characterized by the presence of polar and non-polar phases, opened new possibilities for ink-free lithography transfer applications.<sup>9</sup> In particular, the polar nature of pyridine group allows the P2VP units to be functionalized while the PS units serve as rigid glassy scaffolds. P2VP has also been used to build binary polymer brushes (generally with PS), to control and tune adhesion and friction behavior of solid surfaces.<sup>10</sup> Metal nanoparticle arrays<sup>11</sup> can be efficiently generated from block copolymer micelle lithography, in which P2VP is employed.<sup>12</sup> Morphological behavior of thin films P2VP block co-polymers was studied in the context of fabrication of nonporous membranes, lithography and nanophotonics.<sup>13,14,15</sup> Experimental studies and characterization of P2VP in terms of its synthesis, reactivity, formation of complexes, P2VP-based catalysis and photothermal reactivity, are also reported in literature.<sup>2,16</sup>

Despite several applications of P2VP in the technological field, computational studies, that could allow to understand in detail the P2VP features and to improve its performance, are not huge in number. To the best of our knowledge, only two atomistic models of P2VP have been reported in literature, a united-atom reported by He<sup>17</sup> and an all-atom model reported by Soldera, in which the reproduction of glass transition temperature has been investigated.<sup>18</sup> However, none of these studies is specifically designed for P2VP, and indeed an exhaustive investigation on the main P2VP structural

properties and related comparison with experimental data is missing. Even for coarse-grained models, only few studies have been found.<sup>19</sup> For this reason, we have tested an all-atom model of P2VP, based on the well-known OPLS-AA force field because of its high adaptability to include and combine other organic molecules,<sup>20,21</sup> polymer models,<sup>22,23,24,25,26</sup> nanoparticles and other possible interfaces<sup>27,28</sup> which represent the common applications of P2VP. In particular, equilibrated melt configurations were successfully obtained by using the hybrid particle-field molecular dynamics (PF-MD) method described in chapter 2. Then, structural properties were derived from standard MD simulations and compared with available experimental data, evaluating the accuracy in their reproduction.

## 5.1 Atomistic Model of Atactic P2VP

A schematic picture of the P2VP chemical structure together with the atom types and charges scheme is reported in Figure 36.

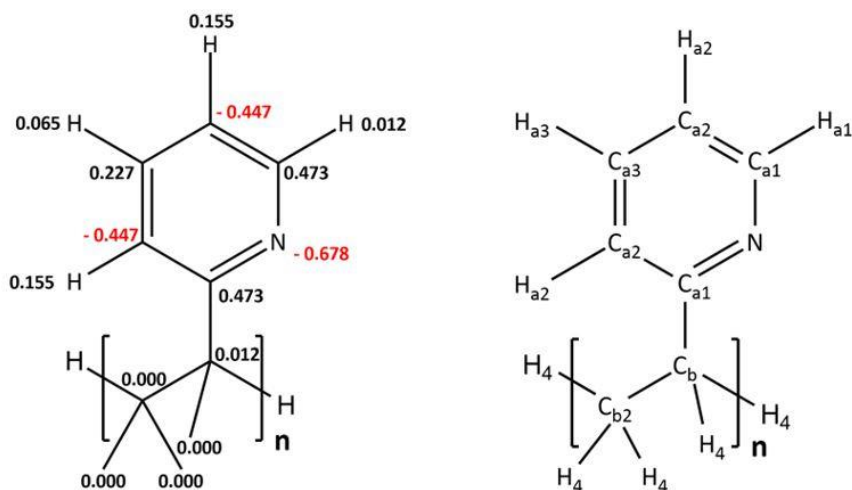


**Figure 36.** P2VP monomer structure with partial charges scheme (left) and atom types (right), taken from Ref.<sup>20</sup>

All the parameters used to describe the pyridine ring were taken from the OPLS-AA force field<sup>20</sup>, which is optimized to fit experimental properties of liquids (such as density and heat of vaporization). For the aliphatic carbons and hydrogens (present on the polymer backbone), the set of parameters reported for atactic polystyrene by Müller-Plathe was used.<sup>29</sup> This choice is based on the wide range of applicability of OPLS-AA and the possibility to combine its force field parameters to study complex polymer systems. Indeed, OPLS-AA was successfully adopted to study different polymers, such as:

polyacrylamides,<sup>25</sup> polyaniline,<sup>26</sup> polyglutamine,<sup>30</sup> macrocyclic polyketides,<sup>31</sup> polymer/carbon nanotube interfaces,<sup>32</sup> and long hydrocarbons.<sup>21,33</sup>

Following the functional forms involved in our model are reported for the bond stretching (Eq. 28), angle bending (Eq 29), dihedral potential for the pyridine ring atoms (Eq. 30) and all other atoms and improper dihedrals (Eq. 31) and non-bonded interactions (Eq. 32):

$$V_b(\mathbf{r}_{ij}) = \frac{1}{2} K_{bond} (\mathbf{r}_{ij} - \mathbf{r}_{ij}^0)^2 \quad (28)$$

$$V_a(\theta_{ijk}) = \frac{1}{2} K_{angle} (\theta_{ijk} - \theta_0)^2 \quad (29)$$

$$V_{rb}(\theta_{ijkl}) = \sum_{n=0}^5 C_n (\cos(\psi))^n \quad (30)$$

$$V_d(\varphi_{ijkl}) = k_{dihedral} (1 + \cos(n\varphi_{ijkl} - \varphi_0)) \quad (31)$$

$$V(r_{ij}) = 4\varepsilon_{ij} \left[ \left( \frac{\sigma_{ij}}{r_{ij}} \right)^{12} - \left( \frac{\sigma_{ij}}{r_{ij}} \right)^6 \right] + \left( \frac{1}{4} \pi \varepsilon_0 \right) \left( \frac{q_i q_j}{r_{ij}} \right) \quad (32)$$

The full list of constants and parameters for each bonded and non-bonded terms is reported in the following tables:

**Table 12.** Constraints and harmonic bond potential

<b>Bonds</b>	<b><math>K_{bond}</math></b> (kJ mol <sup>-1</sup> Å <sup>-2</sup> )	<b><math>r_{ij}^0</math></b> (Å)
C <sub>aro</sub> -N	404.174	1.339
C <sub>aro</sub> -C <sub>aro</sub>	392.458	1.400
C <sub>aro</sub> -H <sub>aro</sub>	/	1.080
C <sub>b</sub> -C <sub>b</sub>	224.264	1.529
C <sub>b</sub> -C <sub>b</sub>	/	1.530
C <sub>b/b2</sub> -H <sub>4</sub>	/	1.100

\*C<sub>aro</sub> includes C<sub>a1</sub>, C<sub>a2</sub>, C<sub>a3</sub>; H<sub>aro</sub> includes H<sub>a1</sub>, H<sub>a2</sub>, H<sub>a3</sub>

**Table 13.** Harmonic angle potential

<b>Angles</b>	<b><math>K_{angle}</math></b> (kJ mol <sup>-1</sup> rad <sup>-2</sup> )	<b><math>\theta_{ijk}^0</math></b> (deg)
C <sub>aro</sub> -C <sub>aro</sub> -C <sub>aro</sub>	527.18	120.00
C <sub>aro</sub> -C <sub>aro</sub> -H <sub>aro</sub>	292.88	120.00
H <sub>aro</sub> -C <sub>aro</sub> -N	292.88	116.00
C <sub>aro</sub> -N-C <sub>aro</sub>	585.76	117.00
N-C <sub>aro</sub> -C <sub>b</sub>	585.76	116.00
C <sub>aro</sub> -C <sub>aro</sub> -C <sub>b</sub>	376.60	120.0
C <sub>b2</sub> -C <sub>b</sub> -C <sub>aro</sub>	482.30	109.45
C <sub>aro</sub> -C <sub>b</sub> -H <sub>4</sub>	366.90	109.45
C <sub>b2</sub> -C <sub>b</sub> -C <sub>b2</sub>	482.30	109.45
C <sub>b</sub> -C <sub>b2</sub> -C <sub>b</sub>	482.30	109.45
C <sub>b2</sub> -C <sub>b</sub> -H <sub>4</sub>	366.90	109.45
C <sub>b</sub> -C <sub>b2</sub> -H <sub>4</sub>	366.90	109.45
H <sub>4</sub> -C <sub>b2</sub> -H <sub>4</sub>	306.40	109.45

\*C<sub>aro</sub> includes C<sub>a1</sub>, C<sub>a2</sub>, C<sub>a3</sub>; H<sub>aro</sub> includes H<sub>a1</sub>, H<sub>a2</sub>, H<sub>a3</sub>

**Table 14.** Ryckaert-Bellemans dihedral potential (for atoms in pyridine ring)

Dihedrals	C <sub>0</sub>	C <sub>1</sub>	C <sub>2</sub>	C <sub>3</sub>	C <sub>4</sub>	C <sub>5</sub>
A <sub>aro</sub> -A <sub>aro</sub> -A <sub>aro</sub> -A <sub>aro</sub>	30.334	0	-30.334	0	0	0
A <sub>aro</sub> -A <sub>aro</sub> -A <sub>aro</sub> -H <sub>aro</sub>	30.334	0	-30.334	0	0	0
C <sub>a1</sub> -C <sub>b</sub> -C <sub>b2</sub> -H <sub>4</sub>	0.9665	2.8995	0	-3.8660	0	0
C <sub>a1</sub> -C <sub>b</sub> -C <sub>b2</sub> -C <sub>b</sub>	2.9288	-1.4644	0.2092	-1.6736	0	0

\*A<sub>aro</sub> includes C<sub>a1</sub>, C<sub>a2</sub>, C<sub>a3</sub>, N; H<sub>aro</sub> includes H<sub>a1</sub>, H<sub>a2</sub>, H<sub>a3</sub>

**Table 15.** Proper and improper dihedral potential. The angle  $\Phi_{ijkl}$  is considered 180.0 deg for all listed dihedral angles reported in table

Dihedrals	<i>K</i> <sub>dihedral</sub> (kJ mol <sup>-1</sup> rad <sup>-2</sup> )	Multiplicity (n)
C <sub>b2</sub> -C <sub>b</sub> -C <sub>b2</sub> -C <sub>b</sub>	6.00	3
C <sub>b</sub> -C <sub>b2</sub> -C <sub>b</sub> -C <sub>b2</sub>	6.00	3
H <sub>4</sub> -C <sub>b</sub> -C <sub>b2</sub> -C <sub>b</sub>	6.00	3
H <sub>a2</sub> -C <sub>a2</sub> -C <sub>a3</sub> -C <sub>a1</sub>	10.46	2
H <sub>a3</sub> -C <sub>a3</sub> -C <sub>a2</sub> -C <sub>a2</sub>	10.46	2
H <sub>a1</sub> -C <sub>a1</sub> -N-C <sub>a2</sub>	10.46	2

**Table 16.** Lennard-Jones parameters and charge assignment to the atom type

Atom types	$\sigma$ (Å)	$\epsilon$ (kJ mol <sup>-1</sup> )	$q_i$
N	0.325	0.711	-0.678
C <sub>a1</sub>	0.355	0.293	0.473
C <sub>a2</sub>	0.355	0.293	-0.447
C <sub>a3</sub>	0.355	0.293	0.227
H <sub>a1</sub>	0.242	0.126	0.012
H <sub>a2</sub>	0.242	0.126	0.155
H <sub>a3</sub>	0.242	0.126	0.065
C <sub>b</sub>	0.321	0.352	0.012
C <sub>b2</sub>	0.321	0.352	0
H <sub>4</sub>	0.232	0.318	0

## 5.2 Simulation Details

The PF-MD simulations have been performed with OCCAM software package.<sup>34</sup> The simulations have been conducted in the *NVT* ensemble at 293 K, by keeping the temperature constant through the Andersen thermostat.<sup>35</sup> A time step of 1 fs was employed in all the simulations. Within the PF-MD framework, the smooth coarse-grained density function  $\phi_K(\mathbf{r})$ , is calculated using a mesh-based approach. In particular, by varying the mesh size  $l$ , different level of coarsening of the density were obtained. In particular we used three different grid sizes: 0.8, 0.4 and 0.2 nm, in relaxation procedure of P2VP10 (10 monomers) melt, while, for P2VP48 (48 monomers) system an additional grid size of 2.5 nm was employed. The standard MD simulations were performed with GROMACS software<sup>36</sup> first in the *NVT* and then in the *NPT* ensemble for 5 and 200 ns, respectively. The temperature was held constant at 293 K by means of a velocity rescale algorithm<sup>37</sup> with a coupling constant  $\tau_T = 0.02$  ps while the pressure was held constant at 1.013 bar using the Berendsen algorithm<sup>38</sup> with a coupling constant  $\tau_P = 0.2$  ps. A time step of 2 fs was employed in all simulations. A cutoff distance of 1 nm was used for both van der Waals and Coulomb interactions. The non-bonded interactions were excluded between first and third neighbors. In addition, non-bonded interactions among atoms within an aromatic ring were excluded. The LINCS constraint algorithm<sup>39</sup> was employed to fix all the distances involving hydrogen atoms and between the

carbons of the backbone. The constraint between backbone carbons were removed in simulations where the only OPLS-AA force field was used alone.

**Table 17** System composition for the simulated systems. The temperature of all the systems is 293K. The MD label indicates a standard molecular dynamics simulation

<b>System</b>	<b>Grid size (nm)</b>	<b>Nr. monomers</b>	<b>Nr. chains</b>	<b>Total nr. Particles</b>	<b>Time (ns)</b>
P2VP10	0.8	10	38	5776	5
	0.4	10	38	5776	5
	0.2	10	38	5776	5
	MD	10	38	5776	200
P2VP48	2.5	48	12	8664	5
	0.8	48	12	8664	25
	0.4	48	12	8664	40
	0.2	48	12	8664	200
	MD*	48	12	8664	200

\* The system has been simulated at both 293 and 303 K

## 5.3 Results and Discussion

### 5.3.1 Relaxation of Atactic P2VP Melt with PF-MD Method

Equilibration of polymer melts is a challenging task, even for low  $M_w$ .<sup>40,41,42</sup> Moreover, a further technical problem of MD simulations is connected to the setup and the obtainment of a suitable initial set of coordinates of polymer melt systems. This is principally due to the large number of atom overlaps, at typical melt density, which causes divergence of force calculations in a MD simulation. In order to avoid such technical problem, in these simulations, we applied a well-tested and validated procedure based on PF-MD.<sup>43</sup> In particular, the procedure employed was the following:

- I) The initial configurations of two P2VP melt systems, having different molecular weights (10 and 48 repeating units, P2VP10 and P2VP48, respectively) were generated by randomly distributing the chains' center of mass in the simulation box. The initial density of the systems was set at the experimental value at 293 K;
- II) For the P2VP10 case, three sequential relaxations runs were performed at 293 K. In particular, a first relaxation, lasting 5 ns, was performed using a grid size  $l = 0.8 \text{ nm}$ , a value that is close to the radius of gyration (Rg) of the polymer chain. Then, two subsequent relaxation, using smaller grid sizes of  $l = 0.4$  and  $0.2 \text{ nm}$ , were performed.
- III) Starting from the last configurations of the PF-MD simulations with the smallest grid size, a short minimization to remove residual

atoms superpositions was executed, followed by a short MD simulation (*NVT* at 293 K) of 5 ns, and *NPT* production runs (200 ns). In case of P2VP48, an additional grid size of  $l = 2.5 \text{ nm}$  (close to  $R_g$ ), was used in the first instance. Then, three subsequent runs were performed by using the same grid sizes employed in the P2VP10 case.

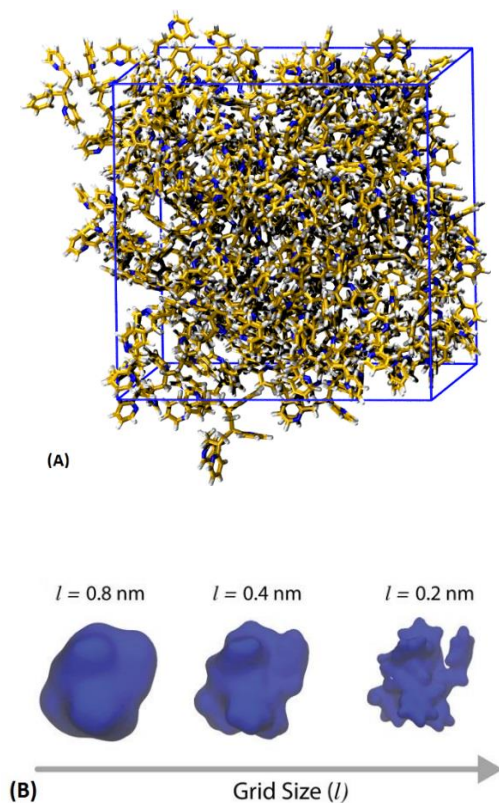


**Figure 37.** (A) Snapshot of the P2VP10 from the equilibrated MD simulation. The nitrogen atom is depicted in blue, the carbons in orange and hydrogens atoms in white. (B) Density isosurfaces (the density is equal to  $\rho_0 = N_{\text{particles}}/V_{\text{box}}$ ) calculated from density fields of a single P2VP10 chain using grids of different resolution ( $l = 0.8 \text{ nm}$ ,  $l = 0.4 \text{ nm}$ ,  $l = 0.2 \text{ nm} \sim \text{atom size}$ ).

In order to correctly apply the relaxation procedure to obtain well-relaxed polymer melt, we analyzed different quantities. In particular, since the equilibrium condition is reached when the diffusion of the chains center of mass covers a length equal or greater than its  $R_g$  (0.8 nm for P2VP10 and 2.5 nm for P2VP48), we computed the root-mean square displacements (RMSD) of the center of mass, as reported in Figure 38, from which it is results that this condition is achieved for both chain lengths. The RMSD is calculated according to the definition reported in the Eq. 33:

$$\text{MSD} \equiv \langle [r(t_0 + t) - r(t_0)]^2 \rangle \quad (33)$$

The angle brackets denote an ensemble average over all the molecules in the system and all the time origins. By time origins, we mean that any timestep can be considered as the time  $t_0$  in the Eq. 33. As shown in the figure, this quantity is calculated at different time origins to make evident that the dynamic is time translational invariant.

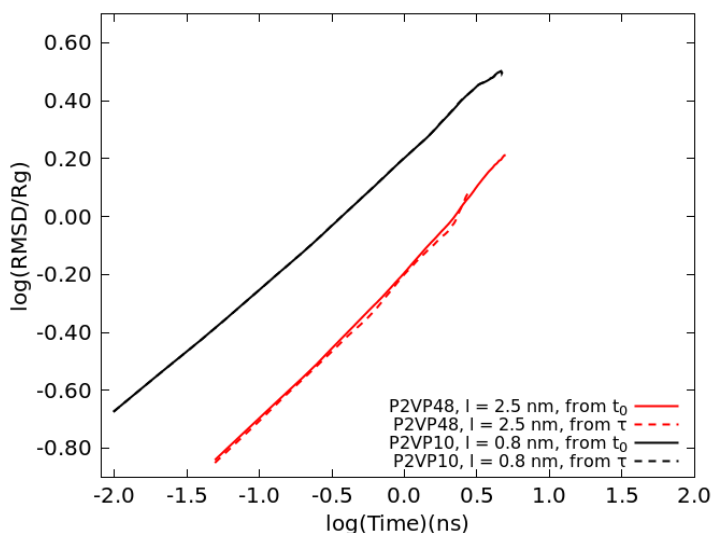


**Figure 38.** Root mean square displacement of the center of mass of the chains (normalized by  $R_g$ ) for P2VP10 and P2VP48, at grid sizes  $l = 0.8 \text{ nm}$  and  $l = 2.5 \text{ nm}$  respectively. Dashed lines are referred to time origins  $\tau$  corresponding to the time necessary to the RMSD to attain the  $R_g$  value.

Different grid sizes provide relaxation of the polymer chains at different scales, as described in the Ref.<sup>44</sup> Indeed, by analyzing the autocorrelation function (ACF) of the end-to-end vector distance, we can verify the relaxation time in which independent chain conformations are explored. In Figure 39, the ACF calculated for PF-MD simulations are reported. As for the RMSD case, also the ACF is calculated at two different time origins. A fast decay to zero of the ACF is observed for all the grid sizes  $l$ . In particular, slower decays are observed as the grid size is decreased. This fact, also observed for the RMSD of the chains center of mass, is due to a decreased smoothness

of the intermolecular potential as the grid becomes finer, since increased detail on the polymer structure is added.<sup>44</sup>

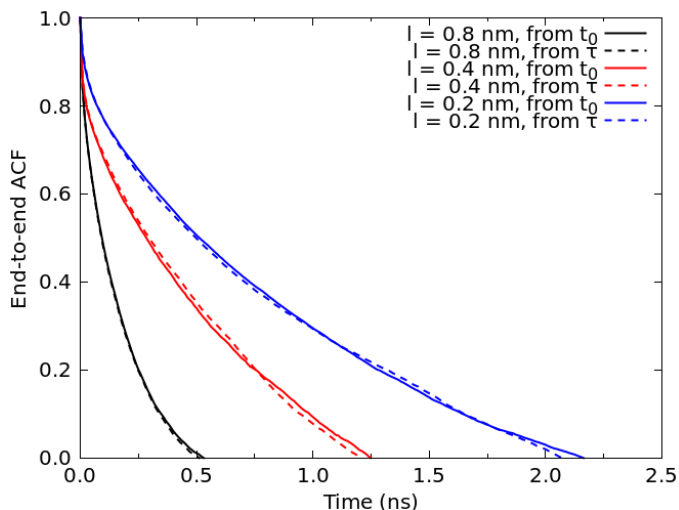


**Figure 39.** End-to-end vector autocorrelation function calculated from PF-MD simulations for P2VP10. Lines with different colors correspond to different grid sizes  $l$ . Dashed lines are referred to time origin  $\tau$  corresponding to the time necessary to the RMSD to attain the  $R_g$  value.

The relaxation time  $\tau$  of the end-to-end vector was evaluated by fitting its autocorrelation function with a stretched exponential (Eq. 34):

$$\tau = \int_0^{\infty} \exp \left[ - \left( \frac{t}{\alpha} \right)^{\beta} \right] dt = \frac{\alpha}{\beta} \Gamma \left( \frac{1}{\beta} \right) \quad (34)$$

Table 18 reports the results of the fitting. In the case of PF-MD simulations, the relaxation of a P2VP10 chain occurs in a time interval

going approximately from 0.16 to 0.86 ns, as function of the grid size. A similar behavior is found for the P2VP48. With the finest grid, the dependence of the relaxation time on chain length agrees well with the prediction of the Rouse model where  $\tau \sim N^{3/2}$ :  $(48/10)^{3/2} = 10.5$ , being N the number of monomers.

**Table 18.** Relaxation times of the end-to-end vector

<b>System</b>	<b>Grid size <i>l</i></b> (nm)	<b><math>\tau</math></b> (ps)
P2VP10	0.8	167 ± 3
	0.4	529 ± 9
	0.2	861 ± 11
P2VP48	2.5	225 ± 29
	0.8	1907 ± 142
	0.4	3175 ± 106
	0.2	8398 ± 164

The whole procedure described above, allows to obtain a suitable initial set of coordinates for the P2VP polymer melts in which the chains are directly packed at a density equal to the experimental one. Short-range correlations among atoms, that cannot be reproduced by the PF-MD method, can be easily reintroduced by performing a short standard MD simulation in which the LJ and Coulombic interactions are treated explicitly. In particular, in less than 1 ns the radial distribution functions (RDF) become indistinguishable with respect to RDF calculated after 200 ns (Figure 40 A-B). This full recovery of short-

range correlations was observed also for other polymers that were modelled with the same procedure.<sup>23,43,45</sup>

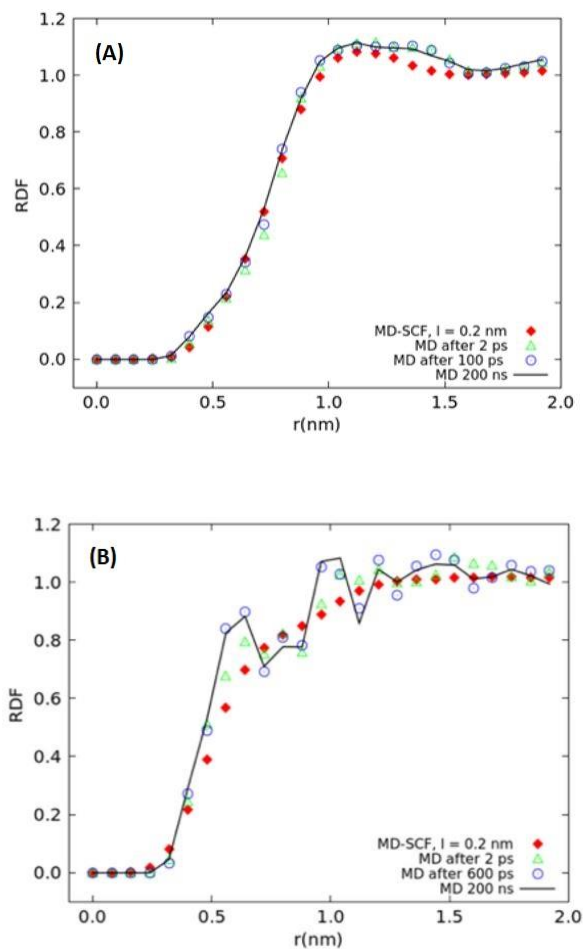


**Figure 40.** Comparison of radial distribution function (RDF) obtained from PF-MD simulations at grid size  $l = 0.2$  nm for P2VP10 (red line) and RDFs from MD simulations at different times. RDFs are calculated among backbone carbon atoms (A) and nitrogen atoms (B) belonging to different chains. Intramolecular correlations are excluded.

### 5.3.2 Structural Properties

To test if the model we proposed was able to reproduce structural experimental properties of P2VP, such as the mass density and X-ray diffraction pattern, MD simulations in the NPT ensemble were performed. In particular, starting from the last configuration obtained from the relaxation procedure (described above), production runs of 200 ns were performed for both P2VP10 and P2VP48, after a short NVT simulation of 5 ns.

The calculated mass densities are compared with the experimental data<sup>46</sup> in Table x8. In particular, an error of about +3.5% for P2VP10 and less than -1% for P2VP48 was found. In particular, the largest error we found (3.5%) is in the range of error 1.8 - 4.2%, which is the typical error interval on densities obtained from simulations performed with the OPLS-AA.<sup>1</sup> In addition to the mass density, also the X-ray diffraction pattern was calculated and compared with the experimental data.<sup>16</sup> In figure 41, a comparison of both X-Ray scattering patterns is reported for the P2VP48. In particular, the experimental X-ray data were measured on a P2VP sample with  $M_w=9$  kg/mol<sup>16</sup>, which corresponds to almost two times the  $M_w$  we simulated (P2VP48). From the comparison of curves in figure 41 it can be observed that the main peaks, at a  $q \sim 8 \text{ nm}^{-1}$  and at  $q \sim 14 \text{ nm}^{-1}$  representing the inter-chains distance and the Van der Waals (VDW) contact between atoms respectively,<sup>16</sup> are centered at similar  $q$  values with the respect to experimental ones. In particular, the

difference in peak positions corresponds to a very small distance difference in real space of about 0.2 Å, suggesting that the X-ray diffraction pattern was well-reproduced in our simulation.

**Table 19.** Calculated densities of P2VP10 and P2VP48

System	Calculated density (g/cm <sup>3</sup> )	Experimental density* (g/cm <sup>3</sup> ) <sup>46</sup>
P2VP10	1.0741 ± 0.0001	1.037 ± 0.002
P2VP48	1.0853 ± 0.0001	1.095 ± 0.003

\*Experimental densities measured from samples with  $M_w$  of 1 kg/mol and 5 kg/mol (corresponding respectively to P2VP10 and P2VP48 in our simulations).

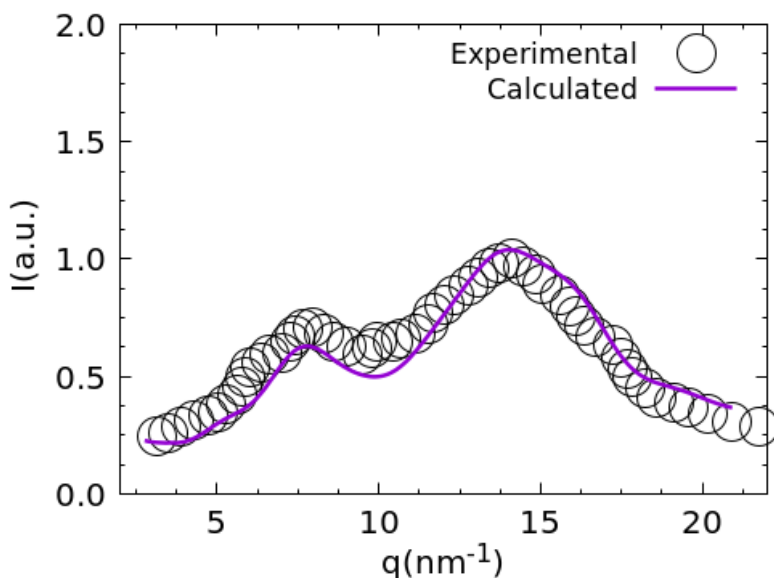


**Figure 41.** Calculated (purple line) and experimental (black circles) X-ray diffraction patterns at 303 K. The intensity has been normalized with respect to the highest peak

Among other structural properties, we calculated also gyration radii ( $R_g$ ). The equilibrium  $R_g$  values obtained from MD simulations calculated for P2VP10 and P2VP48 are 0.62 and 1.51 nm respectively. Comparing our results with the ones obtained from the characteristic ratio of P2VP,<sup>47</sup> which give a value of  $R_g$  equal to 0.632 and 1.414 nm for P2VP10 and P2VP48 chains, we find a good agreement (error range 2-3%). In addition, considering the oligomer of PS with 10 monomers, which has  $M_w$  and structure similar to the ones of P2VP10 the  $R_g$  value (0.68 nm)<sup>29</sup> is comparable with the one obtained from our simulations.

## *5.4 Conclusions*

In this chapter an all-atom model of atactic P2VP has been presented. An efficient relaxation procedure of the P2VP melt, based on hybrid particle-field PF-MD method, has been applied with satisfactory results. The proposed model, based on the OPLS-AA force field, has been tested to reproduce a number of structural properties such as the mass density and X-ray diffraction pattern. In particular, the mass density for the short oligomers (P2VP10) was reproduced within an error of +3.5%, which is in the error range expected from the OPLS-AA force field. For longer polymer chains (P2VP48) the density was reproduced within an error less than -1%, lower than the average error found for the OPLS-AA. Regarding the experimental and calculated X-ray scattering data, we found a good agreement, which

indicates, together with the density mass result, a good description of the structural correlations within the P2VP melt.

Moreover, this model can be used to perform simulations of nanocomposite systems, in which P2VP is present, to further understand and rationalize phenomena that are relevant for technological applications.

### References:

- (1) W. L. Jorgensen, D. S. Maxwell, J. Tirado-Rives, *J. Am. Chem. Soc.* **1996**, *118* (45), 11225–11236.
- (2) J. M. J. Frechet, M. Vivas De Meftahi, *Br. Polym. J.* **1984**, *16*, 193–198.
- (3) U. Borchert, U. Lipprandt, M. Bilanz, A. Kimpfler, A. Rank, R. Peschka-Süss, R. Schubert, P. Lindner, S. Förster, *Langmuir* **2006**, *22* (13), 5843–5847.
- (4) S. G. Jang, A. Khan, C. J. Hawker, E. J. Kramer, *Macromolecules* **2012**, *45* (3), 1553–1561.
- (5) J. E. M. Teoh, Y. Liu, C. K. Chua, S. Yang, J. An, K. F. Leong, W. Y. Yeong, *Virtual Phys. Prototyp.* **2015**, *10* (3), 103–122.
- (6) A. Mitchell, U. Lafont, M. Hołyńska, *Addit. Manuf.* **2018**, *24*, 606–626.
- (7) M. Nadgorny, Z. Xiao, C. Chen, L. A. Connal, *ACS Appl. Mater. Interfaces* **2016**, *8* (42), 28946–28954.
- (8) M. Nadgorny, A. Ameli, *ACS Appl. Mater. Interfaces* **2018**, *10* (21), 17489–17507.
- (9) P. Hou, W. Han, M. Philippi, H. Schäfer, M. Steinhart, *ACS Appl.*

- Nano Mater.* **2018**, *1*, 1413–1419.
- (10) M.Kumar Vyas, K. Schneider, B. Nandan, M. Stamm, *Soft Matter* **2008**, *4*, 1024–1032.
- (11) G. Donati, D. B. Lingerfelt, C. M. Aikens, X. Li, *J. Phys. Chem. C* **2018**, *122*, 10621.
- (12) K.-C. Kao, H. Nishi, T. Tatsuma, *Phys. Chem. Chem. Phys* **2018**, *20*, 3735–3740.
- (13) H. Kim, B.-G. Kang, J. Choi, Z. Sun, M. D. Yu, *Macromolecules* **2018**, *51*, 1181–1188.
- (14) H.-C. Kim, S.-M. Park, W. Hinsberg, *Review. Chem. Rev.* **2010**, *110*, 146–177.
- (15) C. M. Bates, M. J. Maher, D. W. Janes, C. J. Ellison, C. G. Willson, *Macromolecules* **2014**, *47*, 2–12.
- (16) P. Papadopoulos, D. Peristeraki, G. Floudas, G. Koutalas, N. Hadjichristidis, *Macromolecules* **2004**, *37*, 8116–8122.
- (17) B. Du, Z. Wang, X. He, *Adv. Mater. Res.* **2012**, *562*, 123–128.
- (18) A. Soldera, *Mol. Simul.* **2012**, *38*, 762–771.
- (19) Z. Posel, Z. Limpouchova, S. Karel, M. Lísal, K. Procha, *Macromolecules* **2014**, *47*, 2503–2514.
- (20) W. L. Jorgensen, N. A. McDonald, *Journal of Molecular Structure (Theochem)*, **1998**, *424*, 145.
- (21) B. Chen, M. G. Martin, J. I. Siepmann, *J. Phys. Chem. B* **1998**, *102* (14), 2578–2586.
- (22) G. Milano, G. Santangelo, F. Ragone, L. Cavallo, A. Di Matteo, *J. Phys. Chem. C* **2011**, *115* (31), 15154–15163.
- (23) A. De Nicola, R. Avolio, F. Della Monica, G. Gentile, M. Cocca, C. Capacchione, M. E. Errico, G. Milano, *RSC Adv.* **2015**, *5* (87), 71336–71340.

- (24) T. V. M. Nodoro, E. Voyiatzis, A. Ghanbari, D. N. Theodorou, M. C. Böhm, F. Müller-Plathe, *Macromolecules* **2011**, *44* (7), 2316–2327.
- (25) M. Alaghemandi, E. Spohr, *Macromol. Theory Simulations* **2012**, *21* (2), 106–112.
- (26) M. Śniechowski, R. Borek, K. Piwowarczyk, W. Łużny, *Macromol. Theory Simulations* **2015**, *24* (4), 284–290.
- (27) V. Ortiz, S. O. Nielsen, M. L. Klein, D. E. Discher, *J. Polym. Sci. Part B Polym. Phys.* **2006**, *44* (14), 1907–1918.
- (28) C. E. S. Bernardes, A. Joseph, *J. Phys. Chem. A* **2015**, *119* (12), 3023–3034.
- (29) F. Müller-Plathe, *Macromolecules* **1996**, *29*, 4782–4791.
- (30) A. Vitalis, X. Wang, R. V. Pappu, *Biophys. J.* **2007**, *93* (6), 1923–1937.
- (31) K. Kahn, T. C. Bruice, *J. Comput. Chem.* **2002**, *23* (10), 977–996.
- (32) A. Minoia, L. Chen, D. Beljonne, R. Lazzaroni, *Polymer*, **2012**, *53* (24), 5480–5490.
- (33) S. W. I. Siu, K. Pluhackova, R. A. Böckmann, *J. Chem. Theory Comput.* **2012**, *8* (4), 1459–1470.
- (34) Y. Zhao, A. De Nicola, T. Kawakatsu, G. Milano, *J. Comput. Chem.* **2012**, *33*, 868–880.
- (35) H. C. Andersen, *J. Chem. Phys.* **1980**, *72*, 2384–2393.
- (36) H. J. C. Berendsen, D. Van Der Spoel, R. Van Drunen, *Comput. Phys. Commun.* **1995**, *91*, 43–56.
- (37) G. Bussi, D. Donadio, M. Parrinello, *J. Chem. Phys.* **2007**, *126*, 014101.
- (38) H. J. C. Berendsen, J. P. M. Postma, W. F. Van Gunsteren, A. DiNola, J. R. Haak, *J. Chem. Phys.* **1984**, *81*, 3684.

- (39) B. Hess, H. Bekker, H. J. C. Berendsen, J. G. E. M. Fraaije, *J. Comput. Chem.* **1997**, *18* (12), 1463–1472.
- (40) D. Brown, J. H. R. Clarke, M. Okuda, T. Yamazaki, *J. Chem. Phys.* **1994**, *100* (8), 6011–6018.
- (41) G. Milano, F. Müller-Plathe, *J. Phys. Chem. B* **2005**, *109* (39), 18609–18619.
- (42) G. Munaò, A. Pizzirusso, A. Kalogirou, A. De Nicola, T. Kawakatsu, F. Müller-Plathe, G. Milano, *Nanoscale* **2018**, *10*, 21656–21670.
- (43) A. De Nicola, T. Kawakatsu, G. Milano, *J. Chem. Theory Comput.* **2014**, *10*, 5651–5667.
- (44) A. De Nicola, T. Kawakatsu, G. Milano, *J. Chem. Theory Comput.* **2014**, *10*, 5651.
- (45) A. De Nicola, A. Correa, G. Milano, P. La Manna, P. Musto, G. Mensitieri, G. Scherillo, *J. Phys. Chem.* **2017**, *121*, 3162–3176.
- (46) D. N. Voylov, A. P. Holt, B. Doughty, V. Bocharova, H. M. Meyer, S. Cheng, H. Martin, M. Dadmun, A. Kisliuk, A. P. Sokolov, *ACS Macro Lett.* **2017**, *6*, 68–72.
- (47) M. Haizu, C. HongHong, J. LuShi, *Sci. Sin. Chim.* **2012**, *42* (7), 1014.

---

## Appendix

---

A program written in Fortran 90 is reported below, which is able to generate coordinate files of single polymer chains, for polyethylene, polypropylene, polystyrene and poly(2-vinylpyridine). Chains can be obtained both in all-atom and united atom representations. Moreover, for polymers with a substituent, it is possible to obtain atactic, isotactic and syndiotactic chains. The possibility to obtain completely stretched or random conformation chains is also available.

The only input file needed is a Z – matrix fragment of few repetitive units of a chain (reported below for different types of polymers).

### *Z - Matrix United Atom Polyethylene*

```
C 0.00 0 0.00 0 0.00 0 0 0 0
C 1.54 0 0.00 0 0.00 0 1 0 0
C 1.54 0 109.05 0 0.00 0 2 1 0
C 1.54 0 109.05 0 180.00 0 3 2 1
```

### *Z - Matrix All-Atom Polyethylene*

```
C 0.00 0 0.00 0 0.00 0 0 0 0
C 1.54 0 0.00 0 0.00 0 1 0 0
H 1.10 0 110.00 0 0.00 0 1 2 0
H 1.10 0 110.00 0 120.00 0 1 2 3
C 1.54 0 109.05 0 180.00 0 2 1 3
H 1.10 0 110.00 0 120.00 0 2 1 5
H 1.10 0 110.00 0 -120.00 0 2 1 5
```

C	1.54	0	109.05	0	180.00	0	5	2	1
C	1.54	0	109.05	0	180.00	0	8	5	2
H	1.10	0	110.00	0	120.00	0	5	2	8
H	1.10	0	110.00	0	-120.00	0	5	2	8
H	1.10	0	110.00	0	120.00	0	8	5	9
H	1.10	0	110.00	0	-120.00	0	8	5	9
C	1.54	0	109.05	0	180.00	0	9	8	5
C	1.54	0	109.05	0	180.00	0	14	9	8
H	1.10	0	110.00	0	120.00	0	9	8	14
H	1.10	0	110.00	0	-120.00	0	9	8	14
H	1.10	0	110.00	0	120.00	0	14	9	15
H	1.10	0	110.00	0	-120.00	0	14	9	15

*Z - Matrix United Atom Polypropylene*

C	0.00	0	0.00	0	0.00	0	0	0	0
C	1.54	0	0.00	0	0.00	0	1	0	0
C	1.54	0	109.05	0	0.00	0	2	1	0
C	1.54	0	110.00	0	-120.00	0	2	1	3
C	1.54	0	110.00	0	180.00	0	3	2	1
C	1.54	0	110.00	0	180.00	0	5	3	2
C	1.54	0	110.00	0	-120.00	0	5	3	6
C	1.54	0	110.00	0	180.00	0	6	5	3
C	1.54	0	110.00	0	180.00	0	8	6	5
C	1.54	0	110.00	0	-120.00	0	8	6	9

*Z - Matrix All-Atom Polypropylene*

C	0.00	0	0.00	0	0.00	0	0	0	0
C	1.54	0	0.00	0	0.00	0	1	0	0
H	1.10	0	110.00	0	0.00	0	1	2	0
H	1.10	0	110.00	0	120.00	0	1	2	3
C	1.54	0	109.05	0	180.00	0	2	1	3
H	1.10	0	110.00	0	120.00	0	2	1	5
C	1.54	0	110.00	0	-120.00	0	2	1	5
H	1.10	0	110.00	0	60.00	0	7	2	1
H	1.10	0	110.00	0	180.00	0	7	2	1
H	1.10	0	110.00	0	300.00	0	7	2	1
C	1.54	0	109.05	0	180.00	0	5	2	1
C	1.54	0	109.05	0	180.00	0	11	5	2
H	1.10	0	110.00	0	120.00	0	5	2	11
H	1.10	0	110.00	0	-120.00	0	5	2	11

H	1.10	0	110.00	0	120.00	0	11	5	12
C	1.54	0	110.00	0	-120.00	0	11	5	12
H	1.10	0	110.00	0	60.00	0	16	11	5
H	1.10	0	110.00	0	180.00	0	16	11	5
H	1.10	0	110.00	0	300.00	0	16	11	5
C	1.54	0	109.05	0	180.00	0	12	11	5
C	1.54	0	109.05	0	180.00	0	20	12	11
H	1.10	0	110.00	0	120.00	0	12	11	20
H	1.10	0	110.00	0	-120.00	0	12	11	20
H	1.10	0	110.00	0	120.00	0	20	12	21
C	1.54	0	110.00	0	-120.00	0	20	12	21
H	1.10	0	110.00	0	60.00	0	25	20	12
H	1.10	0	110.00	0	180.00	0	25	20	12
H	1.10	0	110.00	0	300.00	0	25	20	12

*Z - Matrix United Atom Polystyrene*

C	0.00	0	0.00	0	0.00	0	0	0	0
C	1.54	0	0.00	0	0.00	0	1	0	0
C	1.54	0	109.05	0	0.00	0	2	1	0
C	1.54	0	110.00	0	-120.00	0	2	1	3
C	1.38	0	120.00	0	60.00	0	4	2	1
C	1.38	0	120.00	0	180.00	0	5	4	2
C	1.38	0	120.00	0	0.00	0	6	5	4
C	1.38	0	120.00	0	0.00	0	7	6	5
C	1.38	0	120.00	0	0.00	0	8	7	6
C	1.54	0	109.05	0	180.00	0	3	2	1
C	1.54	0	109.05	0	180.00	0	10	3	2
C	1.54	0	110.00	0	-120.00	0	10	3	11
C	1.38	0	120.00	0	60.00	0	12	10	3
C	1.38	0	120.00	0	180.00	0	13	12	10
C	1.38	0	120.00	0	0.00	0	14	13	12
C	1.38	0	120.00	0	0.00	0	15	14	13
C	1.38	0	120.00	0	0.00	0	16	15	14
C	1.54	0	109.05	0	180.00	0	11	10	3
C	1.54	0	109.05	0	180.00	0	18	11	10
C	1.54	0	110.00	0	-120.00	0	18	11	19
C	1.38	0	120.00	0	60.00	0	20	18	11
C	1.38	0	120.00	0	180.00	0	21	20	18
C	1.38	0	120.00	0	0.00	0	22	21	20
C	1.38	0	120.00	0	0.00	0	23	22	21
C	1.38	0	120.00	0	0.00	0	24	23	22

### Z - Matrix All-Atom Polystyrene

C	0.00	0	0.00	0	0.00	0	0	0	0
C	1.54	0	0.00	0	0.00	0	1	0	0
H	1.10	0	110.00	0	0.00	0	1	2	0
H	1.10	0	110.00	0	120.00	0	1	2	3
C	1.54	0	109.05	0	180.00	0	2	1	3
H	1.10	0	110.00	0	120.00	0	2	1	5
C	1.54	0	110.00	0	-120.00	0	2	1	5
C	1.38	0	120.00	0	60.00	0	7	2	1
H	1.10	0	120.00	0	0.00	0	8	7	2
C	1.38	0	120.00	0	180.00	0	8	7	2
H	1.10	0	120.00	0	180.00	0	10	8	7
C	1.38	0	120.00	0	0.00	0	10	8	7
H	1.10	0	120.00	0	180.00	0	12	10	8
C	1.38	0	120.00	0	0.00	0	12	10	8
H	1.10	0	120.00	0	180.00	0	14	12	10
C	1.38	0	120.00	0	0.00	0	14	12	10
H	1.10	0	120.00	0	180.00	0	16	14	12
C	1.54	0	109.05	0	180.00	0	5	2	1
C	1.54	0	109.05	0	180.00	0	18	5	2
H	1.10	0	110.00	0	120.00	0	5	2	18
H	1.10	0	110.00	0	-120.00	0	5	2	18
H	1.10	0	110.00	0	120.00	0	18	5	19
C	1.54	0	110.00	0	-120.00	0	18	5	19
C	1.38	0	120.00	0	60.00	0	23	18	5
H	1.10	0	120.00	0	0.00	0	24	23	18
C	1.38	0	120.00	0	180.00	0	24	23	18
H	1.10	0	120.00	0	180.00	0	26	24	23
C	1.38	0	120.00	0	0.00	0	26	24	23
H	1.10	0	120.00	0	180.00	0	28	26	24
C	1.38	0	120.00	0	0.00	0	28	26	24
H	1.10	0	120.00	0	180.00	0	30	28	26
C	1.38	0	120.00	0	0.00	0	30	28	26
H	1.10	0	120.00	0	180.00	0	32	30	28
C	1.54	0	109.05	0	180.00	0	19	18	5
C	1.54	0	109.05	0	180.00	0	34	19	18
H	1.10	0	110.00	0	120.00	0	19	18	34
H	1.10	0	110.00	0	-120.00	0	19	18	34
H	1.10	0	110.00	0	120.00	0	34	19	35
C	1.54	0	110.00	0	-120.00	0	34	19	35
C	1.38	0	120.00	0	60.00	0	39	34	19
H	1.10	0	120.00	0	0.00	0	40	39	34
C	1.38	0	120.00	0	180.00	0	40	39	34

H	1.10	0	120.00	0	180.00	0	42	40	39
C	1.38	0	120.00	0	0.00	0	42	40	39
H	1.10	0	120.00	0	180.00	0	44	42	40
C	1.38	0	120.00	0	0.00	0	44	42	40
H	1.10	0	120.00	0	180.00	0	46	44	42
C	1.38	0	120.00	0	0.00	0	46	44	42
H	1.10	0	120.00	0	180.00	0	48	46	44

*Z - Matrix United Atom Poly(2-vinylpyridine)*

C	0.00	0	0.00	0	0.00	0	0	0	0
C	1.54	0	0.00	0	0.00	0	1	0	0
C	1.54	0	109.05	0	0.00	0	2	1	0
C	1.54	0	110.00	0	-120.00	0	2	1	3
C	1.38	0	120.00	0	60.00	0	4	2	1
C	1.38	0	120.00	0	180.00	0	5	4	2
C	1.38	0	120.00	0	0.00	0	6	5	4
C	1.38	0	120.00	0	0.00	0	7	6	5
N	1.38	0	120.00	0	0.00	0	8	7	6
C	1.54	0	109.05	0	180.00	0	3	2	1
C	1.54	0	109.05	0	180.00	0	10	3	2
C	1.54	0	110.00	0	-120.00	0	10	3	11
C	1.38	0	120.00	0	60.00	0	12	10	3
C	1.38	0	120.00	0	180.00	0	13	12	10
C	1.38	0	120.00	0	0.00	0	14	13	12
C	1.38	0	120.00	0	0.00	0	15	14	13
N	1.38	0	120.00	0	0.00	0	16	15	14
C	1.54	0	109.05	0	180.00	0	11	10	3
C	1.54	0	109.05	0	180.00	0	18	11	10
C	1.54	0	110.00	0	-120.00	0	18	11	19
C	1.38	0	120.00	0	60.00	0	20	18	11
C	1.38	0	120.00	0	180.00	0	21	20	18
C	1.38	0	120.00	0	0.00	0	22	21	20
C	1.38	0	120.00	0	0.00	0	23	22	21
N	1.38	0	120.00	0	0.00	0	24	23	22

*Z - Matrix All-Atom Poly(2-vinylpyridine)*

C	0.00	0	0.00	0	0.00	0	0	0	0
C	1.54	0	0.00	0	0.00	0	1	0	0
H	1.10	0	110.00	0	0.00	0	1	2	0
H	1.10	0	110.00	0	120.00	0	1	2	3

C	1.54	0	109.05	0	180.00	0	2	1	3
H	1.10	0	110.00	0	120.00	0	2	1	5
C	1.54	0	110.00	0	-120.00	0	2	1	5
C	1.38	0	120.00	0	60.00	0	7	2	1
H	1.10	0	120.00	0	0.00	0	8	7	2
C	1.38	0	120.00	0	180.00	0	8	7	2
H	1.10	0	120.00	0	180.00	0	10	8	7
C	1.38	0	120.00	0	0.00	0	10	8	7
H	1.10	0	120.00	0	180.00	0	12	10	8
C	1.38	0	120.00	0	0.00	0	12	10	8
H	1.10	0	120.00	0	180.00	0	14	12	10
N	1.38	0	120.00	0	0.00	0	14	12	10
C	1.54	0	109.05	0	180.00	0	5	2	1
C	1.54	0	109.05	0	180.00	0	17	5	2
H	1.10	0	110.00	0	120.00	0	5	2	17
H	1.10	0	110.00	0	-120.00	0	5	2	17
H	1.10	0	110.00	0	120.00	0	17	5	18
C	1.54	0	110.00	0	-120.00	0	17	5	18
C	1.38	0	120.00	0	60.00	0	22	17	5
H	1.10	0	120.00	0	0.00	0	23	22	17
C	1.38	0	120.00	0	180.00	0	23	22	17
H	1.10	0	120.00	0	180.00	0	25	23	22
C	1.38	0	120.00	0	0.00	0	25	23	22
H	1.10	0	120.00	0	180.00	0	27	25	23
C	1.38	0	120.00	0	0.00	0	27	25	23
H	1.10	0	120.00	0	180.00	0	29	27	25
N	1.38	0	120.00	0	0.00	0	29	27	25
C	1.54	0	109.05	0	180.00	0	18	17	5
C	1.54	0	109.05	0	180.00	0	32	18	17
H	1.10	0	110.00	0	120.00	0	18	17	32
H	1.10	0	110.00	0	-120.00	0	18	17	32
H	1.10	0	110.00	0	120.00	0	32	18	33
C	1.54	0	110.00	0	-120.00	0	32	18	33
C	1.38	0	120.00	0	60.00	0	37	32	18
H	1.10	0	120.00	0	0.00	0	38	37	32
C	1.38	0	120.00	0	180.00	0	38	37	32
H	1.10	0	120.00	0	180.00	0	40	38	37
C	1.38	0	120.00	0	0.00	0	40	38	37
H	1.10	0	120.00	0	180.00	0	42	40	38
C	1.38	0	120.00	0	0.00	0	42	40	38
H	1.10	0	120.00	0	180.00	0	44	42	40
N	1.38	0	120.00	0	0.00	0	44	42	40

The output of the code is a .mop file (internal coordinates, Z - matrix) of a polymer chain with a variable number of repetitive units. The file can be easily converted from .mop to other formats using Open Babel (N. M. O'Boyle, M. Banck, C. A. James, C. Morley, and G. R. Hutchison T. Vandermeersch. "Open Babel: An Open Chemical Toolbox." *Journal of Cheminformatics*, **2011**, 3,2011 33)

The whole code is written below.

```
!!!! THIS PROGRAM WRITES THE Z-MATRIX OF SEVERAL POLYOLEFINS !!!!
```

```
program polymers
```

```
  implicit none
```

```
  interface
```

```
    subroutine ata(n,s)
      real,allocatable::s(:)
    end subroutine ata
```

```
    subroutine syndio(n,s)
      real,allocatable::s(:)
    end subroutine syndio
```

```
    subroutine PE(n,lab,x,i,phi,k,theta,l,d,e,f)
      character,allocatable::lab(:)
      integer,allocatable::i(:),k(:),l(:),d(:),e(:),f(:)
      real,allocatable::x(:),phi(:),theta(:)
    end subroutine PE
```

```
    subroutine hydroPE(n,lab,x,i,phi,k,theta,l,d,e,f)
      character,allocatable::lab(:)
      integer,allocatable::i(:),k(:),l(:),d(:),e(:),f(:)
      real,allocatable::x(:),phi(:),theta(:)
    end subroutine hydroPE
```

```
    subroutine PP(n,lab,x,i,phi,k,theta,l,d,e,f)
      character,allocatable::lab(:)
      integer,allocatable::i(:),k(:),l(:),d(:),e(:),f(:)
      real,allocatable::x(:),phi(:),theta(:)
    end subroutine PP
```

```
    subroutine hydroPP(n,lab,x,i,phi,k,theta,l,d,e,f)
      character,allocatable::lab(:)
```



```

else if (index.eq.2)then
  write(*,*)" Polypropilene chosen. Hydrogens (1) or not (0)"
  read(*,*) choice
  if (choice.eq.1) then
    max_mem=9*n+2
  else if (choice.eq.0) then
    max_mem=3*n
  else
    end if
end if

else if (index.eq.3)then
  write(*,*)"Polystirene (1), poly(2-vinylpyridine) (2)"
  read(*,*)index2
  write(*,*)" Aromatic ring chosen. Hydrogens (1) or not (0)"
  read(*,*) choice
  if (choice.eq.1.and.index2.eq.1) then
    max_mem=16*n+2
  else if (choice.eq.1.and.index2.eq.2) then
    max_mem=16*n+2
  else if (choice.eq.0)then
    max_mem=8*n
  end if
end if

write(*,*)"Stretched (1) of random chain (0)"
read(*,*)index3

allocate(d(max_mem))
allocate(e(max_mem))
allocate(f(max_mem))
allocate(i(max_mem))
allocate(k(max_mem))
allocate(l(max_mem))
allocate(x(max_mem))
allocate(phi(max_mem))
allocate(theta(max_mem))
allocate(lab(max_mem))
allocate(o(n))

!##### PE
#####
#####

if (index.eq.1.and.choice.eq.0) then

  call PE(n,lab,x,i,phi,k,theta,l,d,e,f)

!!!!!!!!!!!!!!!!!!!!!!!!!!!!!!!!!!!!!!!!!!!!!!!!!!!! CONFORMATION OF THE
CHAIN !!!!!!!!!!!!!!!!!!!!!!!!!!!!!!!!!!!!!!!!!!!!!!!!!!!!!!!!!!!!!!!!!!!!!
  if(index3.eq.0)then

    call init_random_seed
    call random_number(o)

```





```

        theta(3*p+3)= 40.0d00+o(p)*120.0d00
    end do

else if(index3.eq.1)then
    write(*,*)"stretched chain"

else

end if

!##### PP WITH HYDROGENS
#####
##

else if (index.eq.2.and.choice.eq.1) then

    call hydroPP(n,lab,x,i,phi,k,theta,l,d,e,f)

!!!!!! TACTICITY OF THE CHAIN
!!!!!!

write(*,*)"Atactic(0), isotactic(1) or syndiotactic(2) polymer?"
read(*,*)choice2

if(choice2.eq.1)then

    write(*,*)"ISOTACTIC POLYMER"

else if(choice2.eq.0)then

    call ata(n,s)

    do p=1,n-1

        if(s(p).eq.-1)then
            theta(9*p-2)=-theta(9*p-2)
            theta(9*p-3)=-theta(9*p-3)
        end if

    end do

    if(s(n).eq.-1)then
        theta(9*n-3)=-theta(9*n-3)
        theta(9*n-4)=-theta(9*n-4)
    end if

    write(*,*)"ATACTIC POLYMER"

else if(choice2.eq.2)then

    call syndio(n,s)

    do p=1,n-1

```





```

        theta(8*p+3)= 40.0d00+o(p)*120.0d00
    end do

    else if(index3.eq.1)then
        write(*,*)"stretched chain"

    else

    end if

##### PS WITH HYDROGENS
#####

    else if (index.eq.3.and.index2.eq.1.and.choice.eq.1) then

        call hydroPS(n,lab,x,i,phi,k,theta,l,d,e,f)

!!!!!!!!!!!!!!!!!!!!!!!!!!!!!!!!!!!!!!!!!!!! TACTICITY OF THE CHAIN
!!!!!!!!!!!!!!!!!!!!!!!!!!!!!!!!!!!!!!!!!!!!
!!!!!!

    write(*,*)"Atactic(0), isotactic(1) or syndiotactic(2) polymer?"
    read(*,*)choice2

    if(choice2.eq.1)then

        write(*,*)"ISOTACTIC POLYMER"

    else if(choice2.eq.0)then

        call ata(n,s)

        do p=1,n-1

            if(s(p).eq.-1)then
                theta(16*p-9)=-theta(16*p-9)
                theta(16*p-8)=-theta(16*p-8)
                theta(16*p-10)=-theta(16*p-10)
            end if

        end do

        if(s(n).eq.-1)then
            theta(16*n-10)=-theta(16*n-10)
            theta(16*n-9)=-theta(16*n-9)
            theta(16*n-11)=-theta(16*n-11)
        end if

        write(*,*)"ATACTIC POLYMER"

    else if(choice2.eq.2)then

        call syndio(n,s)

```





```

do p=1,n-2
  theta(8*p+3)=40.0d00+o(p)*120.0d00
end do

else if(index3.eq.1)then
  write(*,*)"stretched chain"

else

end if

##### P2VP WITH HYDROGENS
#####
#####

else if (index.eq.3.and.index2.eq.2.and.choice.eq.1) then

  call hydroP2VP(n,lab,x,i,phi,k,theta,l,d,e,f)

!!!!!!!!!!!!!!!!!!!!!!!!!!!!!!!!!!!!!!!!!!!!!!!!!!!! TACTICITY OF THE CHAIN
!!!!!!!!!!!!!!!!!!!!!!!!!!!!!!!!!!!!!!!!!!!!!!!!!!!!
!!!!!!

write(*,*)"Atactic(0), isotactic(1) or syndiotactic(2) polymer?"
read(*,*)choice2

if(choice2.eq.1)then

  write(*,*)"ISOTACTIC POLYMER"

else if(choice2.eq.0)then

  call ata(n,s)

  do p=1,n-1

    if(s(p).eq.-1)then
      theta(15*p-8)=-theta(15*p-8)
      theta(15*p-7)=-theta(15*p-7)
      theta(15*p-9)=-theta(15*p-9)
    end if

  end do

  if(s(n).eq.-1)then
    theta(15*n-9)=-theta(15*n-9)
    theta(15*n-8)=-theta(15*n-8)
    theta(15*n-10)=-theta(15*n-10)
  end if

  write(*,*)"ATACTIC POLYMER"

else if(choice2.eq.2)then

  call syndio(n,s)

```



```

end program polymers

!!!!!!!!!!!!!!!!!!!!!!!!!!!!!!!!!!!!!!!!!!!!!!!!!!!!!!!!!!!!!!!!!!!!!!!!!!!!!!
!!!!!!!!!!!!!!!!!!!!!!!!!!!!!!!!!!!!!!!!!!!!!!!!!!!!!!!!!!!!!!!!!!!!!!!!!!!!!!
!!!!!!!!!!!!!!!!!!!!!!!!!!!!

subroutine hydroP2VP(n,lab,x,i,phi,k,theta,l,d,e,f)

    implicit none

    integer::m,j,p
    integer,intent(in)::n
    character,allocatable,intent(out)::lab(:)
    integer,allocatable,intent(out)::i(:),k(:),l(:),d(:),e(:),f(:)
    real,allocatable,intent(out)::x(:),phi(:),theta(:)

    open(UNIT=1,FILE='hydroP2VP.mop',STATUS='old')
    open(UNIT=2,FILE='matrice.mop',STATUS='unknown')
    write(2,*)
    write(2,*)
    write(2,*)
    do j=1,46

read(1,*)lab(j),x(j),i(j),phi(j),k(j),theta(j),l(j),d(j),e(j),f(j)
    end do

    do m=3,n-2

        lab(15*m+2)=lab(17)
        lab(15*m+3)=lab(18)
        lab(15*m+4)=lab(19)
        lab(15*m+5)=lab(20)
        lab(15*m+6)=lab(21)
        lab(15*m+7)=lab(22)
        lab(15*m+8)=lab(23)
        lab(15*m+9)=lab(24)
        lab(15*m+10)=lab(25)
        lab(15*m+11)=lab(26)
        lab(15*m+12)=lab(27)
        lab(15*m+13)=lab(28)
        lab(15*m+14)=lab(29)
        lab(15*m+15)=lab(30)
        lab(15*m+16)=lab(31)

        x(15*m+2)=x(17)
        x(15*m+3)=x(18)
        x(15*m+4)=x(19)
        x(15*m+5)=x(20)
        x(15*m+6)=x(21)
        x(15*m+7)=x(22)
        x(15*m+8)=x(23)
        x(15*m+9)=x(24)
        x(15*m+10)=x(25)
        x(15*m+11)=x(26)
        x(15*m+12)=x(27)
        x(15*m+13)=x(28)
        x(15*m+14)=x(29)
        x(15*m+15)=x(30)
        x(15*m+16)=x(31)

```

i (15\*m+2)=0  
i (15\*m+3)=0  
i (15\*m+4)=0  
i (15\*m+5)=0  
i (15\*m+6)=0  
i (15\*m+7)=0  
i (15\*m+8)=0  
i (15\*m+9)=0  
i (15\*m+10)=0  
i (15\*m+11)=0  
i (15\*m+12)=0  
i (15\*m+13)=0  
i (15\*m+14)=0  
i (15\*m+15)=0  
i (15\*m+16)=0

phi (15\*m+2)=phi (17)  
phi (15\*m+3)=phi (18)  
phi (15\*m+4)=phi (19)  
phi (15\*m+5)=phi (20)  
phi (15\*m+6)=phi (21)  
phi (15\*m+7)=phi (22)  
phi (15\*m+8)=phi (23)  
phi (15\*m+9)=phi (24)  
phi (15\*m+10)=phi (25)  
phi (15\*m+11)=phi (26)  
phi (15\*m+12)=phi (27)  
phi (15\*m+13)=phi (28)  
phi (15\*m+14)=phi (29)  
phi (15\*m+15)=phi (30)  
phi (15\*m+16)=phi (31)

k (15\*m+2)=0  
k (15\*m+3)=0  
k (15\*m+4)=0  
k (15\*m+5)=0  
k (15\*m+6)=0  
k (15\*m+7)=0  
k (15\*m+8)=0  
k (15\*m+9)=0  
k (15\*m+10)=0  
k (15\*m+11)=0  
k (15\*m+12)=0  
k (15\*m+13)=0  
k (15\*m+14)=0  
k (15\*m+15)=0  
k (15\*m+16)=0

theta (15\*m+2)=theta (17)  
theta (15\*m+3)=theta (18)  
theta (15\*m+4)=theta (19)  
theta (15\*m+5)=theta (20)  
theta (15\*m+6)=theta (21)  
theta (15\*m+7)=theta (22)  
theta (15\*m+8)=theta (23)  
theta (15\*m+9)=theta (24)  
theta (15\*m+10)=theta (25)  
theta (15\*m+11)=theta (26)  
theta (15\*m+12)=theta (27)

$\theta(15m+13)=\theta(28)$   
 $\theta(15m+14)=\theta(29)$   
 $\theta(15m+15)=\theta(30)$   
 $\theta(15m+16)=\theta(31)$

$l(15m+2)=0$   
 $l(15m+3)=0$   
 $l(15m+4)=0$   
 $l(15m+5)=0$   
 $l(15m+6)=0$   
 $l(15m+7)=0$   
 $l(15m+8)=0$   
 $l(15m+9)=0$   
 $l(15m+10)=0$   
 $l(15m+11)=0$   
 $l(15m+12)=0$   
 $l(15m+13)=0$   
 $l(15m+14)=0$   
 $l(15m+15)=0$   
 $l(15m+16)=0$

$d(15m+2)=15m-12$   
 $d(15m+3)=15m+2$   
 $d(15m+4)=15m-12$   
 $d(15m+5)=15m-12$   
 $d(15m+6)=15m+2$   
 $d(15m+7)=15m+2$   
 $d(15m+8)=15m+7$   
 $d(15m+9)=15m+8$   
 $d(15m+10)=15m+8$   
 $d(15m+11)=15m+10$   
 $d(15m+12)=15m+10$   
 $d(15m+13)=15m+12$   
 $d(15m+14)=15m+12$   
 $d(15m+15)=15m+14$   
 $d(15m+16)=15m+14$

$e(15m+2)=15m-13$   
 $e(15m+3)=15m-12$   
 $e(15m+4)=15m-13$   
 $e(15m+5)=15m-13$   
 $e(15m+6)=15m-12$   
 $e(15m+7)=15m-12$   
 $e(15m+8)=15m+2$   
 $e(15m+9)=15m+7$   
 $e(15m+10)=15m+7$   
 $e(15m+11)=15m+8$   
 $e(15m+12)=15m+8$   
 $e(15m+13)=15m+10$   
 $e(15m+14)=15m+10$   
 $e(15m+15)=15m+12$   
 $e(15m+16)=15m+12$

$f(15m+2)=15m-27$   
 $f(15m+3)=15m-13$   
 $f(15m+4)=15m+2$   
 $f(15m+5)=15m+2$   
 $f(15m+6)=15m+3$   
 $f(15m+7)=15m+3$

```

f (15*m+8)=15*m-12
f (15*m+9)=15*m+2
f (15*m+10)=15*m+2
f (15*m+11)=15*m+7
f (15*m+12)=15*m+7
f (15*m+13)=15*m+8
f (15*m+14)=15*m+8
f (15*m+15)=15*m+10
f (15*m+16)=15*m+10

end do

lab (15*n-13)=lab (17)
lab (15*n-12)=lab (19)
lab (15*n-11)=lab (20)
lab (15*n-10)=lab (21)
lab (15*n-9)=lab (22)
lab (15*n-8)=lab (23)
lab (15*n-7)=lab (24)
lab (15*n-6)=lab (25)
lab (15*n-5)=lab (26)
lab (15*n-4)=lab (27)
lab (15*n-3)=lab (28)
lab (15*n-2)=lab (29)
lab (15*n-1)=lab (30)
lab (15*n-0)=lab (31)

x (15*n-13)=x (17)
x (15*n-12)=x (19)
x (15*n-11)=x (20)
x (15*n-10)=x (21)
x (15*n-9)=x (22)
x (15*n-8)=x (23)
x (15*n-7)=x (24)
x (15*n-6)=x (25)
x (15*n-5)=x (26)
x (15*n-4)=x (27)
x (15*n-3)=x (28)
x (15*n-2)=x (29)
x (15*n-1)=x (30)
x (15*n-0)=x (31)

i (15*n-13)=0
i (15*n-12)=0
i (15*n-11)=0
i (15*n-10)=0
i (15*n-9)=0
i (15*n-8)=0
i (15*n-7)=0
i (15*n-6)=0
i (15*n-5)=0
i (15*n-4)=0
i (15*n-3)=0
i (15*n-2)=0
i (15*n-1)=0
i (15*n-0)=0

phi (15*n-13)=phi (17)
phi (15*n-12)=phi (19)

```

phi (15\*n-11)=phi (20)  
phi (15\*n-10)=phi (21)  
phi (15\*n-9)=phi (22)  
phi (15\*n-8)=phi (23)  
phi (15\*n-7)=phi (24)  
phi (15\*n-6)=phi (25)  
phi (15\*n-5)=phi (26)  
phi (15\*n-4)=phi (27)  
phi (15\*n-3)=phi (28)  
phi (15\*n-2)=phi (29)  
phi (15\*n-1)=phi (30)  
phi (15\*n-0)=phi (31)

k (15\*n-13)=0  
k (15\*n-12)=0  
k (15\*n-11)=0  
k (15\*n-10)=0  
k (15\*n-9)=0  
k (15\*n-8)=0  
k (15\*n-7)=0  
k (15\*n-6)=0  
k (15\*n-5)=0  
k (15\*n-4)=0  
k (15\*n-3)=0  
k (15\*n-2)=0  
k (15\*n-1)=0  
k (15\*n-0)=0

theta (15\*n-13)=theta (17)  
theta (15\*n-12)=theta (19)  
theta (15\*n-11)=theta (20)  
theta (15\*n-10)=-60.00  
theta (15\*n-9)=60.00  
theta (15\*n-8)=theta (23)  
theta (15\*n-7)=theta (24)  
theta (15\*n-6)=theta (25)  
theta (15\*n-5)=theta (26)  
theta (15\*n-4)=theta (27)  
theta (15\*n-3)=theta (28)  
theta (15\*n-2)=theta (29)  
theta (15\*n-1)=theta (30)  
theta (15\*n-0)=theta (31)

l (15\*n-13)=0  
l (15\*n-12)=0  
l (15\*n-11)=0  
l (15\*n-10)=0  
l (15\*n-9)=0  
l (15\*n-8)=0  
l (15\*n-7)=0  
l (15\*n-6)=0  
l (15\*n-5)=0  
l (15\*n-4)=0  
l (15\*n-3)=0  
l (15\*n-2)=0  
l (15\*n-1)=0  
l (15\*n-0)=0

d (15\*n-13)=15\*n-27

```
d(15*n-12)=15*n-27
d(15*n-11)=15*n-27
d(15*n-10)=15*n-13
d(15*n-9)=15*n-13
d(15*n-8)=15*n-9
d(15*n-7)=15*n-8
d(15*n-6)=15*n-8
d(15*n-5)=15*n-6
d(15*n-4)=15*n-6
d(15*n-3)=15*n-4
d(15*n-2)=15*n-4
d(15*n-1)=15*n-2
d(15*n-0)=15*n-2
```

```
e(15*n-13)=15*n-28
e(15*n-12)=15*n-28
e(15*n-11)=15*n-28
e(15*n-10)=15*n-27
e(15*n-9)=15*n-27
e(15*n-8)=15*n-13
e(15*n-7)=15*n-9
e(15*n-6)=15*n-9
e(15*n-5)=15*n-8
e(15*n-4)=15*n-8
e(15*n-3)=15*n-6
e(15*n-2)=15*n-6
e(15*n-1)=15*n-4
e(15*n-0)=15*n-4
```

```
f(15*n-13)=15*n-42
f(15*n-12)=15*n-13
f(15*n-11)=15*n-13
f(15*n-10)=15*n-28
f(15*n-9)=15*n-28
f(15*n-8)=15*n-27
f(15*n-7)=15*n-27
f(15*n-6)=15*n-13
f(15*n-5)=15*n-9
f(15*n-4)=15*n-9
f(15*n-3)=15*n-8
f(15*n-2)=15*n-8
f(15*n-1)=15*n-6
f(15*n-0)=15*n-6
```

```
lab(15*n+1)="H"
x(15*n+1)=1.10
i(15*n+1)=0
phi(15*n+1)=110.00
k(15*n+1)=0
theta(15*n+1)=-120.00
l(15*n+1)=0
d(15*n+1)=1
e(15*n+1)=2
f(15*n+1)=3
```

```
lab(15*n+2)="H"
x(15*n+2)=1.10
i(15*n+2)=0
phi(15*n+2)=110.00
```

```

k(15*n+2)=0
theta(15*n+2)=180.00
l(15*n+2)=0
d(15*n+2)=15*n-13
e(15*n+2)=15*n-27
f(15*n+2)=15*n-28

do p=1,n-1

    lab(15*n+p+2)="B"
    x(15*n+p+2)=1.38
    i(15*n+p+2)=0
    phi(15*n+p+2)=0
    k(15*n+p+2)=0
    theta(15*n+p+2)=0
    l(15*n+p+2)=0
    d(15*n+p+2)=15*p-3
    e(15*n+p+2)=15*p-8
    f(15*n+p+2)=15*p-7

end do

lab(16*n+2)="B"
x(16*n+2)=1.38
i(16*n+2)=0
phi(16*n+2)=0
k(16*n+2)=0
theta(16*n+2)=0
l(16*n+2)=0
d(16*n+2)=15*n-4
e(16*n+2)=15*n-9
f(16*n+2)=15*n-8

end subroutine hydroP2VP

!!!!!!!!!!!!!!!!!!!!!!!!!!!!!!!!!!!!!!!!!!!!!!!!!!!!!!!!!!!!!!!!!!!!!!!!!!!!!!
!!!!!!!!!!!!!!!!!!!!!!!!!!!!!!!!!!!!!!!!!!!!!!!!!!!!!!!!!!!!!!!!!!!!!!!!!!!!!!
!
subroutine PE(n,lab,x,i,phi,k,theta,l,d,e,f)

    implicit none

    integer::j,m
    integer,intent(in)::n
    character,allocatable,intent(out)::lab(:)
    integer,allocatable,intent(out)::i(:),k(:),l(:),d(:),e(:),f(:)
    real,allocatable,intent(out)::x(:),phi(:),theta(:)

    open(UNIT=1,FILE='PE.mop',STATUS='old')
    open(UNIT=2,FILE='matrice.mop',STATUS='unknown')

    write(2,*)
    write(2,*)
    write(2,*)
    do j=1,4

READ(1,*)lab(j),x(j),i(j),phi(j),k(j),theta(j),l(j),d(j),e(j),f(j)
    end do

```



```

i (6*m+3)=0
i (6*m+4)=0
i (6*m+5)=0
i (6*m+6)=0
i (6*m+7)=0

phi (6*m+2)=phi (14)
phi (6*m+3)=phi (15)
phi (6*m+4)=phi (16)
phi (6*m+5)=phi (17)
phi (6*m+6)=phi (18)
phi (6*m+7)=phi (19)

k (6*m+2)=0
k (6*m+3)=0
k (6*m+4)=0
k (6*m+5)=0
k (6*m+6)=0
k (6*m+7)=0

theta (6*m+2)=theta (14)
theta (6*m+3)=theta (15)
theta (6*m+4)=theta (16)
theta (6*m+5)=theta (17)
theta (6*m+6)=theta (18)
theta (6*m+7)=theta (19)

l (6*m+2)=0
l (6*m+3)=0
l (6*m+4)=0
l (6*m+5)=0
l (6*m+6)=0
l (6*m+7)=0

d (6*m+2)=6*m-3
d (6*m+3)=6*m+2
d (6*m+4)=6*m-3
d (6*m+5)=6*m-3
d (6*m+6)=6*m+2
d (6*m+7)=6*m+2

e (6*m+2)=6*m-4
e (6*m+3)=6*m-3
e (6*m+4)=6*m-4
e (6*m+5)=6*m-4
e (6*m+6)=6*m-3
e (6*m+7)=6*m-3

f (6*m+2)=6*m-9
f (6*m+3)=6*m-4
f (6*m+4)=6*m+2
f (6*m+5)=6*m+2
f (6*m+6)=6*m+3
f (6*m+7)=6*m+3

end do

lab (6*n-4)=lab (14)
lab (6*n-3)=lab (16)

```

```
lab(6*n-2)=lab(17)
lab(6*n-1)=lab(18)
lab(6*n)=lab(19)
```

```
x(6*n-4)=x(14)
x(6*n-3)=x(16)
x(6*n-2)=x(17)
x(6*n-1)=x(18)
x(6*n)=x(19)
```

```
i(6*n-4)=0
i(6*n-3)=0
i(6*n-2)=0
i(6*n-1)=0
i(6*n)=0
```

```
phi(6*n-4)=phi(14)
phi(6*n-3)=phi(16)
phi(6*n-2)=phi(17)
phi(6*n-1)=phi(18)
phi(6*n)=phi(19)
```

```
k(6*n-4)=0
k(6*n-3)=0
k(6*n-2)=0
k(6*n-1)=0
k(6*n)=0
```

```
theta(6*n-4)=theta(14)
theta(6*n-3)=theta(16)
theta(6*n-2)=theta(17)
theta(6*n-1)=60
theta(6*n)=-60
```

```
l(6*n-4)=0
l(6*n-3)=0
l(6*n-2)=0
l(6*n-1)=0
l(6*n)=0
```

```
d(6*n-4)=6*n-9
d(6*n-3)=6*n-9
d(6*n-2)=6*n-9
d(6*n-1)=6*n-4
d(6*n)=6*n-4
```

```
e(6*n-4)=6*n-10
e(6*n-3)=6*n-10
e(6*n-2)=6*n-10
e(6*n-1)=6*n-9
e(6*n)=6*n-9
```

```
f(6*n-4)=6*n-15
f(6*n-3)=6*n-4
f(6*n-2)=6*n-4
f(6*n-1)=6*n-10
f(6*n)=6*n-10
```

```
lab(6*n+1)="H"
```

```

x(6*n+1)=1.10
i(6*n+1)=0
phi(6*n+1)=110.00
k(6*n+1)=0
theta(6*n+1)=-120.00
l(6*n+1)=0
d(6*n+1)=1
e(6*n+1)=2
f(6*n+1)=3

lab(6*n+2)="H"
x(6*n+2)=1.10
i(6*n+2)=0
phi(6*n+2)=110.00
k(6*n+2)=0
theta(6*n+2)=180.00
l(6*n+2)=0
d(6*n+2)=6*n-4
e(6*n+2)=6*n-9
f(6*n+2)=6*n-10

end subroutine hydroPE

!!!!!!!!!!!!!!!!!!!!!!!!!!!!!!!!!!!!!!!!!!!!!!!!!!!!!!!!!!!!!!!!!!!!!!!!!!!!!!
!!!!!!!!!!!!!!!!!!!!!!!!!!!!!!!!!!!!!!!!!!!!!!!!!!!!!!!!!!!!!!!!!!!!!!!!!!!!!!
!!!!!!
subroutine PP(n,lab,x,i,phi,k,theta,l,d,e,f)

    implicit none

    integer,intent(in)::n
    integer::j,m
    character,allocatable,intent(out)::lab(:)
    integer,allocatable,intent(out)::i(:),k(:),l(:),d(:),e(:),f(:)
    real,allocatable,intent(out)::x(:),phi(:),theta(:)

    open(UNIT=1,FILE='PP.mop',STATUS='old')
    open(UNIT=2,FILE='matrice.mop',STATUS='unknown')

    write(2,*)
    write(2,*)
    write(2,*)
    do j=1,10

READ(1,*)lab(j),x(j),i(j),phi(j),k(j),theta(j),l(j),d(j),e(j),f(j)
    end do

    do m=3,n-2

        lab(3*m+2)=lab(8)
        lab(3*m+3)=lab(9)
        lab(3*m+4)=lab(10)

        x(3*m+2)=x(8)
        x(3*m+3)=x(9)
        x(3*m+4)=x(10)

        i(3*m+2)=0
        i(3*m+3)=0

```

```

i(3*m+4)=0

phi(3*m+2)=phi(8)
phi(3*m+3)=phi(9)
phi(3*m+4)=phi(10)

k(3*m+2)=0
k(3*m+3)=0
k(3*m+4)=0

theta(3*m+2)=theta(8)
theta(3*m+3)=theta(9)
theta(3*m+4)=theta(10)

l(3*m+2)=0
l(3*m+3)=0
l(3*m+4)=0

d(3*m+2)=3*m
d(3*m+3)=3*m+2
d(3*m+4)=3*m+2

e(3*m+2)=3*m-1
e(3*m+3)=3*m
e(3*m+4)=3*m

f(3*m+2)=3*m-3
f(3*m+3)=3*m-1
f(3*m+4)=3*m+3

end do

lab(3*n-1)="C"
x(3*n-1)=1.54
i(3*n-1)=0
phi(3*n-1)=109.05
k(3*n-1)=0
theta(3*n-1)=180.00
l(3*n-1)=0
d(3*n-1)=3*n-3
e(3*n-1)=3*n-4
f(3*n-1)=3*n-6

lab(3*n)="C"
x(3*n)=1.54
i(3*n)=0
phi(3*n)=109.05
k(3*n)=0
theta(3*n)=60
l(3*n)=0
d(3*n)=3*n-1
e(3*n)=3*n-3
f(3*n)=3*n-4

end subroutine PP

!!!!!!!!!!!!!!!!!!!!!!!!!!!!!!!!!!!!!!!!!!!!!!!!!!!!!!!!!!!!!!!!!!!!!!!!!!!!!!!!!!!!!!
!!!!!!!!!!!!!!!!!!!!!!!!!!!!!!!!!!!!!!!!!!!!!!!!!!!!!!!!!!!!!!!!!!!!!!!!!!!!!!!!!!!!!!
subroutine hydroPP(n,lab,x,i,phi,k,theta,l,d,e,f)

```

```

implicit none

integer, intent(in)::n
integer::j,m
character, allocatable, intent(out)::lab(:)
integer, allocatable, intent(out)::i(:),k(:),l(:),d(:),e(:),f(:)
real, allocatable, intent(out)::x(:),phi(:),theta(:)

open(UNIT=1,FILE='hydroPP.mop',STATUS='old')
open(UNIT=2,FILE='matrice.mop',STATUS='unknown')

write(2,*)
write(2,*)
write(2,*)
do j=1,28

READ(1,*)lab(j),x(j),i(j),phi(j),k(j),theta(j),l(j),d(j),e(j),f(j)
end do

do m=3,n-2

lab(9*m+2)=lab(20)
lab(9*m+3)=lab(21)
lab(9*m+4)=lab(22)
lab(9*m+5)=lab(23)
lab(9*m+6)=lab(24)
lab(9*m+7)=lab(25)
lab(9*m+8)=lab(26)
lab(9*m+9)=lab(27)
lab(9*m+10)=lab(28)

x(9*m+2)=x(20)
x(9*m+3)=x(21)
x(9*m+4)=x(22)
x(9*m+5)=x(23)
x(9*m+6)=x(24)
x(9*m+7)=x(25)
x(9*m+8)=x(26)
x(9*m+9)=x(27)
x(9*m+10)=x(28)

i(9*m+2)=0
i(9*m+3)=0
i(9*m+4)=0
i(9*m+5)=0
i(9*m+6)=0
i(9*m+7)=0
i(9*m+8)=0
i(9*m+9)=0
i(9*m+10)=0

phi(9*m+2)=phi(20)
phi(9*m+3)=phi(21)
phi(9*m+4)=phi(22)
phi(9*m+5)=phi(23)
phi(9*m+6)=phi(24)
phi(9*m+7)=phi(25)
phi(9*m+8)=phi(26)

```

$\phi(9m+9) = \phi(27)$   
 $\phi(9m+10) = \phi(28)$

$k(9m+2) = 0$   
 $k(9m+3) = 0$   
 $k(9m+4) = 0$   
 $k(9m+5) = 0$   
 $k(9m+6) = 0$   
 $k(9m+7) = 0$   
 $k(9m+8) = 0$   
 $k(9m+9) = 0$   
 $k(9m+10) = 0$

$\theta(9m+2) = \theta(20)$   
 $\theta(9m+3) = \theta(21)$   
 $\theta(9m+4) = \theta(22)$   
 $\theta(9m+5) = \theta(23)$   
 $\theta(9m+6) = \theta(24)$   
 $\theta(9m+7) = \theta(25)$   
 $\theta(9m+8) = \theta(26)$   
 $\theta(9m+9) = \theta(27)$   
 $\theta(9m+10) = \theta(28)$

$l(9m+2) = 0$   
 $l(9m+3) = 0$   
 $l(9m+4) = 0$   
 $l(9m+5) = 0$   
 $l(9m+6) = 0$   
 $l(9m+7) = 0$   
 $l(9m+8) = 0$   
 $l(9m+9) = 0$   
 $l(9m+10) = 0$

$d(9m+2) = 9m-6$   
 $d(9m+3) = 9m+2$   
 $d(9m+4) = 9m-6$   
 $d(9m+5) = 9m-6$   
 $d(9m+6) = 9m+2$   
 $d(9m+7) = 9m+2$   
 $d(9m+8) = 9m+7$   
 $d(9m+9) = 9m+7$   
 $d(9m+10) = 9m+7$

$e(9m+2) = 9m-7$   
 $e(9m+3) = 9m-6$   
 $e(9m+4) = 9m-7$   
 $e(9m+5) = 9m-7$   
 $e(9m+6) = 9m-6$   
 $e(9m+7) = 9m-6$   
 $e(9m+8) = 9m+2$   
 $e(9m+9) = 9m+2$   
 $e(9m+10) = 9m+2$

$f(9m+2) = 9m-15$   
 $f(9m+3) = 9m-7$   
 $f(9m+4) = 9m+2$   
 $f(9m+5) = 9m+2$   
 $f(9m+6) = 9m+3$   
 $f(9m+7) = 9m+3$

```

f (9*m+8)=9*m-6
f (9*m+9)=9*m-6
f (9*m+10)=9*m-6

end do

lab (9*n-7)=lab (20)
lab (9*n-6)=lab (22)
lab (9*n-5)=lab (23)
lab (9*n-4)=lab (24)
lab (9*n-3)=lab (25)
lab (9*n-2)=lab (26)
lab (9*n-1)=lab (27)
lab (9*n)=lab (28)

x (9*n-7)=x (20)
x (9*n-6)=x (22)
x (9*n-5)=x (23)
x (9*n-4)=x (24)
x (9*n-3)=x (25)
x (9*n-2)=x (26)
x (9*n-1)=x (27)
x (9*n)=x (28)

i (9*n-7)=0
i (9*n-6)=0
i (9*n-5)=0
i (9*n-4)=0
i (9*n-3)=0
i (9*n-2)=0
i (9*n-1)=0
i (9*n)=0

phi (9*n-7)=phi (20)
phi (9*n-6)=phi (22)
phi (9*n-5)=phi (23)
phi (9*n-4)=phi (24)
phi (9*n-3)=phi (25)
phi (9*n-2)=phi (26)
phi (9*n-1)=phi (27)
phi (9*n)=phi (28)

k (9*n-7)=0
k (9*n-6)=0
k (9*n-5)=0
k (9*n-4)=0
k (9*n-3)=0
k (9*n-2)=0
k (9*n-1)=0
k (9*n)=0

theta (9*n-7)=theta (20)
theta (9*n-6)=theta (22)
theta (9*n-5)=theta (23)
theta (9*n-4)=-60
theta (9*n-3)=60
theta (9*n-2)=theta (26)
theta (9*n-1)=theta (27)
theta (9*n)=theta (28)

```

$l(9*n-7)=0$   
 $l(9*n-6)=0$   
 $l(9*n-5)=0$   
 $l(9*n-4)=0$   
 $l(9*n-3)=0$   
 $l(9*n-2)=0$   
 $l(9*n-1)=0$   
 $l(9*n)=0$

$d(9*n-7)=9*n-15$   
 $d(9*n-6)=9*n-15$   
 $d(9*n-5)=9*n-15$   
 $d(9*n-4)=9*n-7$   
 $d(9*n-3)=9*n-7$   
 $d(9*n-2)=9*n-3$   
 $d(9*n-1)=9*n-3$   
 $d(9*n)=9*n-3$

$e(9*n-7)=9*n-16$   
 $e(9*n-6)=9*n-16$   
 $e(9*n-5)=9*n-16$   
 $e(9*n-4)=9*n-15$   
 $e(9*n-3)=9*n-15$   
 $e(9*n-2)=9*n-7$   
 $e(9*n-1)=9*n-7$   
 $e(9*n)=9*n-7$

$f(9*n-7)=9*n-24$   
 $f(9*n-6)=9*n-7$   
 $f(9*n-5)=9*n-7$   
 $f(9*n-4)=9*n-16$   
 $f(9*n-3)=9*n-16$   
 $f(9*n-2)=9*n-15$   
 $f(9*n-1)=9*n-15$   
 $f(9*n)=9*n-15$

$lab(9*n+1)=""$   
 $x(9*n+1)=1.10$   
 $i(9*n+1)=0$   
 $phi(9*n+1)=110.00$   
 $k(9*n+1)=0$   
 $theta(9*n+1)=-120.00$   
 $l(9*n+1)=0$   
 $d(9*n+1)=1$   
 $e(9*n+1)=2$   
 $f(9*n+1)=3$

$lab(9*n+2)=""$   
 $x(9*n+2)=1.10$   
 $i(9*n+2)=0$   
 $phi(9*n+2)=110.00$   
 $k(9*n+2)=0$   
 $theta(9*n+2)=180.00$   
 $l(9*n+2)=0$   
 $d(9*n+2)=9*n-7$   
 $e(9*n+2)=9*n-15$   
 $f(9*n+2)=9*n-16$

```

end subroutine hydroPP

!!!!!!!!!!!!!!!!!!!!!!!!!!!!!!!!!!!!!!!!!!!!!!!!!!!!!!!!!!!!!!!!!!!!!!!!!!!!!!
!!!!!!!!!!!!!!!!!!!!!!!!!!!!!!!!!!!!!!!!!!!!!!!!!!!!!!!!!!!!!!!!!!!!!!!!!!!!!!
subroutine PS(n,lab,x,i,phi,k,theta,l,d,e,f)

    implicit none

    integer,intent(in)::n
    integer::j,m
    character,allocatable,intent(out)::lab(:)
    integer,allocatable,intent(out)::i(:),k(:),l(:),d(:),e(:),f(:)
    real,allocatable,intent(out)::x(:),phi(:),theta(:)

    open(UNIT=1,FILE='PS.mop',STATUS='old')
    open(UNIT=2,FILE='matrice.mop',STATUS='unknown')
    write(2,*)
    write(2,*)
    write(2,*)
    do j=1,25

read(1,*)lab(j),x(j),i(j),phi(j),k(j),theta(j),l(j),d(j),e(j),f(j)
    end do

    do m=3,n-2

        lab(8*m+2)=lab(18)
        lab(8*m+3)=lab(19)
        lab(8*m+4)=lab(20)
        lab(8*m+5)=lab(21)
        lab(8*m+6)=lab(22)
        lab(8*m+7)=lab(23)
        lab(8*m+8)=lab(24)
        lab(8*m+9)=lab(25)

        x(8*m+2)=x(18)
        x(8*m+3)=x(19)
        x(8*m+4)=x(20)
        x(8*m+5)=x(21)
        x(8*m+6)=x(22)
        x(8*m+7)=x(23)
        x(8*m+8)=x(24)
        x(8*m+9)=x(25)

        i(8*m+2)=0
        i(8*m+3)=0
        i(8*m+4)=0
        i(8*m+5)=0
        i(8*m+6)=0
        i(8*m+7)=0
        i(8*m+8)=0
        i(8*m+9)=0

        phi(8*m+2)=phi(18)
        phi(8*m+3)=phi(19)
        phi(8*m+4)=phi(20)
        phi(8*m+5)=phi(21)
        phi(8*m+6)=phi(22)
        phi(8*m+7)=phi(23)

```

```
phi (8*m+8)=phi (24)
phi (8*m+9)=phi (25)
```

```
k (8*m+2)=0
k (8*m+3)=0
k (8*m+4)=0
k (8*m+5)=0
k (8*m+6)=0
k (8*m+7)=0
k (8*m+8)=0
k (8*m+9)=0
```

```
theta (8*m+2)=theta (18)
theta (8*m+3)=theta (19)
theta (8*m+4)=theta (20)
theta (8*m+5)=theta (21)
theta (8*m+6)=theta (22)
theta (8*m+7)=theta (23)
theta (8*m+8)=theta (24)
theta (8*m+9)=theta (25)
```

```
l (8*m+2)=0
l (8*m+3)=0
l (8*m+4)=0
l (8*m+5)=0
l (8*m+6)=0
l (8*m+7)=0
l (8*m+8)=0
l (8*m+9)=0
```

```
d (8*m+2)=8*m-5
d (8*m+3)=8*m+2
d (8*m+4)=8*m+2
d (8*m+5)=8*m+4
d (8*m+6)=8*m+5
d (8*m+7)=8*m+6
d (8*m+8)=8*m+7
d (8*m+9)=8*m+8
```

```
e (8*m+2)=8*m-6
e (8*m+3)=8*m-5
e (8*m+4)=8*m-5
e (8*m+5)=8*m+2
e (8*m+6)=8*m+4
e (8*m+7)=8*m+5
e (8*m+8)=8*m+6
e (8*m+9)=8*m+7
```

```
f (8*m+2)=8*m-13
f (8*m+3)=8*m-6
f (8*m+4)=8*m+3
f (8*m+5)=8*m-5
f (8*m+6)=8*m+2
f (8*m+7)=8*m+4
f (8*m+8)=8*m+5
f (8*m+9)=8*m+6
```

```
end do
```

```
lab(8*n-6)=lab(18)
lab(8*n-5)=lab(20)
lab(8*n-4)=lab(21)
lab(8*n-3)=lab(22)
lab(8*n-2)=lab(23)
lab(8*n-1)=lab(24)
lab(8*n)=lab(25)
```

```
x(8*n-6)=x(18)
x(8*n-5)=x(20)
x(8*n-4)=x(21)
x(8*n-3)=x(22)
x(8*n-2)=x(23)
x(8*n-1)=x(24)
x(8*n)=x(25)
```

```
i(8*n-6)=0
i(8*n-5)=0
i(8*n-4)=0
i(8*n-3)=0
i(8*n-2)=0
i(8*n-1)=0
i(8*n)=0
```

```
phi(8*n-6)=phi(18)
phi(8*n-5)=phi(20)
phi(8*n-4)=phi(21)
phi(8*n-3)=phi(22)
phi(8*n-2)=phi(23)
phi(8*n-1)=phi(24)
phi(8*n)=phi(25)
```

```
k(8*n-6)=0
k(8*n-5)=0
k(8*n-4)=0
k(8*n-3)=0
k(8*n-2)=0
k(8*n-1)=0
k(8*n)=0
```

```
theta(8*n-6)=theta(18)
theta(8*n-5)=60
theta(8*n-4)=theta(21)
theta(8*n-3)=theta(22)
theta(8*n-2)=theta(23)
theta(8*n-1)=theta(24)
theta(8*n)=theta(25)
```

```
l(8*n-6)=0
l(8*n-5)=0
l(8*n-4)=0
l(8*n-3)=0
l(8*n-2)=0
l(8*n-1)=0
l(8*n)=0
```

```
d(8*n-6)=8*n-13
d(8*n-5)=8*n-6
d(8*n-4)=8*n-5
```

```

d(8*n-3)=8*n-4
d(8*n-2)=8*n-3
d(8*n-1)=8*n-2
d(8*n)=8*n-1

e(8*n-6)=8*n-14
e(8*n-5)=8*n-13
e(8*n-4)=8*n-6
e(8*n-3)=8*n-5
e(8*n-2)=8*n-4
e(8*n-1)=8*n-3
e(8*n)=8*n-2

f(8*n-6)=8*n-21
f(8*n-5)=8*n-14
f(8*n-4)=8*n-13
f(8*n-3)=8*n-6
f(8*n-2)=8*n-5
f(8*n-1)=8*n-4
f(8*n)=8*n-3

end subroutine PS

!!!!!!!!!!!!!!!!!!!!!!!!!!!!!!!!!!!!!!!!!!!!!!!!!!!!!!!!!!!!!!!!!!!!!!!!!!!!!!
!!!!!!!!!!!!!!!!!!!!!!!!!!!!!!!!!!!!!!!!!!!!!!!!!!!!!!!!!!!!!!!!!!!!!!!!!!!!!!

subroutine P2VP(n,lab,x,i,phi,k,theta,l,d,e,f)

implicit none

integer,intent(in)::n
integer::j,m
character,allocatable,intent(out)::lab(:)
integer,allocatable,intent(out)::i(:),k(:),l(:),d(:),e(:),f(:)
real,allocatable,intent(out)::x(:),phi(:),theta(:)

open(UNIT=1,FILE='P2VP.mop',STATUS='old')
open(UNIT=2,FILE='matrice.mop',STATUS='unknown')
write(2,*)
write(2,*)
write(2,*)
do j=1,25

read(1,*)lab(j),x(j),i(j),phi(j),k(j),theta(j),l(j),d(j),e(j),f(j))
end do

do m=3,n-2

lab(8*m+2)=lab(18)
lab(8*m+3)=lab(19)
lab(8*m+4)=lab(20)
lab(8*m+5)=lab(21)
lab(8*m+6)=lab(22)
lab(8*m+7)=lab(23)
lab(8*m+8)=lab(24)
lab(8*m+9)=lab(25)

x(8*m+2)=x(18)
x(8*m+3)=x(19)

```

$x(8*m+4)=x(20)$   
 $x(8*m+5)=x(21)$   
 $x(8*m+6)=x(22)$   
 $x(8*m+7)=x(23)$   
 $x(8*m+8)=x(24)$   
 $x(8*m+9)=x(25)$

$i(8*m+2)=0$   
 $i(8*m+3)=0$   
 $i(8*m+4)=0$   
 $i(8*m+5)=0$   
 $i(8*m+6)=0$   
 $i(8*m+7)=0$   
 $i(8*m+8)=0$   
 $i(8*m+9)=0$

$\phi(8*m+2)=\phi(18)$   
 $\phi(8*m+3)=\phi(19)$   
 $\phi(8*m+4)=\phi(20)$   
 $\phi(8*m+5)=\phi(21)$   
 $\phi(8*m+6)=\phi(22)$   
 $\phi(8*m+7)=\phi(23)$   
 $\phi(8*m+8)=\phi(24)$   
 $\phi(8*m+9)=\phi(25)$

$k(8*m+2)=0$   
 $k(8*m+3)=0$   
 $k(8*m+4)=0$   
 $k(8*m+5)=0$   
 $k(8*m+6)=0$   
 $k(8*m+7)=0$   
 $k(8*m+8)=0$   
 $k(8*m+9)=0$

$\theta(8*m+2)=\theta(18)$   
 $\theta(8*m+3)=\theta(19)$   
 $\theta(8*m+4)=\theta(20)$   
 $\theta(8*m+5)=\theta(21)$   
 $\theta(8*m+6)=\theta(22)$   
 $\theta(8*m+7)=\theta(23)$   
 $\theta(8*m+8)=\theta(24)$   
 $\theta(8*m+9)=\theta(25)$

$l(8*m+2)=0$   
 $l(8*m+3)=0$   
 $l(8*m+4)=0$   
 $l(8*m+5)=0$   
 $l(8*m+6)=0$   
 $l(8*m+7)=0$   
 $l(8*m+8)=0$   
 $l(8*m+9)=0$

$d(8*m+2)=8*m-5$   
 $d(8*m+3)=8*m+2$   
 $d(8*m+4)=8*m+2$   
 $d(8*m+5)=8*m+4$   
 $d(8*m+6)=8*m+5$   
 $d(8*m+7)=8*m+6$   
 $d(8*m+8)=8*m+7$

```

d(8*m+9)=8*m+8

e(8*m+2)=8*m-6
e(8*m+3)=8*m-5
e(8*m+4)=8*m-5
e(8*m+5)=8*m+2
e(8*m+6)=8*m+4
e(8*m+7)=8*m+5
e(8*m+8)=8*m+6
e(8*m+9)=8*m+7

f(8*m+2)=8*m-13
f(8*m+3)=8*m-6
f(8*m+4)=8*m+3
f(8*m+5)=8*m-5
f(8*m+6)=8*m+2
f(8*m+7)=8*m+4
f(8*m+8)=8*m+5
f(8*m+9)=8*m+6

end do

lab(8*n-6)=lab(18)
lab(8*n-5)=lab(20)
lab(8*n-4)=lab(21)
lab(8*n-3)=lab(22)
lab(8*n-2)=lab(23)
lab(8*n-1)=lab(24)
lab(8*n)=lab(25)

x(8*n-6)=x(18)
x(8*n-5)=x(20)
x(8*n-4)=x(21)
x(8*n-3)=x(22)
x(8*n-2)=x(23)
x(8*n-1)=x(24)
x(8*n)=x(25)

i(8*n-6)=0
i(8*n-5)=0
i(8*n-4)=0
i(8*n-3)=0
i(8*n-2)=0
i(8*n-1)=0
i(8*n)=0

phi(8*n-6)=phi(18)
phi(8*n-5)=phi(20)
phi(8*n-4)=phi(21)
phi(8*n-3)=phi(22)
phi(8*n-2)=phi(23)
phi(8*n-1)=phi(24)
phi(8*n)=phi(25)

k(8*n-6)=0
k(8*n-5)=0
k(8*n-4)=0
k(8*n-3)=0
k(8*n-2)=0

```

```

k(8*n-1)=0
k(8*n)=0

theta(8*n-6)=theta(18)
theta(8*n-5)=60
theta(8*n-4)=theta(21)
theta(8*n-3)=theta(22)
theta(8*n-2)=theta(23)
theta(8*n-1)=theta(24)
theta(8*n)=theta(25)

l(8*n-6)=0
l(8*n-5)=0
l(8*n-4)=0
l(8*n-3)=0
l(8*n-2)=0
l(8*n-1)=0
l(8*n)=0

d(8*n-6)=8*n-13
d(8*n-5)=8*n-6
d(8*n-4)=8*n-5
d(8*n-3)=8*n-4
d(8*n-2)=8*n-3
d(8*n-1)=8*n-2
d(8*n)=8*n-1

e(8*n-6)=8*n-14
e(8*n-5)=8*n-13
e(8*n-4)=8*n-6
e(8*n-3)=8*n-5
e(8*n-2)=8*n-4
e(8*n-1)=8*n-3
e(8*n)=8*n-2

f(8*n-6)=8*n-21
f(8*n-5)=8*n-14
f(8*n-4)=8*n-13
f(8*n-3)=8*n-6
f(8*n-2)=8*n-5
f(8*n-1)=8*n-4
f(8*n)=8*n-3

end subroutine P2VP

!!!!!!!!!!!!!!!!!!!!!!!!!!!!!!!!!!!!!!!!!!!!!!!!!!!!!!!!!!!!!!!!!!!!!!!!!!!!!!
!!!!!!!!!!!!!!!!!!!!!!!!!!!!!!!!!!!!!!!!!!!!!!!!!!!!!!!!!!!!!!!!!!!!!!!!!!!!!!
!!!!!!!!!!
subroutine hydroPS(n,lab,x,i,phi,k,theta,l,d,e,f)

implicit none

integer::m,j
integer,intent(in)::n
character,allocatable,intent(out)::lab(:)
integer,allocatable,intent(out)::i(:),k(:),l(:),d(:),e(:),f(:)
real,allocatable,intent(out)::x(:),phi(:),theta(:)

open(UNIT=1,FILE='hydroPS.mop',STATUS='old')

```

```

open (UNIT=2, FILE='matrice.mop', STATUS='unknown')
write (2, *)
write (2, *)
write (2, *)
do j=1,49

read(1,*) lab(j), x(j), i(j), phi(j), k(j), theta(j), l(j), d(j), e(j), f(j)
end do

do m=3,n-2

lab(16*m+2)=lab(34)
lab(16*m+3)=lab(35)
lab(16*m+4)=lab(36)
lab(16*m+5)=lab(37)
lab(16*m+6)=lab(38)
lab(16*m+7)=lab(39)
lab(16*m+8)=lab(40)
lab(16*m+9)=lab(41)
lab(16*m+10)=lab(42)
lab(16*m+11)=lab(43)
lab(16*m+12)=lab(44)
lab(16*m+13)=lab(45)
lab(16*m+14)=lab(46)
lab(16*m+15)=lab(47)
lab(16*m+16)=lab(48)
lab(16*m+17)=lab(49)

x(16*m+2)=x(34)
x(16*m+3)=x(35)
x(16*m+4)=x(36)
x(16*m+5)=x(37)
x(16*m+6)=x(38)
x(16*m+7)=x(39)
x(16*m+8)=x(40)
x(16*m+9)=x(41)
x(16*m+10)=x(42)
x(16*m+11)=x(43)
x(16*m+12)=x(44)
x(16*m+13)=x(45)
x(16*m+14)=x(46)
x(16*m+15)=x(47)
x(16*m+16)=x(48)
x(16*m+17)=x(49)

i(16*m+2)=0
i(16*m+3)=0
i(16*m+4)=0
i(16*m+5)=0
i(16*m+6)=0
i(16*m+7)=0
i(16*m+8)=0
i(16*m+9)=0
i(16*m+10)=0
i(16*m+11)=0
i(16*m+12)=0
i(16*m+13)=0
i(16*m+14)=0
i(16*m+15)=0

```

$i(16*m+16)=0$   
 $i(16*m+17)=0$

$\text{phi}(16*m+2)=\text{phi}(34)$   
 $\text{phi}(16*m+3)=\text{phi}(35)$   
 $\text{phi}(16*m+4)=\text{phi}(36)$   
 $\text{phi}(16*m+5)=\text{phi}(37)$   
 $\text{phi}(16*m+6)=\text{phi}(38)$   
 $\text{phi}(16*m+7)=\text{phi}(39)$   
 $\text{phi}(16*m+8)=\text{phi}(40)$   
 $\text{phi}(16*m+9)=\text{phi}(41)$   
 $\text{phi}(16*m+10)=\text{phi}(42)$   
 $\text{phi}(16*m+11)=\text{phi}(43)$   
 $\text{phi}(16*m+12)=\text{phi}(44)$   
 $\text{phi}(16*m+13)=\text{phi}(45)$   
 $\text{phi}(16*m+14)=\text{phi}(46)$   
 $\text{phi}(16*m+15)=\text{phi}(47)$   
 $\text{phi}(16*m+16)=\text{phi}(48)$   
 $\text{phi}(16*m+17)=\text{phi}(49)$

$k(16*m+2)=0$   
 $k(16*m+3)=0$   
 $k(16*m+4)=0$   
 $k(16*m+5)=0$   
 $k(16*m+6)=0$   
 $k(16*m+7)=0$   
 $k(16*m+8)=0$   
 $k(16*m+9)=0$   
 $k(16*m+10)=0$   
 $k(16*m+11)=0$   
 $k(16*m+12)=0$   
 $k(16*m+13)=0$   
 $k(16*m+14)=0$   
 $k(16*m+15)=0$   
 $k(16*m+16)=0$   
 $k(16*m+17)=0$

$\text{theta}(16*m+2)=\text{theta}(34)$   
 $\text{theta}(16*m+3)=\text{theta}(35)$   
 $\text{theta}(16*m+4)=\text{theta}(36)$   
 $\text{theta}(16*m+5)=\text{theta}(37)$   
 $\text{theta}(16*m+6)=\text{theta}(38)$   
 $\text{theta}(16*m+7)=\text{theta}(39)$   
 $\text{theta}(16*m+8)=\text{theta}(40)$   
 $\text{theta}(16*m+9)=\text{theta}(41)$   
 $\text{theta}(16*m+10)=\text{theta}(42)$   
 $\text{theta}(16*m+11)=\text{theta}(43)$   
 $\text{theta}(16*m+12)=\text{theta}(44)$   
 $\text{theta}(16*m+13)=\text{theta}(45)$   
 $\text{theta}(16*m+14)=\text{theta}(46)$   
 $\text{theta}(16*m+15)=\text{theta}(47)$   
 $\text{theta}(16*m+16)=\text{theta}(48)$   
 $\text{theta}(16*m+17)=\text{theta}(49)$

$l(16*m+2)=0$   
 $l(16*m+3)=0$   
 $l(16*m+4)=0$   
 $l(16*m+5)=0$   
 $l(16*m+6)=0$

$l(16*m+7)=0$   
 $l(16*m+8)=0$   
 $l(16*m+9)=0$   
 $l(16*m+10)=0$   
 $l(16*m+11)=0$   
 $l(16*m+12)=0$   
 $l(16*m+13)=0$   
 $l(16*m+14)=0$   
 $l(16*m+15)=0$   
 $l(16*m+16)=0$   
 $l(16*m+17)=0$

$d(16*m+2)=16*m-13$   
 $d(16*m+3)=16*m+2$   
 $d(16*m+4)=16*m-13$   
 $d(16*m+5)=16*m-13$   
 $d(16*m+6)=16*m+2$   
 $d(16*m+7)=16*m+2$   
 $d(16*m+8)=16*m+7$   
 $d(16*m+9)=16*m+8$   
 $d(16*m+10)=16*m+8$   
 $d(16*m+11)=16*m+10$   
 $d(16*m+12)=16*m+10$   
 $d(16*m+13)=16*m+12$   
 $d(16*m+14)=16*m+12$   
 $d(16*m+15)=16*m+14$   
 $d(16*m+16)=16*m+14$   
 $d(16*m+17)=16*m+16$

$e(16*m+2)=16*m-14$   
 $e(16*m+3)=16*m-13$   
 $e(16*m+4)=16*m-14$   
 $e(16*m+5)=16*m-14$   
 $e(16*m+6)=16*m-13$   
 $e(16*m+7)=16*m-13$   
 $e(16*m+8)=16*m+2$   
 $e(16*m+9)=16*m+7$   
 $e(16*m+10)=16*m+7$   
 $e(16*m+11)=16*m+8$   
 $e(16*m+12)=16*m+8$   
 $e(16*m+13)=16*m+10$   
 $e(16*m+14)=16*m+10$   
 $e(16*m+15)=16*m+12$   
 $e(16*m+16)=16*m+12$   
 $e(16*m+17)=16*m+14$

$f(16*m+2)=16*m-29$   
 $f(16*m+3)=16*m-14$   
 $f(16*m+4)=16*m+2$   
 $f(16*m+5)=16*m+2$   
 $f(16*m+6)=16*m+3$   
 $f(16*m+7)=16*m+3$   
 $f(16*m+8)=16*m-13$   
 $f(16*m+9)=16*m+2$   
 $f(16*m+10)=16*m+2$   
 $f(16*m+11)=16*m+7$   
 $f(16*m+12)=16*m+7$   
 $f(16*m+13)=16*m+8$   
 $f(16*m+14)=16*m+8$

```

f(16*m+15)=16*m+10
f(16*m+16)=16*m+10
f(16*m+17)=16*m+12

end do

lab(16*n-14)=lab(34)
lab(16*n-13)=lab(36)
lab(16*n-12)=lab(37)
lab(16*n-11)=lab(38)
lab(16*n-10)=lab(39)
lab(16*n-9)=lab(40)
lab(16*n-8)=lab(41)
lab(16*n-7)=lab(42)
lab(16*n-6)=lab(43)
lab(16*n-5)=lab(44)
lab(16*n-4)=lab(45)
lab(16*n-3)=lab(46)
lab(16*n-2)=lab(47)
lab(16*n-1)=lab(48)
lab(16*n)=lab(49)

x(16*n-14)=x(34)
x(16*n-13)=x(36)
x(16*n-12)=x(37)
x(16*n-11)=x(38)
x(16*n-10)=x(39)
x(16*n-9)=x(40)
x(16*n-8)=x(41)
x(16*n-7)=x(42)
x(16*n-6)=x(43)
x(16*n-5)=x(44)
x(16*n-4)=x(45)
x(16*n-3)=x(46)
x(16*n-2)=x(47)
x(16*n-1)=x(48)
x(16*n)=x(49)

i(16*n-14)=0
i(16*n-13)=0
i(16*n-12)=0
i(16*n-11)=0
i(16*n-10)=0
i(16*n-9)=0
i(16*n-8)=0
i(16*n-7)=0
i(16*n-6)=0
i(16*n-5)=0
i(16*n-4)=0
i(16*n-3)=0
i(16*n-2)=0
i(16*n-1)=0
i(16*n)=0

phi(16*n-14)=phi(34)
phi(16*n-13)=phi(36)
phi(16*n-12)=phi(37)
phi(16*n-11)=phi(38)
phi(16*n-10)=phi(39)

```

phi(16\*n-9)=phi(40)  
phi(16\*n-8)=phi(41)  
phi(16\*n-7)=phi(42)  
phi(16\*n-6)=phi(43)  
phi(16\*n-5)=phi(44)  
phi(16\*n-4)=phi(45)  
phi(16\*n-3)=phi(46)  
phi(16\*n-2)=phi(47)  
phi(16\*n-1)=phi(48)  
phi(16\*n)=phi(49)

k(16\*n-14)=0  
k(16\*n-13)=0  
k(16\*n-12)=0  
k(16\*n-11)=0  
k(16\*n-10)=0  
k(16\*n-9)=0  
k(16\*n-8)=0  
k(16\*n-7)=0  
k(16\*n-6)=0  
k(16\*n-5)=0  
k(16\*n-4)=0  
k(16\*n-3)=0  
k(16\*n-2)=0  
k(16\*n-1)=0  
k(16\*n)=0

theta(16\*n-14)=theta(34)  
theta(16\*n-13)=theta(36)  
theta(16\*n-12)=theta(37)  
theta(16\*n-11)=-60  
theta(16\*n-10)=60  
theta(16\*n-9)=theta(40)  
theta(16\*n-8)=theta(41)  
theta(16\*n-7)=theta(42)  
theta(16\*n-6)=theta(43)  
theta(16\*n-5)=theta(44)  
theta(16\*n-4)=theta(45)  
theta(16\*n-3)=theta(46)  
theta(16\*n-2)=theta(47)  
theta(16\*n-1)=theta(48)  
theta(16\*n)=theta(49)

l(16\*n-14)=0  
l(16\*n-13)=0  
l(16\*n-12)=0  
l(16\*n-11)=0  
l(16\*n-10)=0  
l(16\*n-9)=0  
l(16\*n-8)=0  
l(16\*n-7)=0  
l(16\*n-6)=0  
l(16\*n-5)=0  
l(16\*n-4)=0  
l(16\*n-3)=0  
l(16\*n-2)=0  
l(16\*n-1)=0  
l(16\*n)=0

```
d(16*n-14)=16*n-29
d(16*n-13)=16*n-29
d(16*n-12)=16*n-29
d(16*n-11)=16*n-14
d(16*n-10)=16*n-14
d(16*n-9)=16*n-10
d(16*n-8)=16*n-9
d(16*n-7)=16*n-9
d(16*n-6)=16*n-7
d(16*n-5)=16*n-7
d(16*n-4)=16*n-5
d(16*n-3)=16*n-5
d(16*n-2)=16*n-3
d(16*n-1)=16*n-3
d(16*n)=16*n-1
```

```
e(16*n-14)=16*n-30
e(16*n-13)=16*n-30
e(16*n-12)=16*n-30
e(16*n-11)=16*n-29
e(16*n-10)=16*n-29
e(16*n-9)=16*n-14
e(16*n-8)=16*n-10
e(16*n-7)=16*n-10
e(16*n-6)=16*n-9
e(16*n-5)=16*n-9
e(16*n-4)=16*n-7
e(16*n-3)=16*n-7
e(16*n-2)=16*n-5
e(16*n-1)=16*n-5
e(16*n)=16*n-3
```

```
f(16*n-14)=16*n-45
f(16*n-13)=16*n-14
f(16*n-12)=16*n-14
f(16*n-11)=16*n-30
f(16*n-10)=16*n-30
f(16*n-9)=16*n-29
f(16*n-8)=16*n-14
f(16*n-7)=16*n-14
f(16*n-6)=16*n-10
f(16*n-5)=16*n-10
f(16*n-4)=16*n-9
f(16*n-3)=16*n-9
f(16*n-2)=16*n-7
f(16*n-1)=16*n-7
f(16*n)=16*n-5
```

```
lab(16*n+1)="H"
x(16*n+1)=1.10
i(16*n+1)=0
phi(16*n+1)=110.00
k(16*n+1)=0
theta(16*n+1)=-120.00
l(16*n+1)=0
d(16*n+1)=1
e(16*n+1)=2
f(16*n+1)=3
```

```

lab(16*n+2)="H"
x(16*n+2)=1.10
i(16*n+2)=0
phi(16*n+2)=110.00
k(16*n+2)=0
theta(16*n+2)=180.00
l(16*n+2)=0
d(16*n+2)=16*n-14
e(16*n+2)=16*n-29
f(16*n+2)=16*n-30

end subroutine hydroPS

!!!!!!!!!!!!!!!!!!!!!!!!!!!!!!!!!!!!!!!!!!!!!!!!!!!!!!!!!!!!!!!!!!!!!!!!!!!!!!!!!!!!!!
!!!!!!!!!!!!!!!!!!!!!!!!!!!!!!!!!!!!!!!!!!!!!!!!!!!!!!!!!!!!!!!!!!!!!!!!!!!!!!!!!!!!!!
subroutine ata(n,s)

  implicit none

  interface

    subroutine pseudoran(s)
      real, allocatable::s(:)
    end subroutine pseudoran

  end interface

  integer, allocatable::diad_val(:), triad_val(:)
  real, allocatable, intent(out)::s(:)
  integer, intent(in)::n
  integer::u,v,z,ntry
  real::tol1,tol2,tol_diad,tol_mm,tol_mr,tol_rr
  real::num_m,num_r,num_mm,num_mr,num_rr
  real::tot_m,tot_r,tot_mm,tot_mr,tot_rr
  real::pm,pr,pmm,pmr,prr,f_r,f_mm,f_mr,f_rr

  ntry=100000
  pm=0.5
  pr=0.5
  pmm=pm*pm
  pmr=2*pm*pr
  prr=pr*pr
  tol1=0.12
  tol2=0.12

  allocate(s(n))
  allocate(diad_val(n-1))
  allocate(triad_val(n-2))

  do z=1,ntry

    num_m=0
    num_r=0
    num_mm=0
    num_mr=0
    num_rr=0

```

```

call pseudoran(s)
do u=1,n-1
    diad_val(u)=s(u)*s(u+1)
    if(diad_val(u).eq.-1)then
        diad_val(u)=0
        num_r=num_r+1
    else if(diad_val(u).eq.1)then
        num_m=num_m+1
    end if
end do

tot_r=num_r

f_r=tot_r/(n-1)
tol_diad=abs(f_r-pr)/pr

do v=1,n-2
    triad_val(v)=diad_val(v)+diad_val(v+1)
    if(triad_val(v).eq.0)then
        num_rr=num_rr+1
    end if

    if(triad_val(v).eq.1)then
        num_mr=num_mr+1
    end if

    if(triad_val(v).eq.2)then
        num_mm=num_mm+1
    end if
end do

tot_mm=num_mm
tot_mr=num_mr
tot_rr=num_rr

f_mm=tot_mm/(n-2)
f_mr=tot_mr/(n-2)
f_rr=tot_rr/(n-2)

tol_mm=abs(f_mm-pmm)/pmm
tol_mr=abs(f_mr-pmr)/pmr
tol_rr=abs(f_rr-prr)/pr

if(tol_diad.le.tol1)then
    if(tol_mm.le.tol2.and.tol_mr.le.tol2.and.tol_rr.le.tol2)then
        exit
    end if
end if

```

```

        end if
    end if
end do

write(80,*)"sequence accepted"
write(80,*)"#####"
write(80,*)"fraction of r diads"
write(80,*)f_r
write(80,*)"reference value of r diads fraction (according to
Bernoulli dist.)"
write(80,*)pr
write(80,*)"maximum tolerance for r diads fraction"
WRITE(80,*)tol1
write(80,*)"TOLERANCE CALCULATED FOR r DIADS FRACTION"
write(80,*)tol_diad
write(80,*)"fraction of mm diads"
write(80,*)f_mm
write(80,*)"fraction of mr diads"
write(80,*)f_mr
write(80,*)"fraction of rr diads"
write(80,*)f_rr
write(80,*)"reference value of mm triads fraction (according to
Bernoulli dist.) "
write(80,*)pmm
write(80,*)"reference value of mr triads fraction (according to
Bernoulli dist.)"
write(80,*)pmr
write(80,*)"reference value of rr triads fraction (according to
Bernoulli dist.)"
write(80,*)prr
write(80,*)"maximum tolerance for mm,mr and rr triads fractions"
write(80,*)tol2
write(80,*)"TOLERANCE CALCULATED FOR mm TRIADS FRACTION"
write(80,*)tol_mm
write(80,*)"TOLERANCE CALCULATED FOR mr TRIADS FRACTION"
write(80,*)tol_mr
write(80,*)"TOLERANCE CALCULATED FOR rr TRIADS FRACTION"
write(80,*)tol_rr
write(80,*)"Sequence numbers"
write(80, '(f4.1)')s(:)
write(80,*)"#####"

```

end subroutine ata

```

!!!!!!!!!!!!!!!!!!!!!!!!!!!!!!!!!!!!!!!!!!!!!!!!!!!!!!!!!!!!!!!!!!!!!!!!!!!!!!!!!!!!!!!!!!!!!!!!!!!!!!!!!!!!!!!!!!!!!!!!
!!!!!!!!!!!!!!!!!!!!!!!!!!!!!!!!!!!!!!!!!!!!!!!!!!!!!!!!!!!!!!!!!!!!!!!!!!!!!!!!!!!!!!!!!!!!!!!!!!!!!!!!!!!!!!!!!!!!!!!!
!!!!!!!!!!!!!!!!!!!!!!!!!!!!!!!!!!!!!!!!!!!!!!!!!!!!!!!!!!!!!!!!!!!!!!!!!!!!!!!!!!!!!!!!!!!!!!!!!!!!!!!!!!!!!!!!!!!!!!!!

```

```

subroutine syndio(n,s)

    implicit none

    integer::i
    integer,intent(in)::n
    real,allocatable,intent(out)::s(:)

    allocate(s(n))

```

```

do i = 1,n-1,2
  s(i) = 1
end do

do i = 2,n,2
  s(i) = -1
end do

end subroutine syndio

!!!!!!!!!!!!!!!!!!!!!!!!!!!!!!!!!!!!!!!!!!!!!!!!!!!!!!!!!!!!!!!!!!!!!!!!!!!!!!!!!!!!!!!!!!!!!!!!!!!!!!!!!!!!!!!!!!!!!!!!
!!!!!!!!!!!!!!!!!!!!!!!!!!!!!!!!!!!!!!!!!!!!!!!!!!!!!!!!!!!!!!!!!!!!!!!!!!!!!!!!!!!!!!!!!!!!!!!!!!!!!!!!!!!!!!!!!!!!!!!!
!!!!!!!!!!!!!!!!!!!!!!!!!!!!!!!!!!!!!!!!!!!!!!!!!!!!!!!!!!!!!!!!!!!!!!!!!!!!!!!!!!!!!!!!!!!!!!!!!!!!!!!!!!!!!!!!!!!!!!!!
subroutine pseudoran(s)

  implicit none

  real,intent(out),allocatable :: s(:)

  CALL init_random_seed
  CALL RANDOM_NUMBER(s)

  where(s(:).le.0.5)
    s(:)=1
  elsewhere
    s(:)=-1
  end where

end subroutine pseudoran

!!!!!!!!!!!!!!!!!!!!!!!!!!!!!!!!!!!!!!!!!!!!!!!!!!!!!!!!!!!!!!!!!!!!!!!!!!!!!!!!!!!!!!!!!!!!!!!!!!!!!!!!!!!!!!!!!!!!!!!!
!!!!!!!!!!!!!!!!!!!!!!!!!!!!!!!!!!!!!!!!!!!!!!!!!!!!!!!!!!!!!!!!!!!!!!!!!!!!!!!!!!!!!!!!!!!!!!!!!!!!!!!!!!!!!!!!!!!!!!!!
!!!!!!!!!!!!!!!!!!!!!!!!!!!!!!!!!!!!!!!!!!!!!!!!!!!!!!!!!!!!!!!!!!!!!!!!!!!!!!!!!!!!!!!!!!!!!!!!!!!!!!!!!!!!!!!!!!!!!!!!

SUBROUTINE init_random_seed

  implicit none

  INTEGER :: c, clock
  INTEGER, ALLOCATABLE :: seed(:)

  CALL RANDOM_SEED(size = c)
  ALLOCATE(seed(c))

  CALL SYSTEM_CLOCK(clock)

  seed = clock

  CALL RANDOM_SEED(PUT = seed)

END SUBROUTINE init_random_seed

```



